Aus dem

Department für Augenheilkunde Tübingen

Universitäts-Augenklinik

Characterization of Mechanosensitive Channels in the Eye

Inaugural-Dissertation
zur Erlangung des Doktorgrades
der Medizin

der Medizinischen Fakultät
der Eberhard Karls Universität
zu Tübingen

vorgelegt von
Zheng, Wenxu

2023

Dekan: Professor Dr. B. Pichler

1. Berichterstatter: Professor Dr. F. Ziemssen
2. Berichterstatter: Professorin Dr. M. Knipper-Breer

Tag der Disputation: 22.03.2023

Contents

List of figures

List of tables

Index of abbreviations

AANAT	arylalkymine N-acetyltransferase
ADPKD	autosomal-dominant polycystic kidney disease
ASICs	acid-sensing ion channels
ATP	adenosine triphosphate
BCs	bipolar cells
Brn3a	brain-specific homeobox/POU domain protein 3A
BSA	bovine serum albumin
CB	ciliary body
COR	consensual ophthalmotonic reaction
DAPI	4'6-diamidine-2'phenylinodole dihydrochloride
DEG/ENaC	degenerin/epithelial sodium channel
DMEM	Dulbecco's Modified Eagle Medium
ECM	extracellular matrix
GAPDH	glyceraldehyde 3-phosphate dehydrogenase
GCL	ganglion cell layer
HNPCE	human non-pigment ciliary epithelial
INL	inner nuclear layer
INPP5	inositol polyphosphate 5-phosphatase
IOP	Intraocular pressure
IPL	inner plexiform layer
K2P	two-pore domain K+
miR-204	microRNA-204
mmHg	millimeter of mercury (unit)
MSCs	mechanosensitive channels
MscL	mechanosensitive channel of large conductance
MscS	mechanosensitive channel of small conductance
NaCl	sodium chloride
NC	negative control
NAP	normal atmospheric pressure
NPE	non-pigmented epithelium
OCRL	Lowe oculocerebrorenal syndrome protein
ON	optic nerve

ONL	outer nuclear layer
OPL	outer plexiform layer
PBS	phosphate buffered saline
PCR	polymerase chain reaction
PE	pigmented epithelium
PFA	paraformaldehyde
PI(4)P	Phosphatidylinositol-4-phosphate
$PI(4,5)P_2$	phosphatidylinositol-4,5-bisphosphate
PKD	polycystic kidney disease
PL	photoreceptor layer
PLL	Poly-L-Lysine
PMSF	phenylmethylsulfonylfluorid
RGCs	retinal ganglion cells
RPE	retinal pigment epithelial cells
RT	room temperature
RT-PCR	reverse transcription polymerase chain reaction
SDS	sodium dodecyl sulfate
SDS-PAGE	sodium dodecyl sulfate polyacrylamide gel electrophoresis
siRNA	small interfering RNA
TBS	Tris-buffered saline
TBST	Tris-buffered saline supplemented with Triton X-100
TG	trigeminal ganglion
TM	trabecular meshwork
TMC	transmembrane channel
TMEM16/Ano	transmembrane protein 16/Anoctamin
TRIS	Tris-(hydroxymethyl)-aminomethan)-base
TRP	transient receptor potential
TRPA1	transient receptor potential ankyrin-1
TRPC6	transient receptor potential canonical-6
TRPM3	transient receptor potential melastatin-3
TRPM4	transient receptor potential melastatin-4
TRPM7	transient receptor potential melastatin-7
TRPV1	transient receptor potential vanilloid-1

TRPV2	transient receptor potential vanilloid-2
TRPV4	transient receptor potential vanilloid-4
WB	Western blot
Wpk	Wistar polycystic kidney

1. Introduction

1.1 Glaucoma and intraocular pressure

Glaucoma encompasses a spectrum of manifestations of different diseases in which progressive atrophy of ganglion cells and optic neuropathy occur. Its common feature is slow degeneration of retinal cells and their axons, leading to the characteristic appearance of optic disc damage accompanying with different patterns of visual loss (Weinreb and Khaw, 2004). It has been estimated that more than 76 million people worldwide suffer from glaucoma, of which about 10% have bilateral blindness (Tham et al., 2014). Glaucoma is the second leading reason caused blindness in the world (Kingman, 2004). The vision loss is irreversible, so it is especially important to detect the disease early in order to be able to intervene with preventive measures and therapies before permanent damage has occurred. However, the underlying mechanisms of the disease have not been fully understood. The potential factors leading to its development and the progress have not been fully characterized. Although early investigations and studies underestimated the differential resistance and survival of ganglion cells as a factor. **Intraocular pressure** (IOP) has been identified as major modifiable risk factor. Achieving a finely regulated equilibrium of aqueous humor production and outflow ensures that healthy individuals do not experience excessive fluctuations or increased values of IOP. In addition, the reduction of IOP was the first and most widespread therapeutic option in the last 100 years (Weinreb and Khaw, 2004).

Increased IOP, depending on the individual target pressure range (e.g., $\leqslant$16, 18 or 21 mmHg), is considered to be the most important risk factor for progression. The imbalance between aqueous humor secretion in the **ciliary body** (CB, Figure 1) and outflow in the anterior chamber angle is responsible for the increased IOP in glaucoma. Aqueous humor is secreted by non-pigmented epithelial cells of the CB into the posterior chamber, passes through the pupil into the anterior chamber, and exits through the trabecular meshwork or uveoscleral outflow pathways. However, the exact mechanisms of IOP regulation are still unclear.

Previous findings were mainly limited to the development of increased IOP (disease scenario), which may often be caused by an increase in outflow resistance in the area of the **trabecular meshwork** (TM) or behind it. Deposits of proteins or changes of the extracellular matrix, e.g., after application of steroids, were identified as triggers (Clark and Wordinger, 2009; Vranka et al., 2015).

Few studies, however, have addressed the question of which mechanisms ensure that despite fluctuations in aqueous humor production (for example in the circadian rhythm), a "normal" IOP (physiologic scenario) can still be maintained for the vast majority. Several studies have suggested the existence of a "**consensual ophthalmotonic reaction**" (COR). The phenomenon consists of a change in IOP of one eye that provokes an alteration in IOP in the contralateral eye (Gibbens, 1988). Therefore, the often-observed response, e.g. in the context of pressure-lowering glaucoma surgery, represents evidence for a regulation of aqueous humor production. The reaction may indicate IOP regulation, probably through a reflex arc (for further details see Denis et al.) (Denis et al., 1994).

A mandatory part of the COR reflex arc includes an afferent pathway with sensitive cells or baroreceptors in the center. If this element exists, these baroreceptors might be localized in the region of TM，the CB or the wall of the bulb (cornea or sclera). Of course, it would make sense if sensitive structures were placed immediately near or in proximity to those formations where the aqueous humor is produced. A feedback from hydrostatic pressure to the processes of aqueous humor formation has not been proven yet. Although no clear evidence has confirmed the importance of specific baroreceptors in the eye so far, recent studies revealed some possible candidates (Kalapesi et al., 2005). The typical characteristics of known mechanosensitive channels might help us to identify possible baroreceptors in the eye (Baxter et al., 2020).

The CB of eye is generally thought as the anatomical site of aqueous humor production (Civan and Macknight, 2004). More precisely, the formation of aqueous humor is located in the ciliary epithelium of CB, which is composed of the **non-pigmented epithelium** (NPE) facing to posterior chamber and **pigmented epithelium** (PE) facing to stroma. The two

layers of cells are connected by gap junctions. The unidirectional fluid is secreted from stroma to NPE by transferring solute (mainly NaCl) and water follows passively (Civan and Macknight, 2004). To what we know, there are three mechanisms involved in aqueous humor formation: diffusion, ultrafiltration and active secretion. Bicarbonate (HCO_3^-) and chloride (Cl^-) play a significant role in aqueous humor formation (Civan and Macknight, 2004).

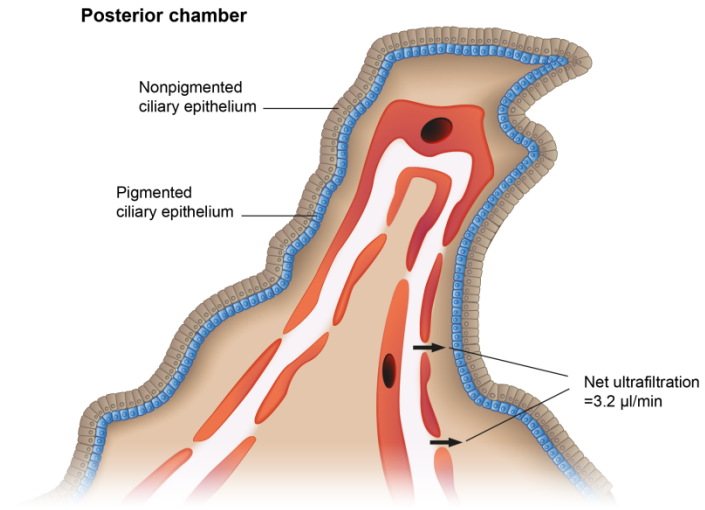

Figure 1. Schematic drawing of the anatomy of CB. Adapted from (Sruthi Sampathkumar and Carol B. Toris, 2022).

1.2 Mechanosensitive channels (MSCs)

Mechanosensitive channels (MSCs), also called mechanically activated channels, are membrane proteins which can directly respond to the mechanical stress of external mechanical stimuli and can convert mechanical force into biological signals (Sachs, 2010). The mechanical force could be varied, like fluid shear stress and pressure, membrane stretch, vibration, indentation and so on (Ranade et al., 2015). Over the last few years, many potential MSCs have been reported, especially in eukaryotic cells, including members of the PIEZO family, some members of **transient receptor potential** (TRP) family, and members of **two-pore domain K^+** (K2P) channel family, as well as some members of the **degenerin/epithelial sodium channel** (DEG/ENaC) superfamily and the **transmembrane**

protein 16/Anoctamin (TMEM16/Ano) superfamily (Jin et al., 2020). The term “PIEZO” is derived from the Greek πιέζω, which means to squeeze or press.

1.2.1 PIEZO family

The PIEZO family was identified as an important component of a mechanically activated ion channel ten years ago (Coste et al., 2010). The family has two members, PIEZO1 (Fam38A) and PIEZO2 (Fam38B) (Figure 2) (Coste et al., 2010). PIEZO1 is broadly expressed in many different organs, like bladder, colon, kidney, lung and skin (Coste et al., 2010). Its abundance has been described for different cell types, like vascular endothelial cells (Li et al., 2014), erythrocytes (Faucherre et al., 2014) or periodontal ligament cells (Jin et al., 2015). PIEZO2 is prominently expressed in the bladder, the colon, the lung and dorsal root ganglia (Coste et al., 2010). Its function seems to be of importance for trigeminal ganglion neurons (Bron et al., 2014) and the Merkel cells (Woo et al., 2014). The Piezo proteins play an important role in response to membrane tension (~1–3 mN/m) (Coste et al., 2010), indentation (Kim et al., 2012), shear stress (~10 dyn/cm2) (Rode et al., 2017) and/or stretch (Gudipaty et al., 2017). Expression of PIEZO1 in the plasma membrane is consistent with its function as a stretch-activated channel that mediates Ca^{2+} influx. Miyamoto et al. showed that in urothelial cell, the PIEZO1 can regulate the mechanotransduction by stretch-evoked Ca^{2+} influx and adenosine triphosphate (ATP) releasing (Miyamoto et al., 2014). Cinar et al. also reported the same function of PIEZO1 in human red blood cells (Cinar et al., 2015).

In ocular tissues, PIEZO1 and PIEZO2 were reported to be broadly expressed in cornea, TM, epithelial cells of lens, the retinal ganglion cell layer (Morozumi et al., 2020) and the astrocytes of the optic nerve head in mice (Choi et al., 2015). Recently, PIEZO1 has been identified as a potential transducer of tensile stretch, shear flow and pressure in TM (Yarishkin et al., 2021; Zhu et al., 2021). In murine glaucoma models, the level of PIEZO2 expression is increased in mice retina (Morozumi et al., 2020) and astrocytes of the optic nerve head (Choi et al., 2015).

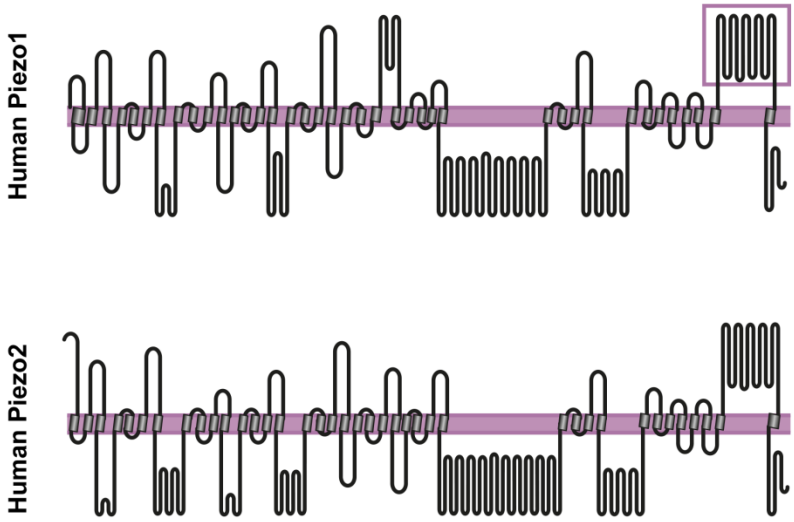

Figure 2. Putative topology of human PIEZO1 (top) and PIEZO2 (bottom). Adapted from (Soattin et al., 2016).

1.2.2 Transient receptor potential (TRP) family

The **transient receptor potential** (TRP) channels family has a series of six-transmembrane cation-permeable channels. These channels are involved in processing of many physiological and pathophysiological senses, such as hearing (Zanini and Göpfert, 2014), smelling (Zufall, 2014), tasting (Roper, 2014), feeling pain (Jardín et al., 2017), sight (Katz et al., 2017), registering temperature (Nilius and Flockerzi, 2014) and senses of force (Lin and Corey, 2005). TRP channels play an essential role in several pathways of mechanotransduction following the increased tension of membrane, fluid shear stress and the change of cell volume or osmotic pressure (Startek et al., 2019). Based on the homology of amino acid sequences, the mammalian TRP channels are divided into six subfamilies: TRPA (Ankyrin), TRPC (Canonical), TRPM (Melastatin), TRPV (Vanilloid), TRPP (Polycystin) and TRPML (Mucolipin) (Samanta et al., 2018) (Figure 3). Evidence from many recent studies revealed that some members of TRP channels, like **transient receptor potential ankyrin-1** (TRPA1), **transient receptor potential canonical-6** (TRPC6), **transient receptor potential melastatin-3** (TRPM3), **transient receptor potential melastatin-4** (TRPM4), **transient receptor potential melastatin-7** (TRPM7), **transient receptor potential vanilloid-1** (TRPV1), **transient receptor potential vanilloid-**

2 (TRPV2) and **transient receptor potential vanilloid-4** (TRPV4), may have the function like mechanoreceptor properties (Startek et al., 2019).

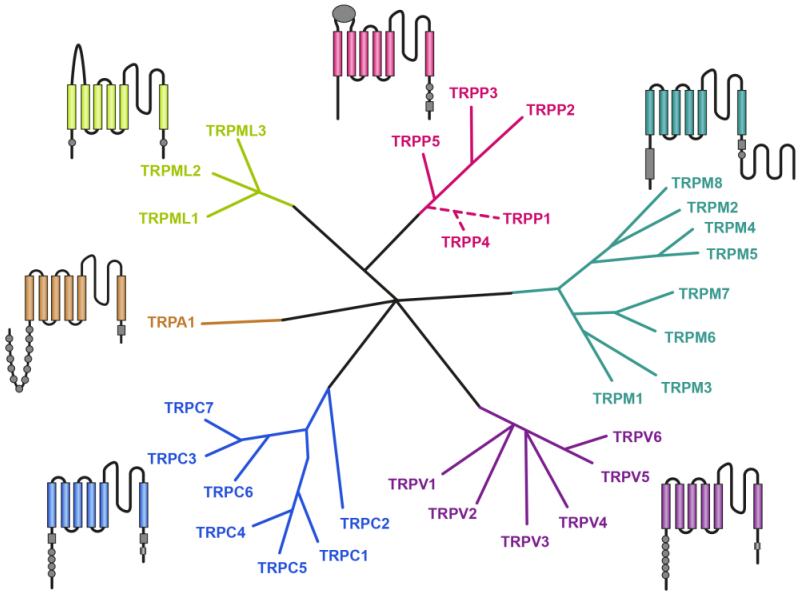

Figure 3. A schematic representation of the TRP superfamily ion channels. Each branching group is representative of a subfamily of channels. Adapted from (Samanta et al., 2018).

1.2.2.1 Transient receptor potential ankyrin-1 (TRPA1)

Transient receptor potential ankyrin-1 (TRPA1) is a Ca^{2+}-permeable cation channel and is the only member of the mammalian TRPA subfamily (Jaquemar et al., 1999) (Figure 3). Studies found TRPA1 to be mainly expressed in sensory neurons and epithelial cells and functions as chemical nocisensor, noxious or cold sensor (Talavera et al., 2020). Investigations identified its role in mechanosensation. This function of TRPA1 was first reported for inner-ear hair cells (Corey et al., 2004). TRPA1 has been discussed as a component of the transduction channel. The inhibition of TRPA1 protein expression in inner ear cells inhibits receptor cell function (Corey et al., 2004).

Many reports allude to the role of TRPA1 in detecting mechanical stimulation in different cells types, including sensory neurons (Kerstein et al., 2009), human periodontal ligament cells (Tsutsumi et al., 2013), Merkel cells (Soya et al., 2014), and odontoblasts (Shibukawa et al., 2015).

1.2.2.2 Transient receptor potential melastatin-3 (TRPM3)

Transient receptor potential melastatin-3 (TRPM3) belongs to a type of Ca^{2+}-permeable nonselective cation channel. The protein is one of eight members of the mammalian TRPM subfamily (Lee et al., 2003) (Figure 3). Previous studies identified its function as a chemical and heat nociceptor channel (Vriens et al., 2011). TRPM3 also showed putative mechanosensitive function, which has been shown to get activated upon stimulation of hypotonic extracellular solution (Grimm et al., 2003). Treatment of hypertonic solution could lead to decreased activity of TRPM3, while hypotonic solution treatment causes activation of TRPM3 in HEK293 cells (Grimm et al., 2003). Furthermore, mutation in the TRPM3 gene leads to inherited eye disease. For example, mutations in TRPM3 gene are associated to complex ocular syndromes, presenting with cataract and high-tension glaucoma with variable anterior segment defects (Bennett et al., 2014). The expression of TRPM3 was localized mainly in the CB (Gilliam and Wensel, 2011; Ryskamp et al., 2016b). Therefore, TRPM3 might play a role in detecting changes secondary to the hydrostatic pressure of the eye.

1.2.2.3 Transient receptor potential Vanilloid-4 (TRPV4)

Transient receptor potential Vanilloid-4 (TRPV4) is one of the nonselective cation channels, allowing permission of Ca^{2+} and Mg^{2+}. It belongs to the family of TRPV proteins (Voets et al., 2002) (Figure 3). TRPV4 was first known as an osmosensor, as it can sense osmotic pressure in the central nervous system (Liedtke et al., 2000). Further studies revealed its additional function in temperature sensation, as well as the integration of thermal and osmotic information (Güler et al., 2002).

Based on its permeability properties for calcium, it was recognized as mechanoreceptor as well (O'Neil and Heller, 2005). In recent years, TRPV4 was found widely expressed in ocular tissues, including in the retina, corneal epithelium, ciliary body, and the lens (Guarino et al., 2020). TRPV4 can also interact with OCRL (Lowe

oculocerebrorenal syndrome protein), which had been identified as the responsible MSC of primary cilia in TM (Luo et al., 2014). Mutations in OCRL can cause Lowe syndrome (Loi, 2006), a multisystem disorder, including glaucoma. More interestingly, the systemic delivery of TRPV4 antagonist prodrug analogs have been shown to lower IOP in a murine glaucoma model (Ryskamp et al., 2016b).

1.2.2.4 Transient receptor potential polycystin-2 (TRPP2)

Transient receptor potential polycystin-2 (TRPP2, polycystin 2 or PC2) belongs to a type of Ca^{2+} permeable cation channel. Deficiency of TRPP2 channel has been reported as a causative of **autosomal-dominant polycystic kidney disease** (ADPKD) (Mochizuki et al., 1996) (Figure 3). Several lines of evidence indicate the role of TRPP2 in sensing mechanical pressure. For example, the polycystin complex, which is assembled by TRPP2 and its molecular chaperones polycystin 1, can be activated and induced Ca^{2+} influx to primary cilia by mechanical pressure on several stress-bearing cells, like kidney cells (Nauli et al., 2003), vascular endothelial cells (AbouAlaiwi et al., 2009), vascular smooth muscle cells (Lu et al., 2008) and bronchial smooth muscle cells (Wu et al., 2009). In the eye, the expression of TRPP2 has been detected in different structures, including the TM (Tran et al., 2014), the cornea (Obermüller et al., 1999), the retina (Gallagher et al., 2006; Gilliam and Wensel, 2011) and the optic nerve head (Choi et al., 2015) of animals.

1.2.3 Two-pore domain K^+ (K2P) channel family

Two-pore domain K^+ (K2P) channel family contains a series of K^+ channel, which consists of four transmembrane segments and two pore domains (Enyedi and Czirják, 2010). The protein has been shown to maintain the resting level of membrane potential in different cell types such as TREK currents in embryonic atrial myocytes (Zhang et al., 2008), TASK-3 in cerebellar granule neurons (Zanzouri et al., 2006) and TASK-2 in pulmonary arteries (Gönczi et al., 2006) and so on. To date, 15 members of the K2P family have been identified. According to the range of different activities, K2P family members are divided into

six subfamilies (Table 1): (1) mechano-gated, (2) alkaline-activated, (3) Ca^{2+}-activated, (4) weak inward rectifiers, (5) acid-inhibited, and (6) halothane-inhibited channels (Honoré, 2007).

TREK1, a member of mechano-gated subfamily, is found to directly transmit mechanical force by modifying membrane tension (Patel et al., 1998). The expression of TREK1 was detected within TM of human eyes on protein and RNA level (Tran et al., 2014). The transduction of mechanosensing via cochlin/TREK1 may associated with remodeling of TM cell cytoskeleton. These changes might finally lead to an increased outflow of aqueous humor and this decreased in IOP (Goel et al., 2011). Additionally, TRPV4 and TREK1 have been considered to regulate the calcium homeostasis and transcellular permeability in order to control the tensile homeostasis and IOP (Yarishkin et al., 2018).

Table 1. The members of K2P family are divided into six subfamilies by potential function.

Subfamily	Member	
Mechano-gated	TRAAK	K_{2P}4.1[KCNK4]
	TREK1	K_{2P}2.1[KCNK2]
	TREK2	K_{2P}10.1[KCNK10]
Alkaline-activated	TALK1	K_{2P}16.1[KCNK16]
	TALK2	K_{2P}17.1[KCNK17]
	TASK2	K_{2P}5.1[KCNK5]
Calcium-activated	TRESK1	K_{2P}18.1[KCNK18]
Weak inward rectifiers	KCNK7	K_{2P}7.1[KCNK7]
	TWIK1	K_{2P}1.1[KCNK1]
	TWIK2	K_{2P}6.1[KCNK6]
Acid-inhibited	TASK1	K_{2P}3.1[KCNK3]
	TASK3	K_{2P}9.1[KCNK9]
	TASK5	K_{2P}15.1[KCNK15]
Halothane-inhibited	THIK1	K_{2P}13.1[KCNK13]
	THIK2	K_{2P}12.1[KCNK12]

1.2.4 Other MSCs

MEC-10 and MEC-4 (the *mec-4* and *mec-10* protein, *mec* is abbreviation of mechanosensory), which belongs to the **degenerin/epithelial sodium channel** (DEG/ENaC) superfamily (Ben-Shahar, 2011), were first verified as a requirement for touch sensation in Caenorhabditis elegans (Huang and Chalfie, 1994). Many evidences showed that some members of mammalian DEG/ENaC proteins may play a critical role in mechanosensation. Among these, a group of **acid-sensing ion channels** (ASICs) have

been implicated in mechanical transduction of proprioceptors, mechanoreceptors and nociceptors to monitor the homoeostatic state of muscle contraction, blood volume, blood pressure and pain stimulation (Cheng et al., 2018). Furthermore, **transmembrane channel-1** (TMC1) and **transmembrane channel** (TMC2), two members of **transmembrane channel** (TMC), belonging to the **transmembrane protein 16/Anoctamin** (TMEM16/Ano) family, were considered to be candidates for the long-sought pore-forming subunits of MSCs in the hair cells of inner-ear (Corey and Holt, 2016).

Besides the above mentioned MSCs, the bacterial **mechanosensitive channel of large conductance** (MscL) and **mechanosensitive channel of small conductance** (MscS) are the best-characterized MSCs (Cox et al., 2018).

1.2.5 MSCs of the eye

Mechanical transduction is a process in which cells transduce mechanical signals into biological reactions (Polacheck et al., 2013). This process is triggered by different types of mechanical stimuli, including hydrostatic pressure, compression, connective tissue tensile stretch and, fluid shear stress and interstitial fluid flow (Thompson et al., 2020). The mechanical stimuli for intraocular cells and tissues can be direct through the hydrostatic pressure and indirect through the connective tissue tensile stretch. Then, biological responses are triggered in the cells and tissues, like altered gene expression and protein secretion, to change the influence of the effect caused by the mechanical cues. As in the ocular tissue, increased IOP may stimulate mechanotransducers in the TM, which leads to increased fluid outflow and motivates the mechanotransducers in the CB, finally decrease fluid formation to maintain IOP homeostasis (Figure 4). Therefore, mechanical transduction usually involves a feedback process (Polacheck et al., 2013). Thus, as the mechanosensing is at the beginning of the process, MSCs play a crucial role in adjustment of steady-state intraocular pressure. For example, PIEZO1 has been identified as the key TM mechanosensor for stretch, shear flow and pressure since its activation causes

intracellular signals to change the cytoskeleton and cell-extracellular matrix contact tissues and regulate the trabecular components of aqueous humor outflow (Yarishkin et al., 2021).

Some MSCs are considered to be putative mechanosensors in TM cells and have been found, including PIEZO1 (Yarishkin et al., 2021; Zhu et al., 2021), TRPV4 channels (Luo et al., 2014; Ryskamp et al., 2016a) and TREK-1 (Carreon et al., 2017b; Yarishkin et al., 2018). However, the expression and location of multiple MSCs in the source of fluid production --- ciliary body are not well characterized so far.

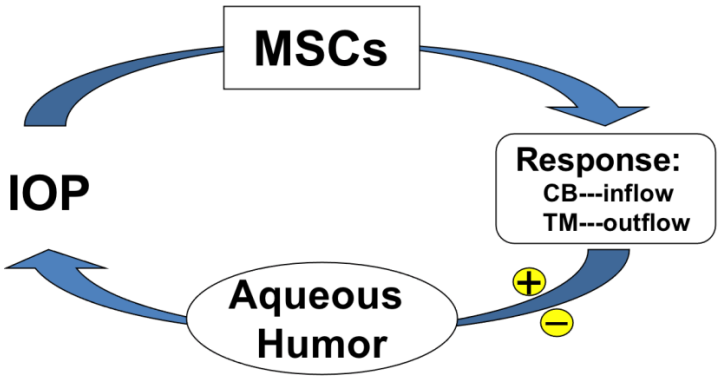

Figure 4. Schematic diagram of IOP regulation by MSCs.

1.3 Primary cilia

1.3.1 Primary cilia

While the present study focuses on the distribution and location of the PIEZO channels, some selected TRP members, and TREK1 in rat and human eyes as well as in human non-pigment ciliary epithelial (HNPCE) cells cultures, cilia must be considered as structural elements of these cells. Cilia are located on the surface of most eukaryotic cells and are membrane-bound projections (Satir and Christensen, 2007). Cilia can be structurally divided into four sub-compartments, including a basal body, a so-called axoneme, a ciliary membrane and transition fibers (Berbari et al., 2009). Cilia are discussed as acting like ‘antennae’ which can sense the extracellular signals, such as growth factors, hormones, odorants and developmental morphogens (Berbari et al., 2009). In mammals, ciliary axonemes can form two major, different patterns: one is the 9+2 cilia, consisting of nine doublet microtubules surrounded by a central pair of singlet microtubules, and the other one

is 9 + 0 cilia, which is similar to the other cilia, but without having the central pair (Satir, 2005). Most of cell types can show only one cilium (a monocilium or primary cilium), whereas some type of cells exhibit cilia bundles that consisting of 200–300 individual organelles (multiple cilia) (Fliegauf et al., 2007). According to mobility, the cilia can also be classified as motile cilia and immotile cilia (Berbari et al., 2009).

A primary cilium is single and immotile, with the ciliary axoneme pattern of a 9+0 cilia (Figure 5). Primary cilia were found not only on epithelial cells, like the kidney tubule, the bile duct, the endocrine pancreas, and the thyroid, but also on non-epithelial cells, like the chondrocytes, fibroblasts, smooth muscle cells, neurons, and Schwann cells (Satir and Christensen, 2007).

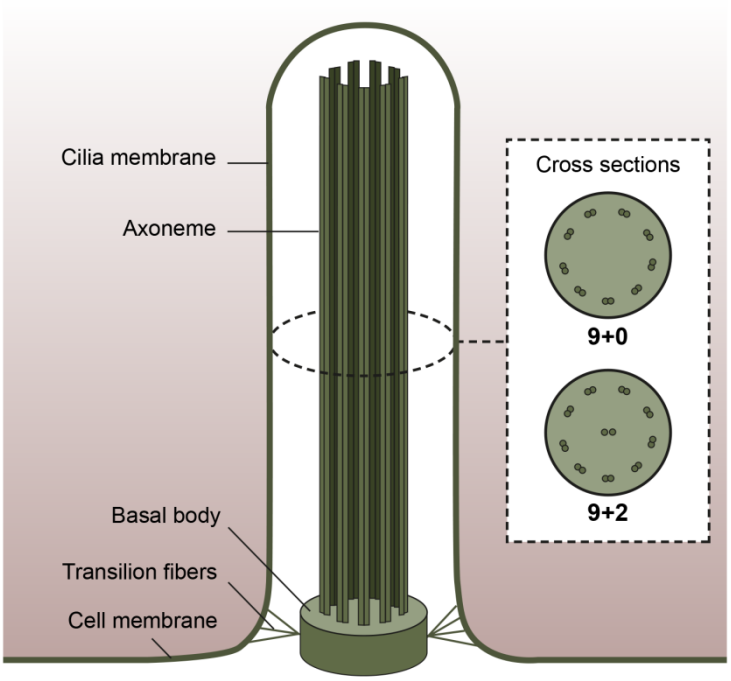

Figure 5. Schematic drawing of the structure primary cilia. Adapted from (Berbari, 2009).

1.3.2 Primary cilia and IOP

Primary cilia have been identified as cell organelles twenty years ago (Wheatley, 1995). However, their potential role of acting as a mechanosensor was reported in recent publication (Berbari et al., 2009; Satir and Christensen, 2007). Such primary cilia have been described in several cell types, particular in the cells exposed to flow, such as

cholangiocytes (Masyuk et al., 2006), vascular endothelia (Iomini et al., 2004; Nauli et al., 2008), renal collecting duct epithelium (Liu et al., 2018) and chondrocytes (Wann et al., 2012). In 1980, Ohnishi and Tanaka observed that primary cilia exist in the ciliary PE and NPE of the Rhesus monkey eye by using electron microscopy (Ohnishi and Tanaka, 1980). Immunostaining showed that TM cells also have primary cilia which can response to the change of IOP. For example, in response to elevated hydrostatic pressure the primary cilia in TM cells become shorten (Luo et al., 2014). Furthermore, mutation in a key protein, inositol polyphosphate 5-phosphatase (INPP5), seems to be required for the response of primary cilia, secondary to pressure stimulation and thus contributing to the oculocerebrorenal syndrome (Lowe syndrome, OCRL) (Luo et al., 2014).

1.3.3 Primary cilia and MSCs

Many reports show that some MSCs identified in the primary cilia could respond to mechanical stimuli of surrounding environment. For example, TRPM3 expressed in primary cilia in renal epithelial cells in mice are required for the maximal osmotic response (Siroky et al., 2017). The TRPV4 expressed in cholangiocytes cilia can also detect the changes in the luminal tonicity (Gradilone et al., 2007). In ocular tissue, the expression of TRPV4 was detected in primary cilia of TM, and TRPV4 agonist treatment could also reduce IOP in Wistar polycystic kidney (Wpk) rats, which is a model with polycystic kidney disease (Nauta et al., 2000). Furthermore, TRPV4 knockout in mice displays elevated IOP and shortened primary cilia (Luo et al., 2014).

Another MSCs TRPP2 and its molecular chaperones, polycystin1, could assemble the polycystin complex which located on primary cilia and associated with cellular mechanosensitivity on several stress-bearing cells, like kidney cells (Nauli et al., 2003), vascular endothelial cells (AbouAlaiwi et al., 2009), vascular smooth muscle cells (Lu et al., 2008) and bronchial smooth muscle cells (Wu et al., 2009). In addition, TRPV4 and TRPP2 are considered to be a mechanosensitive molecular sensor in primary cilia of renal epithelial cells (Köttgen et al., 2008).

1.4 Objectives

To date, a large number of MSCs candidates have been identified in different organs, but little is known about their expression and potential function in ocular tissues, especially in CB. As MSCs can sense mechanical strength, whether MSCs in eyes can also sense the IOP and subsequently control the aqueous humor regulation is largely unclear.

In this study, an overview of several selected MSCs (PIEZO1, PIEZO2, TRPA1, TRPM3, TRPV4, TRPP2 and TREK1) will be provided in order to characterize the expression, distribution and localization of MSCs in different structures in the eye. First, (ultra-)structure properties of ocular MSCs should be clarified, using immunofluorescence in sections from frozen rat eyes. Next, to determine the protein level of selected MSCs, WB will be performed using the protein lysate from different structures of rat eyes. To analyze mRNA levels, reverse transcription PCR and qRT-PCR will be used on different rat eye tissues. Then, the expression of MSCs in human eye on paraffin sections will be tested by using the same antibody. Afterwards, western blotting, conventional PCR and ICC will be carried out on HNPCE cells to extract analyze the expression and localization of MSCs on the area where aqueous humor is produced.

The primary cilium in HNPCE cells will be detected to investigate the existence and whether it can sense elevated hydrostatic pressure in HNPCE cells. Thus, in order to indicate the structure of primary cilia, mouse anti-acetylated α-tubulin and rabbit anti-γ-tubulin antibodies will be used to detect the primary cilia axoneme and basal body of HNPCE cells by using immunofluorescence staining. For further confirm the formation of primary cilia, electron microscopy will be performed on HNPCE cultured cells and immunohistochemistry staining will be performed on human eye tissue sections. As primary cilia and MSCs are both related to the mechanic sense of cells, whether MSCs and primary cilia work together should also be studied. Thus, the co-localization of MSCs candidates and primary cilia marker, acetylated α-tubulin, will be examined using double immunofluorescence staining.

In the third part of this study, whether MSCs candidates in the HNPCE can be related to sensation of increase in IOP is going to be further examined. The interaction between MSCs candidates and high pressure will be explored by using an apparatus of pressure elevation model which imitates IOP increasing in human eye. The protein and mRNA expression change in MSCs candidates in the HNPCE after subjecting to increased hydrostatic pressure will be determined. In order to further characterize the influence of TRPP2 and PIEZO2 proteins in HNPCE cells, repressing the expression of TRPP2 and PIEZO2 will be performed with aid from the technology of **small interfering RNA** (siRNA). To investigate the influence of TRPP2 on the expression of other MSCs candidates in HNPCE cells, the protein level of PIEZO1, PIEZO2, TRPA1, TRPM3, TRPV4 and TREK1 will be tested in TRPP2-siRNA treated HNPCE cells with or without high pressure treatment. To investigate the influence of PIEZO2 on the expression of other MSCs candidates in HNPCE cells, the protein level changes of PIEZO1, TRPA1, TRPM3, TRPV4, TRPP2 and TREK1 in HNPCE cells will be tested in PIEZO2-siRNA under normal atmospheric pressure (NAP) and the high-pressure treatment condition.

Characterizing the MSCs in ocular tissue, in particular in CB, may provide a new view on the potential function of mechanotransduction in IOP sensing and regulation, and provide clues on suggesting new molecular targets for glaucoma treatment.

2. Materials and Methods

2.1 Methods

2.1.1 Animal tissue preparation

Animals were treated according to the Principles of Laboratory Animal Care (NIH publication No. 85–23, revised 1985), the OPRR Public Health Service Policy on the Human Care and Use of Laboratory Animals (revised 1986) and the German animal protection law. Six wild type female Sprague–Dawley rats (12 weeks old) were euthanized using carbon dioxide inhalation and 12 eyes were enucleated immediately after death. After careful dissecting of the whole eyeball, three eyes were fixed for immunohistochemistry staining, six eyes were processed for protein analysis and three eyes were processed for mRNA expression analysis. For protein and mRNA analysis the eyes were transferred under a sterile hood and dissected under a microscope into seven different parts: the retina, CB, cornea, sclera, optic nerve (ON), iris and lens. The dissected tissues were immediately frozen in liquid nitrogen and further stored at −80°C for long term storage until further analysis.

2.1.2 Human ocular specimens

Human eye experiments performed in this study were conducted according to the tenets of the Declaration of Helsinki. Three human eyes that were obtained from patient with choroidal melanoma but with a normal anterior segment were obtained (Patients code: University of Tübingen, no. 38072, 38282, 38375). All specimens were prepared by the pathology lab at the University Eye Hospital, Tübingen, Germany. Only eyes with normal structure of ciliary body were used for analysis.

2.1.3 HNPCE cell culture

Primary HNPCE cells were purchased from ScienCell Research Laboratories (cat no. 6580, CA, USA). The cells were cultured in epithelial cell medium (ScienCell Research

Laboratories, cat no. 4101, CA, USA) at 37°C in an incubator with 5% CO_2 and 95% humidity according to the instructions from the manufacturer.

2.1.4 Immunofluorescence staining

The rat eyes were cryo-sectioned into 12 μm sections for immunofluorescence staining. The slices were fixed with ice-cold methanol for 10 minutes at room temperature (RT). In order to mark NPE cells, after washing with Tris-buffered saline (TBS), slices were incubated with Jacalin-FITC (a marker for NPE cell) for 30 minutes in a dark chamber at RT before performing immunostaining. After blocking slices at RT for 1 hour with 5% bovine serum albumin (BSA) in TBS, slices were incubated with the primary antibody (PIEZO1, PIEZO2, TRPA1, TRPM3, TRPV4, TRPP2 and TREK1) (Table 7) at 4°C overnight. After washing three times, slices were added and incubated with the secondary antibody (Alexa Fluor 555-conjugated donkey anti-rabbit IgG) (Table 8) for 1 hour at RT. Slides were observed on Axioskop fluorescent microscope (Zeiss, Germany).

In order to mark RGC, after washing with TBS, slices were blocked at RT for 1 hour with 5% BSA in TBS and incubated with different primary antibody PIEZO1, PIEZO2, TRPA1, TRPM3, TRPV4, TRPP2, TREK1 and Brn3a (brain-specific homeobox/POU domain protein 3A) (Table 7) at 4°C overnight. After washing, slices were incubated with the secondary antibody Alexa Fluor 488-conjugated goat anti-rabbit IgG and Alexa Fluor 555-conjugated goat anti-mouse IgG (Table 8) for 1 hour at RT. Slides were observed on fluorescent microscope (Zeiss, Germany). The color of fluorescence on retina was exchanged to remain consistent with the color of fluorescence on CB and cornea.

2.1.5 Immunohistochemistry staining

Immunohistochemistry was performed to detect the expression and localization of MSCs candidates in human eye tissues. After removing paraffin from human eye tissue sections (4 μm) by using xylol, the eye slices were rehydrated in a graded alcohol series. After antigen retrieval using citric buffer (pH 6.0), slices were incubated with different

primary antibodies, like PIEZO1, PIEZO2, TRPA1, TRPM3, TRPV4, TRPP2 and TREK1 and mouse anti-acetylated α-tubulin for detection of primary cilia axoneme (Table 7) at 4°C overnight. After incubating with secondary antibody, immunoreaction was conducted using a commercially available alkaline phosphatase-anti-alkaline phosphatase kit (Dako REAL™ Detection System, Alkaline phosphatase/red, rabbit/mouse, DakoCytomation GmbH, Hamburg, Germany). Sections were counterstained with Mayer's hematoxylin to observe the nucleus. For negative controls, sections underwent the same immunohistochemical staining procedures but without adding the primary antibody during primary antibody incubation (Suesskind et al., 2012). Slides were finally observed on VHX-S550E microscope (KEYENCE, Japan).

2.1.6 Western Blotting

Tissue and cellular samples were homogenized in cell lysis buffer (cat no. FNN0011, Invitrogen, CA, USA), supplemented with phenylmethylsulfonyl fluoride and a protease inhibitor cocktail (#539134, Calbiochem, San Diego, USA). After homogenized at 13,000 x g (4°C) for 10 minutes, the supernatant was collected for concentration determination by using a BCA protein assay kit (#23227, Pierce, Rockford, USA) and protein analysis. The same amount of protein samples was separated on sodium dodecyl sulfate polyacrylamide gel electrophoresis (SDS-PAGE) gels for protein level analysis. To detect PIEZO1 and TRPM3, 4%–15% SDS-PAGE gels (Mini-PROTEAN® TGX™ Gel, #456-1083, Bio-Rad., CA, USA) were used, whereas 10% SDS-PAGE gels (Mini-PROTEAN® TGX™ Gel, #456-1033, Bio-Rad., CA, USA) were used for PIEZO2, TRPA1, TRPV4, TRPP2 and TREK1 detection. After SDS gel separation, proteins were transferred onto nitrocellulose membranes using a wet transfer technique (150 mA 4 hours for PIEZO1 and TRPM3, 350 mA 1 hour for other proteins). Membranes were blocked by 5% nonfat dry milk for 1 hour and incubated with primary antibodies (PIEZO1, PIEZO2, TRPA1, TRPM3, TRPV4, TRPP2, TREK1, β-actin and GAPDH) (Table 7) at 4°C overnight, respectively. After washing three times with TBST and incubating with the secondary antibody IRDye® 800CW goat anti-rabbit IgG (Table 8)

for 1 hour at RT, membranes were then detected using the Odyssey Imaging system (Li-Cor Bioscience) (Castellani et al., 2014). Positive control was performed using rat kidney tissue.

2.1.7 Serum-starvation of HNPCE cells

To evaluate cilia length, HNPCE cells were treated by serum starvation. Primary HNPCE cell cultures were seeded on Poly-L-Lysine (PLL)-coated cover slips in 24-well plate at a density of 4.0×10^4 cells/well. On the following day, the grown medium of HNPCE cells was changed from 1% serum medium to no serum medium for serum starvation. HNPCE cells were collected and used for immunocytochemistry staining after serum starvation for 24, 48, and 72 hours.

2.1.8 Immunocytochemistry staining

The serum starved HNPCE cells were fixed by 4% paraformaldehyde (PFA) for 15 minutes at RT. Afterwards, cells were permeabilized by 0.2% Triton X-100. Cells were then blocked with 1% BSA/PBS for 1 hour 30 minutes at RT and were incubated with primary antibodies at 4°C overnight. In this step, mouse anti-acetylated α-tubulin and rabbit anti-γ-tubulin (Table 7) were used to detect the primary cilia axoneme and basal body. For co-localization analysis, different MSCs antibodies were co-stained with mouse anti-acetylated α-tubulin (Table 7) to observe the co-localization of MSCs and primary cilia. After incubation with secondary antibodies (Alexa Fluor 488-conjugated goat anti-rabbit IgG and Alexa Fluor 555-conjugated goat anti-mouse IgG) (Table 8) for 1 hour at RT, slides were observed on fluorescent microscope (Zeiss, Germany). Imaging was analyzed with a software of microscope to measure the length of primary cilia.

2.1.9 Electron Microscopy

In order to observe primary cilia, the HNPCE cells were first fixed overnight at 4°C with 2% glutaraldehyde in 0.1M cacodylate buffer (pH 7.4), then fixed with 1% OsO4% in 0.1M

cacodylate buffer at room temperature for 1 hour. After further staining with uranyl acetate and embeding in Epon after dehydration in a graded series of ethanol, ultra-thin cell sections were made and analyzed with a Zeiss 900 electron microscope (Zeiss, Jena, Germany) (Tschulakow et al., 2018).

2.1.10 Total RNA extraction and Reverse Transcription PCR

Total mRNA of rat eye tissues or HNPCE cells were extracted and directly synthesized to cDNA using the Milteny MultiMACS cDNA Synthesis Kits as per the manufacturer's instructions. Synthesized cDNA was stored at -20℃for further analysis. Conventional PCR was performed with Go Taq® Hot Start Polymerase (M5001, Promega, US) in the UNO Cycler PCR system (VWR, UK). The primer sequences used for PCR are shown in Table 9. In total 2µl of undiluted cDNA was used to do PCR in a 25µl reaction volume. The thermocycling conditions were: 5 minutes at 94 °C, 45 cycles of 30 seconds at 94 °C, 30 seconds at 58 °C, and 30 seconds at 72 °C. The final elongation step was 7 minutes at 72 °C. After conventional PCR, the amplicons were resolved on 1.0% agarose gels for electrophoresis. Gels were then detected using the Odyssey Imaging System (Li-Cor Bioscience, USA).

Table 2. Taq polymerase PCR system

5×GreenGoTaq®Buffer	10 µl
Forward Primer (10 pmol/µl)	2 µl
Reverse Primer (10 pmol/µl)	2 µl
dNTP MIX (10mM/µl)	1 µl
GoTaq®DNA polymerase	0.25µl
Template DNA	1 µl
Nuclease free water	up to 50 µl

2.1.11 Quantitative real-time PCR

The cDNA samples were prepared dilution at 1:10 dilution to detect the expression of some human and rat genes, like PIEZO1, PIEZO2, TRPA1, TRPM3, TRPV4, TRPP2 and TREK1, respectively. The qPCR was performed on a CFX Real-Time-System (BIO-RAD, Singapore). The sequences of primers used in study are shown in Table 10 and 11. For

each reaction, 2µl cDNA was used for qPCR analysis. The used quantitative PCR conditions are as following: 10 minutes at 95 °C, 40 cycles of 15 seconds at 95 °C and 1 minute at 60 °C. Melting curve analysis confirmed the specificity of the amplification and the absence of nonspecific amplification and primer dimers. Three replicates were used for each condition. In the analysis of the RNA expression, housekeeping gene Actin was used as a reference gene. We used ΔCT = CT (Target gene) - CT (GAPDH or Rpl32) and ΔΔCT = ΔCT (Samples) - ΔCT (controls) to calculate the ΔCT and ΔΔCT, where CT refers to cycle threshold. We used the formula, change fold = $2^{(-\Delta\Delta CT)}$ to demonstrate the change in RNA expression. Student's t-test was performed to analyze RNA expression changes between experiment and control groups.

Table 3. Quantitative real-time PCR system

Template DNA	5 µl
Forward Primer (10 pmol/µl)	1 µl
Reverse Primer (10 pmol/µl)	1 µl
SsoAdvanced™ Universal SYBR® Green Supermix	10 µl
Nuclease free water	up to 20 µl

2.1.12 siRNA transfection

In order to knock down the expression of TRPP2 or PIEZO2, siRNA studies have to be performed. HNPE cells were seeded on 12-well plate (4×10^4 per well) for 24 hours before transfection. Transfection was done by using Lipofectamine 2000 (Invitrogen) transfection reagent according to instructions from the manufacture. In order to obtain higher transfection efficiency, two different transfection methods were used (Figure 6).

The first transfection method was the method according to the instructions from manufacturer. In brief, 1µl Lipofectamine 2000 and 80pmol siRNA were added into two vials of 100µl Opti-MEM I reduced serum media separately, and incubated for 5 minutes at room temperature. After incubation the siRNA and Lipofectamine 2000 solution were gently mixed and incubated for another 20 minutes at room temperature before added to cultured cells in 12-well plates with 1 ml cell culture medium and incubated for 4 hours at 37°C.

The second method is modified Lipofectamine 2000_optimized protocol according to the literature (Avci-Adali et al., 2014). The transfection mixture was prepared by adding 1µl Lipofectamine 2000 and 80pmol siRNA into 500µl Opti-MEM I reduced serum media. After 20 minutes at room temperature, the mixture was directly added to the adherent growing cells which were washed once with 1ml of DPBS in advance and incubated for 4 hours at 37°C.

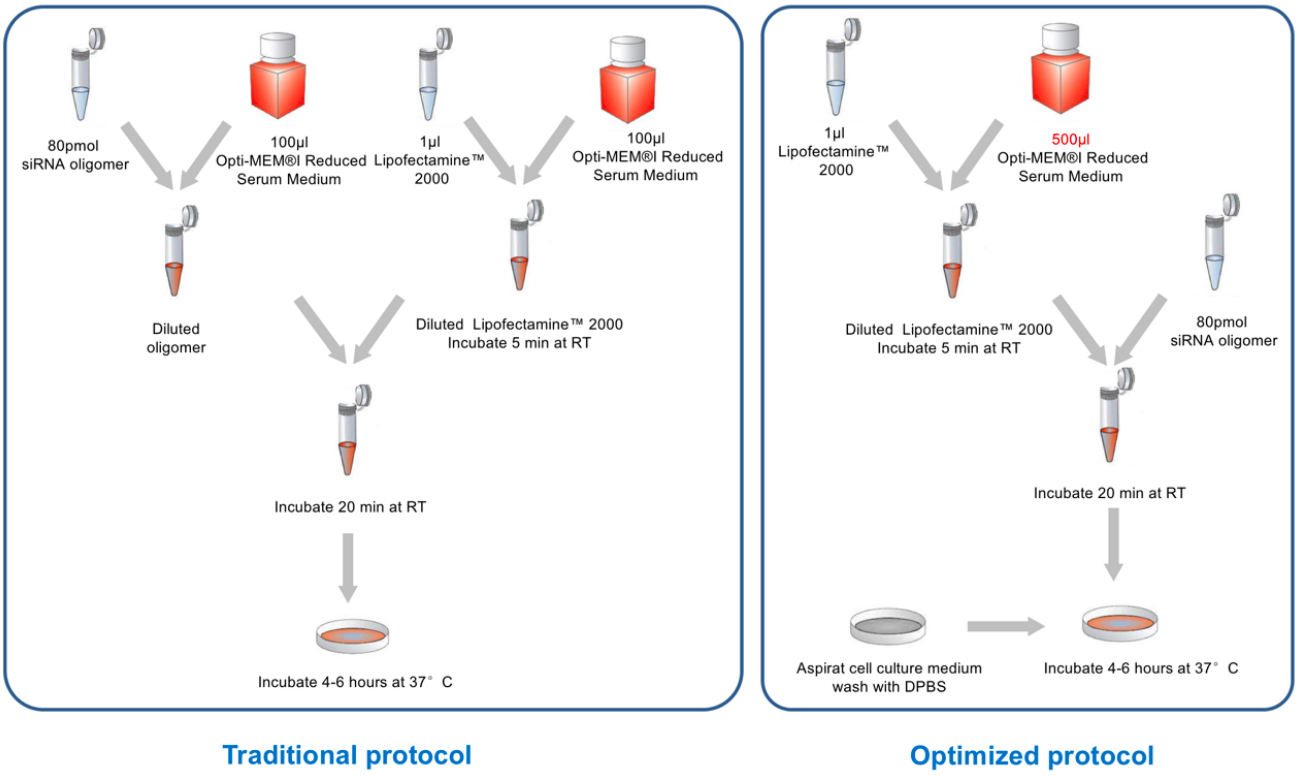

Figure 6. Two transfection methods protocol

2.1.13 Hydrostatic pressure model

To study the effect of pressure on cellular changes in the HNPCE cells, a modified hydrostatic pressure chamber was developed based on the chamber used in the report of Ishikawa et al (Ishikawa et al., 2014) (Figure 7). Briefly, the cells were grown on the bottom side of PLL-coated T-75 flasks. The flask was sealed by a cap connected with a long tube (Corning, cat no. 3282, USA). The flask and the tube were all filled with cell culture medium to produce pressure upon cells, and flasks were incubated in a water bath at 37 °C. In this experiment, the height of medium was set at 79.8cm, which could produce a pressure

similar to the IOP of human acute glaucoma attack (60 mmHg) and thus mimic the normal IOP circumstance. For further experiments, cells were collected at different time points after incubation at the high-pressure.

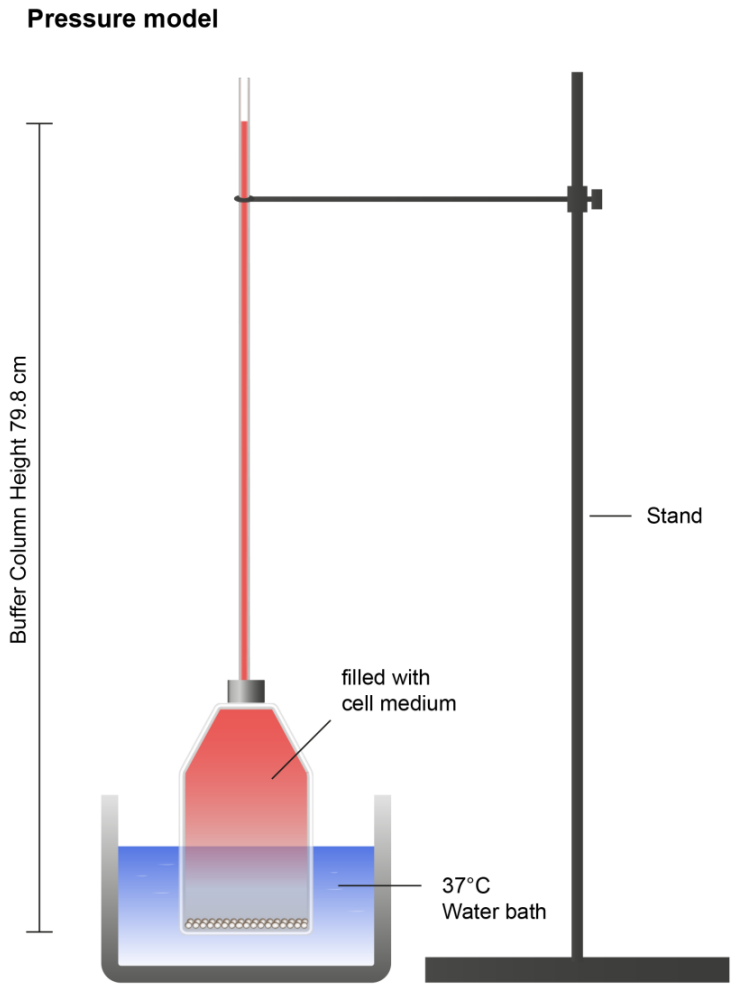

Figure 7. Schematic diagram of Hydrostatic pressure model

To investigate the interaction between putative MSCs on the HNPCE in sensing an increased IOP, the difference in expression of putative MSCs were compared to TRPP2/PIEZO2 siRNA groups and control siRNA under a high pressure at 60mmHg for 24 hours by using the hydrostatic pressure model (Table 4).

Table 4. List of different Group

Group 1	Group 2	Group 3	Group 4
Control siRNA		TRPP2/PIEZO2 siRNA	
NAP	60mmHg, 24h	NAP	60mmHg, 24h

2.1.14 Statistical analyses

Data was presented as the mean ± standard error of the means (SEMs). Statistical comparisons were calculated by using unpaired Student's t-test under SPSS Statistics (Version 26.0) software (IBM, Armonk, NY, USA). A p value ≤0.05 was considered as statistically significant.

2.2 Materials

2.2.1 Materials

Table 5. List of materials

Product	Manufacturer, Place of origin
15 ml, 50ml falcon tube	Falcon, Corning Inc., USA
6 well, 12 well, 96 wells Transparent plate	Falcon, BD Biosciences, USA
Cell scraper	Corning Inc. #3010, Mexico
Eppendorf tubes (different sizes, plastic or glass)	Eppendorf AG, Germany
Filling screwcap with tubing	Corning® # 3282, USA
Glass slides	Superfrost plus, R. Langenbrinck, Germany
G25 needle	Sterican® Safety, B.Braun, Germany
Multi-8 Filter (12x8 Reaktionen)	Miltenyi Biotec #130-092-546, Germany
Nitrocellulose Blotting Membrane	Amersham #10600001, Germany
Precast Protein Gels,	Mini-PROTEAN® TGX™ #4561034/ 4561084, BIO-RAD, USA
T25, T75, T175 cell culture flask	CELLSTAR®, Germany

2.2.2 Chemicals

Table 6. List of chemicals

Product	Manufacturer, Place of origin
BCA Protein Assay Kit	PIERCE #23227, Thermo SCIENTIFIC, USA
Bovine serum albumin	SIGMA #A8806-5G, USA
β-Mercaptoethanol	SIGMA #M3148-25ml, USA
Cell extraction buffer	Invitrogen # FNN0011, USA
Citric Acid	SIGMA #251275-500G, Germany
Dako Real Antibody Diluent	DakoCytomation GmbH, #S3022, Germany
Dako REAL™ Detection System, Alkaline phosphatase/red, rabbit/mouse	DakoCytomation GmbH, Germany
DAPI (4'6-diamidine-2'phenylinodole dihydrochloride)	Sigma Aldrich #1246530100, USA
Dulbecco's Modified Eagle Medium (DMEM)	Gibco # 31885-023, Germany
Dulbecco' s Phosphate Buffered Saline (PBS)	SIGMA #D8537-500 ml, Germany
Epithelial cell medium	ScienCell Research Laboratories #4101, USA
Ethanol	SAV-LIQUID PRODUCTION GMBH, #ETO-5000-99-1, Germany
Fetal bovine serum	Gibco #10082-147, USA
FluorSave™ Reagent	Merck Millipore #345789, Germany
Glycin	Carl Roth #3187.3, Germany
Go Taq® Hot Start Polymerase	Promega #M5001, USA
Hematoxylin	Sigma Aldrich #HHS32-1L, USA
Hydrochloric acid 25%	Merck Millipore #100316, Germany
Lipofectamine™ 2000	Invitrogen #11668-027, USA
liquid nitrogen	WestfalenGas, Germany
Methanol	Honeywell #32213-2.5L, France
MultiMACS ™ cDNA Sythesis Kit (12x8)	Miltenyi Biotec #130-094-410, Germany
Mounting medium	Sigma Aldrich #03989-500ml, Germany
Opti-MEM® I Reduced-Serum Medium	Gibco #31985, Germany

PBS	Merck Millipore #L1825, Germany
PFA (paraformaldehyde)	Merck #104005, Germany
Phenylmethylsulfonylfluorid(PMSF)	Carl Roth #6367.4, Germany
Poly-L-lysine(PLL) solution	SIGMA #P4707, USA
Powdered milk	Carl Roth #T145.3, Germany
Precision Plus Protein Standards Kaleidoscope	BIO-RAD#161-0375, USA
Protease Inhibitor Cocktail Set III	Calbiochem # 539134, Germany
SDS (sodium dodecyl sulfate)	Carl Roth #2326.2, Germany
Sodium chloride	VWR CHEMICALS #27.810.295, Germany
Sodium Citrate dihydrate	Merck Millipore #106448, Germany
SsoAdvanced™ Universal SYBR® Green Supermix	BIO-RAD #1725270, USA
Tissue-Tek O.C.T.Compound	Sakura Finetek #4583, Netherlands
TRIS (Tris-(hydroxymethyl)-aminomethan)-base	Sigma Aldrich, #T1503-1KG, Germany
Triton X-100	Sigma#9002-93-1, USA
Tween 20	Serva #39796.01, Germany
Xylene	VWR CHEMICALS #28975.325, France

2.2.3 Solutions

- TBS(10×)

  For 1 L:

  60.75 g TrisBase

  87.66 g NaCl

  900 ml Millipore water

Adjust the pH to 7.6 by adding 25% HCL and make up the volume to 1L using Millipore water. Store at 4°C.

- TBS(1×)-Tween(0.1%)

Dilute 100L TBS stock solution by adding 900 ml Millipore water to make one liter of 1×TBS buffer solution. 1 ml of tween 20 was pipetted with a pipette. Due to the high viscosity of the tween, the pipette at the tip were cut off to enlarge the free end.

- 5% BSA / TBS

  For 100mL:

  5 g BSA

  100 mL 1×TBS

- 1% BSA / PBS

  For 100mL:

  1 g BSA

  100 mL 1×PBS

- Permeabilization Buffer (1X PBS/0.2% Triton X-100)

  For 25 mL:

  50 µl Triton X-100

  25 mL 1×PBS

- 4% paraformaldehyde (PFA)

  For 1L:

  40 g paraformaldehyde

  1 L 1×PBS

Mixed with a magnetic stirrer at 50°C overnight. Stored in aliquots at −20°C. For safety reason, the process was done under a ventilated fume hood.

- 20%SDS

  For 500 mL:

  20 g SDS

Add Millipore water to 500 ml. Because SDS powder is hazardous, the solution was prepared under a ventilated fume hood. Stored at room temperature.

- Sodium citrate buffer(10×)

  For 1 L:

  24.096 g Sodium Citrate dihydrate

  3.471 g Citric Acid

800 ml Millipore water

Solution was adjusted to final desired pH 6.0 using 25% HCL. Millipore water was added until volume was 1 L. For 1 L 1× sodium citrate buffer solution, 100 ml 10 × sodium citrate buffer was diluted by adding 900 ml Millipore water. Stored at 4°C

- Running buffer(10×)

  For 500 mL:

  15 g TrisBase

  72 g Glycin

  5 g SDS

Add Millipore water to 500 ml. Because SDS powder is hazardous, the solution was prepared under a ventilated fume hood. Stored at 4°C.

- WB Transfer buffer

  For 1 L:

  3 g TrisBase

  14.4 g Glycin

  200 ml (pre-cold) methonal

  250 µl 20% SDS

Add Millipore water to 1L.

2.2.4 Animals and eyes

Wildtype female Sprague–Dawley rats (12 weeks old), Transgenic Facility Tübingen (University of Tübingen), Germany.

Choroidal melanoma with a normal anterior segment Human eyes (University of Tübingen, no. 38072, 38282, 38375), Pathology lab at the University Eye Hospital, Tübingen, Germany.

2.2.5 Cells

Primary Human Non-Pigmented Ciliary Epithelial Cells, ScienCell Research Laboratories #6580, USA.

2.2.6 Antibodies

All antibodies used in the research are listed in the following:

Table 7. List of Used Primary Antibodies

Antibody	Source	Detection	Dilution
rabbit anti-PIEZO1	Proteintech (Manchester, UK), 15939-1-AP	PIEZO1	IF (1:200), IHC (1:800), WB (1:500), ICC (1:100)
rabbit anti-PIEZO2	Aviva Systems Biology (San Diego, USA), ARP49683_P050	PIEZO2	IF (1:400), IHC (1:1000), WB (1:500), ICC (1:100)
rabbit anti-TRPA1	Novus Biologicals (Abingdon, UK), NB110-40763	TRPA1	IF (1:100), IHC (1:400), WB (1:500), ICC (1:200)
rabbit anti-TRPM3	Abcam (Cambridge, UK), ab56171	TRPM3	IF (1:100), IHC (1:800), WB (1:800), ICC (1:100)
rabbit anti-TRPV4	Alomone Labs (Jerusalem, Israel), ACC-034	TRPV4	IF (1:100), IHC (1:800), WB (1:500), ICC (1:100)
rabbit anti-TRPP2	Proteintech (Manchester, UK), 19126-1-AP	TRPP2	IF (1:200), IHC (1:400), WB (1:300), ICC (1:100)
rabbit anti-TREK1	Abcam (Cambridge, UK), ab83932	TREK1	IF (1:300), IHC (1:1000), WB (1:500), ICC (1:100)
mouse anti-acetylated α-tubulin	Sigma-Aldrich (St.Louis, USA), T7451	primary cilia axoneme	IHC (1:100), ICC (1:200)
rabbit anti-γ-tubulin	BioLegend (San Diego, USA), 620901	primary cilia basal body	ICC (1:200)
mouse anti-Brn3a	Santa Cruz Biotechnology (Heidelberg, Germany), sc-8429	RGC	IF(1:50)
Jacalin-FITC	EY Laboratories (San Mateo, USA), F-6301-2	NPE cells	IF (1:100)
Rabbit anti-β-actin	Cell Signaling Technology (Danvers, USA), 4970	β-actin	WB (1:1000)
rabbit anti-GAPDH	Cell Signaling Technology (Danvers, USA), 2118	GAPDH	WB (1:1000)

IF, immunofluorescence; IHC, immunohistochemistry; WB, western blot; ICC, immunocytochemistry; RGC, retinal ganglion cell; NPE, non-pigmented ciliary epithelium.

Table 8. List of Used Secondary Antibodies

Antibody	Source	Dilution
Alexa Fluor 555-conjugated donkey anti-rabbit IgG	Abcam (Cambridge, UK), ab150074	IF (1:2000)
Alexa Fluor 488-conjugated goat anti-rabbit IgG	Thermo Fisher Scientific (Waltham, USA), A-11008	IF (1:2000)
Alexa Fluor 555-conjugated goat anti-mouse IgG	Thermo Fisher Scientific (Waltham, USA), A-21422	IF (1:2000)

IRDye® 800CW goat anti-rabbit IgG	Li-Cor Biosciences Inc. (Lincoln, USA), 926-32211	WB (1:15,000)

2.2.7 Primers

Primers were designed for *TRPP2* by using NCBI's Primer-BLAST and were purchased from Biomers.net (Ulm, Germany). All primers used for reverse transcription PCR and quantitative real-time PCR are listed in the following:

Table 9. Reverse Transcription PCR primers for TRPP2

Oligo name		**sequence**(5' -.....-3')
hTRPP2	**F**	TCGACAAGATCTCAAAGGGA
	R	GTCTCACCAGGACTTGAAAC
rTRPP2	**F**	AGGACCTAGACTTGGAACAC
	R	GTGGATCTCACTATCCCGAC

Table 10. Quantitative real-time PCR primers for rat

Oligo name		**sequence**(5' -.....-3')
PIEZO1	**F**	TTTATCATCAAGTGCAGCCG
	R	AAGAGGATGATGAGACCTCC
PIEZO2	**F**	TTCAATGACAAAGTCAGCCC
	R	GAATTCGCGAACAAACTTCC
TRPA1	**F**	ATGCAAGAAACACGACAAGA
	R	CCAAAAGAGAAGTGAGGTCC
TRPM3	**F**	CCGCTTCAATTCATCCAATG
	R	TCTCTCATTGACTTCCTCCAG
TRPV4	**F**	AGATCTACCAGTACTATGGCTT
	R	ATCTGTGCCTGAGTTCTTGTT
TRPP1	**F**	CGTCCATGGGAACCAGTCTA
	R	TGTGCTCTGAGCTAGAAGG
TRPP2	**F**	TGAAGAGGCGAGAGGTGTTA
	R	TCCCTGTGGATCTCACTATC
TREK1	**F**	TGGCTACGGGTGATATCTAA
	R	TCCTTGTTTCCTTGAACTCG
Actin	**F**	AGAAGGAGATTACCCTG
	R	CCACCAATCACAGAGTA

Table 11. Quantitative real-time PCR primers for human

Oligo name		sequence(5' -.....-3')
PIEZO1	F	TCATCATCAAATGCAGCCGA
	R	CATGCCGTACTTGACGATCT
PIEZO2	F	TATGTGAAAGCACCTAGTGA
	R	TCTCTGGACAAAATGATGGT
TRPA1	F	AATCCACCATCGTGTATCCC
	R	CTTGTCTTATTTCCCCAGTGC
TRPM3	F	GATGAGAGGATACGGGTGAC
	R	TTCATGGAGTGCTCTCTCTC
TRPV4	F	TTATGGCTTCTCGCATACCG
	R	GGGTTCGAGTTCTTGTTCAG
TRPP1	F	CTCTCGCTGCCTCTGCTC
	R	CTTCCCTGTGCCAAGTACG
TRPP2	F	CAAACTGAAGAGGAGGGAGG
	R	TACTAGCCGTTCCATCTGTT
TREK1	F	GAGATTGGCTCCGAGTGATA
	R	TCTTTGAATTCGGCTGTGAC
Actin	F	TCCCTGGAGAAGAGCTACGA
	R	AGGAAGGAAGGCTGGAAGAG

2.2.8 siRNA

All siRNA used in this study were modified by adding AlexaFluor488 at 3', which will present green fluorescence under fluorescence microscope if the cells were transfected successfully. All siRNA were purchased from QIAGEN (Hilgen, Germany). The target sequences of each siRNA are listed in the following table:

Table 12. List of Used siRNA

Product name		Catalog no.	Target sequence
TRPP2	Hs_PKD2_3	SI00006489	CTCGACAATCAAGAATGTTAT
	Hs_PKD2_4	SI00006496	TTGCTAATCTTCTGCATTTA
	Hs_PKD2_5	SI03050446	ATGGAACGGCTAGTACGTGAA
PIEZO2	Hs_FAM38B_1	SI00383677	CACCTAGTGATTCTAACTCAA
	Hs_FAM38B_5	SI04148515	CAAGAGCTACAATTACGTCAA
	Hs_FAM38B_6	SI04261411	TAGCGCCGTGACTGACGTGTA
	Hs_FAM38B_7	SI04321688	TTCGACGGAAATGGTTTGTTT
AllStars Neg. Control siRNA		1027281	-

2.2.9 Machines and software

Table 13. List of machines and software

Product	Type	Manufacturer, Place of origin
Blotting chamber	MP Tetra Ready Gels / Mini Trans-Blot	BIO-RAD, Singapore
Centrifuge	IKA mini G	IKA, Germany
Centrifuge	MEGA STAR 3.0 R	VWR, Germany
Centrifuge	Heraeus Megafuge 8R	Thermo SCIENTIFIC, Germany
Cryostat	Leica CM 1950	LEICA, Germany
Cycler	CFX96 Real-Time-System	BIO-RAD, Singapore
Fluorescent microscope	Axioplane2 imaging®, Germany with Openlab software	Zeiss, Improvision, Germany
Imaging system	Odyssey® FC	LI-COR, USA
Incubator	HERACELL150i	ThermoSCIENTIFIC, Germany
Magnetic stirrer	IKA lab disc	IKA,Germany
Microplate Reader	Infinite 200 PRO NanoQuant	Tecan, Austria
Microscope	Axio Observer	Zeiss, Germany
MultiMAS Separation Unit	MultiMACS™ M96	MACS, USA
pH Meter	pH 211 Microprocessor	HANNA instrumentals, Germany
Power Supply	PowerPac HC	BIO-RAD, Singapore
Rocking shaker	ST5	CAT, Germany
Stereomicroscope	Stemi 2000-C	Zeiss, Germany
Sterile workbench	MSC-ADVANTAGE	Thermo SCIENTIFIC, Germany
Thermomixer	Thermomixer comfort	Eppendorf, Germany
Ultrapure water system	GenPure Pro UV/UF	Thermo SCIENTIFIC, Germany
UNO Cycler PCR system	VWRI732-1200	VWR, UK
Vortex mixer	Vortex 4 basic	IKA, Germany
Water bath	VWB 18	VWR, Germany
Weight scale	EW 3000-2M	Kern, Germany

3. Results

3.1 Expression and localization of MSCs candidates in eye tissue

3.1.1 Expression and localization of PIEZO family in eye tissues

3.1.1.1 PIEZO1

Using immunofluorescence staining, cells positive for PIEZO1 were identified in the retina, CB and cornea of the rat. In the retina, rat eye sections were double-labeled with PIEZO1 and Brn3a (brain-specific homeobox/POU domain protein 3A), a specific marker for retinal ganglion cells (RGCs) (Nadal-Nicolas et al., 2009). Highly immunoreactivity of PIEZO1 was detected in the ganglion cell layer (GCL) and inner nuclear layer (INL), while weak immunoreactivity was seen in inner plexiform layer (IPL), outer plexiform layer (OPL), outer nuclear layer (ONL) and photoreceptor layer (PL) of rods and cones. PIEZO1 was mainly located in cytoplasm of RGCs. In CB, anti-Jacalin antibody, a marker of ciliary NPE cells, was used to characterize the localization of PIEZO1 in the CB (Hu et al., 2011). PIEZO1 protein appeared abundantly expressed in NPE and PE. The expression of PIEZO1 was also observed in the epithelium of cornea (Figure 8).

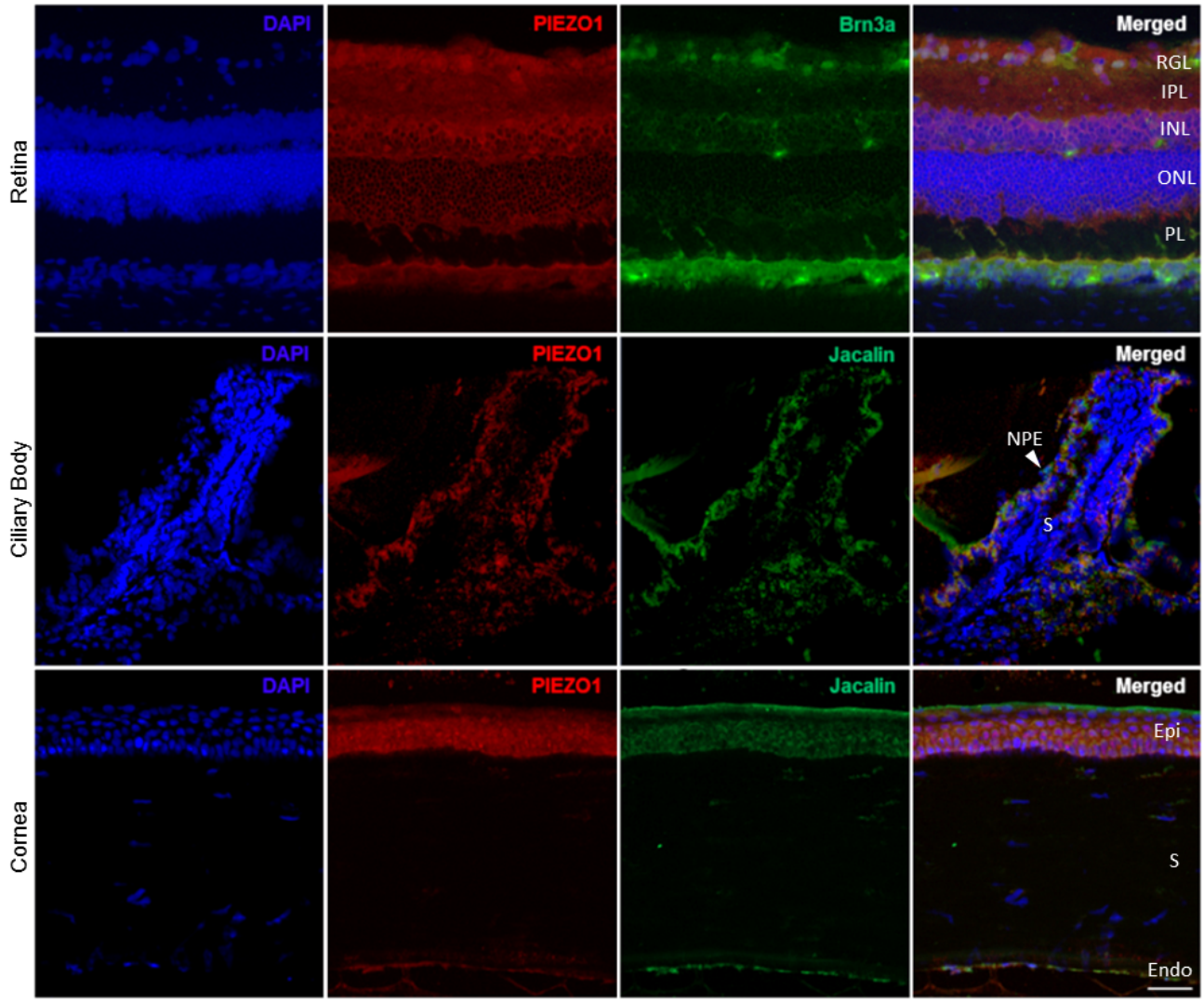

Figure 8. Localization of PIEZO1 in rat eye tissue. PIEZO1 was found distributed in the rat retina, ciliary body and cornea. PIEZO1 antibody (red); Brn3a antibody (green); Jacalin-FITC (green); DAPI (blue). Scale bar: 50μm, n > 20 sections. GCL, ganglion cell layer; IPL, inner plexiform layer; INL, inner nuclear layer; ONL, outer nuclear layer; PL, and photoreceptor layer; NPE, non-pigmented epithelium; Epi, epithelium; Endo, endothelium; S, stroma.

Western blot analysis showed a protein of ~230 kDa (the expected molecular weight for full length PIEZO1) in all eye tissues with a positive signal in immunohistology. The quantitative analysis of the expression of PIEZO1 in different eye tissue showed by comparing its expression in rat kidney tissues. PIEZO1 is highly expressed in CB (3.37 ± 0.32), cornea (5.91 ± 1.56), sclera (9.71 ± 2.04) and ON (3.69 ± 1.28), but weakly expressed in retina (1.37 ± 0.33) and lens (2.00 ± 0.52) (the protein level of PIEZO1 in rat kidney tissue was set as 1) (Figure 9A and 9B). Quantitative RT-PCR detected high

expression of PIEZO1 mRNA in the CB (2.00 ± 0. 65) and sclera (3.60 ± 1.16), but moderately expressed in retina (1.29 ± 0.58), cornea (0.81 ± 0.11) and ON (1.20 ± 0.17) (The expression level of PIEZO1 in the lysate of all the tissues was set as 1 during the comparison) (Figure 9C).

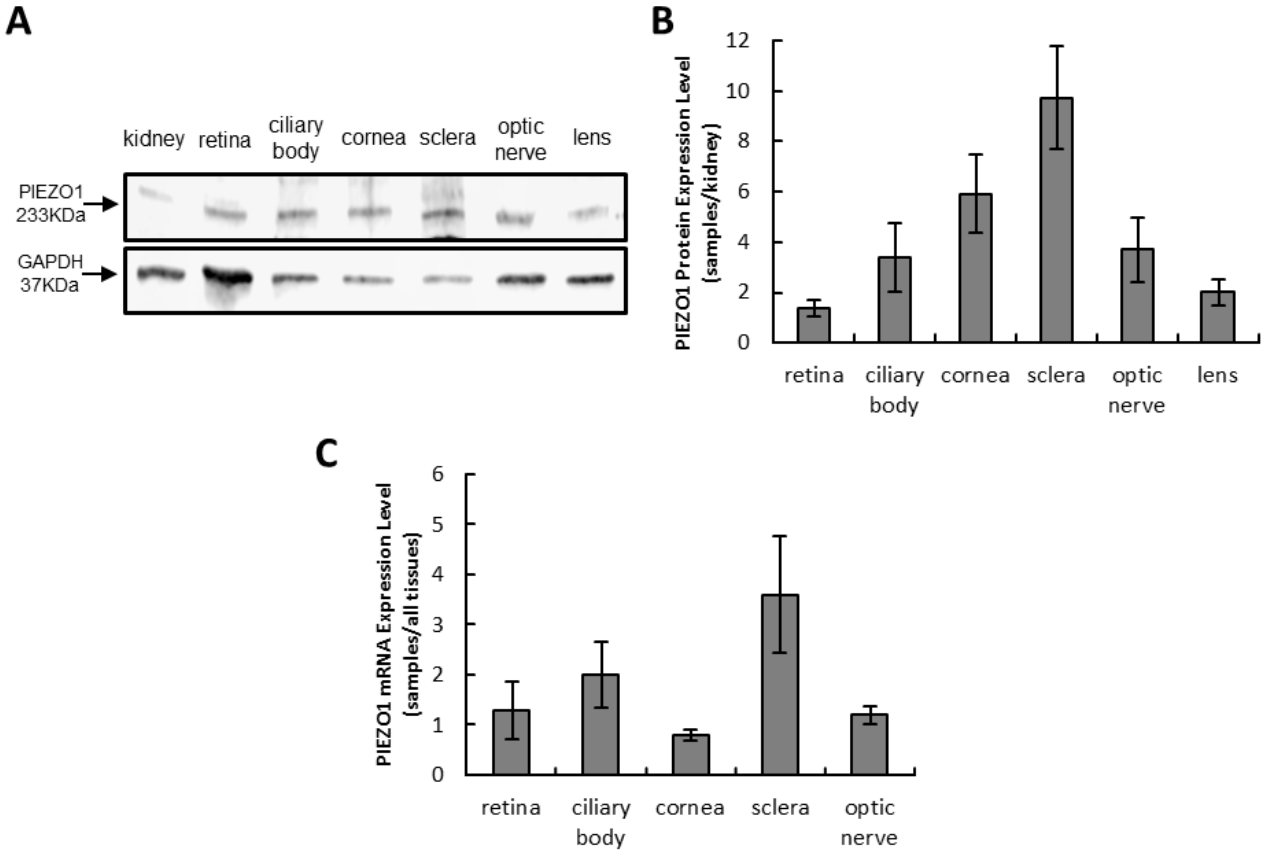

Figure 9. Localization of PIEZO1 in rat eye tissue. (A) Western blot analysis showed the protein expression level of PIEZO1 in different tissues of a rat eye(n=3). (B) Quantitative analysis of three different forms of PIEZO1 protein in different tissue. The expression of PIEZO1 was normalized to GAPDH. (C) Quantitative real-time PCR demonstrated the mRNA expression level of PIEZO1 in different tissues of rat eye. Three replications were done (n=3).

The expression of PIEZO1 in non-pigmented as well as pigmented cells of human CB (Figure.10A) was observed. In agreement with the result of immunohistochemistry staining of human ciliary body, both the results of western blot (Figure.10B) and PCR (Figure.10C) proved the expression of PIEZO1 in HNPCE. Reverse transcription PCR showed a 209bp band represents the PCR product of PIEZO1 (Figure.10C).

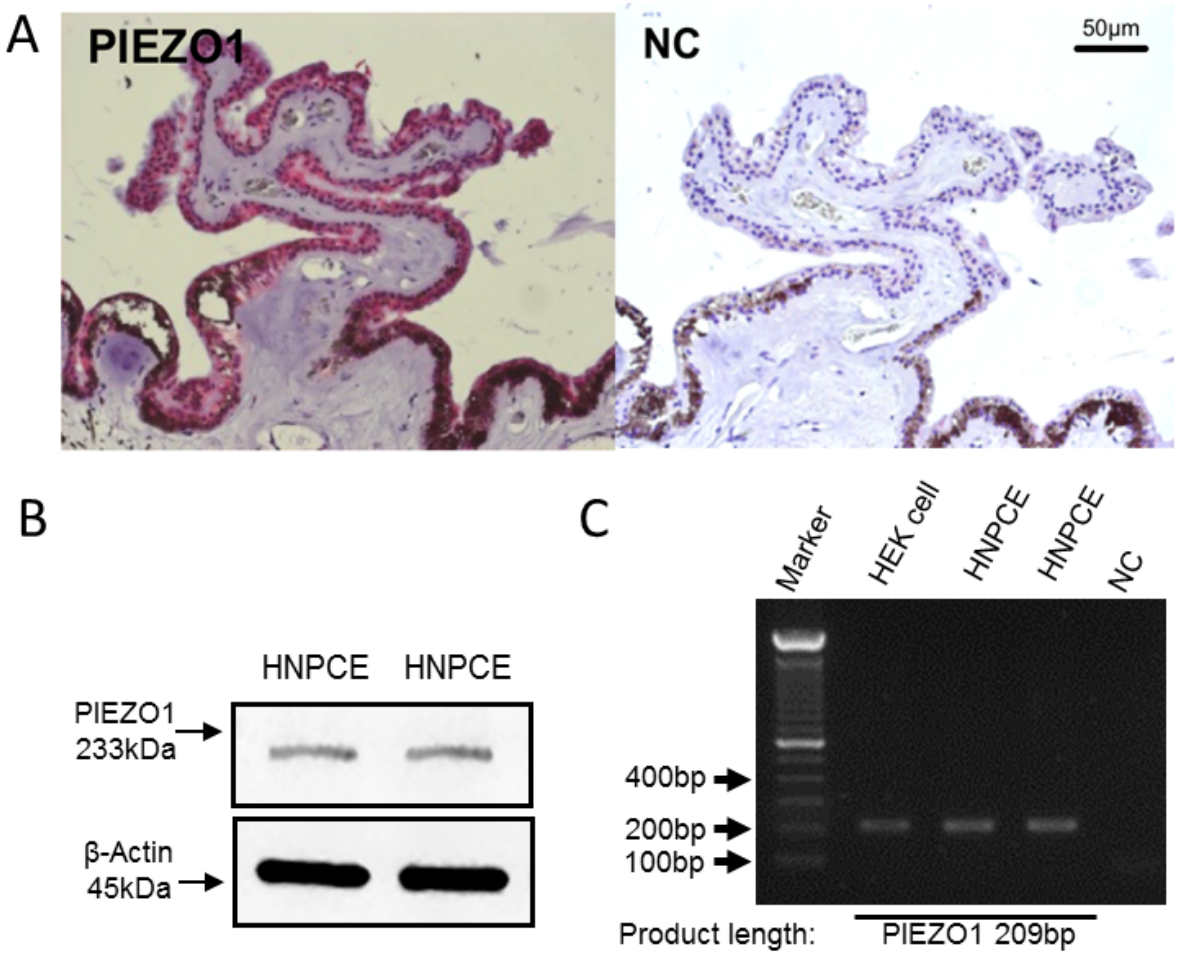

Figure 10. The expression of PIEZO1 in human ciliary body and HNPCE cells. (A) PIEZO1 is expressed in the human ciliary body epithelium. PIEZO1 antibody (red); nuclei (blue). Scale bar: 50μm (n=3). (B) Western blot analysis showed the expression of PIEZO1 in HNPCE cells, β-actin was used as loading control. (C) PIEZO1 mRNA expression was detected by reverse transcript PCR.

3.1.1.2 PIEZO2

Similar to PIEZO1, positive PIEZO2 staining was also observed in rat retina, CB and cornea. Similar to the expression of PIEZO1, PIEZO2 antibody was observed broadly expressed in different layers of retina, including IPL, IN L, OPL, ONL and PL, while the highest immunoreactivity was observed in cytoplasm of RGCs. PIEZO2 protein was also observed predominantly expressed NPE and PE of CB. The epithelium of cornea expressed PIEZO2 as well (Figure.11).

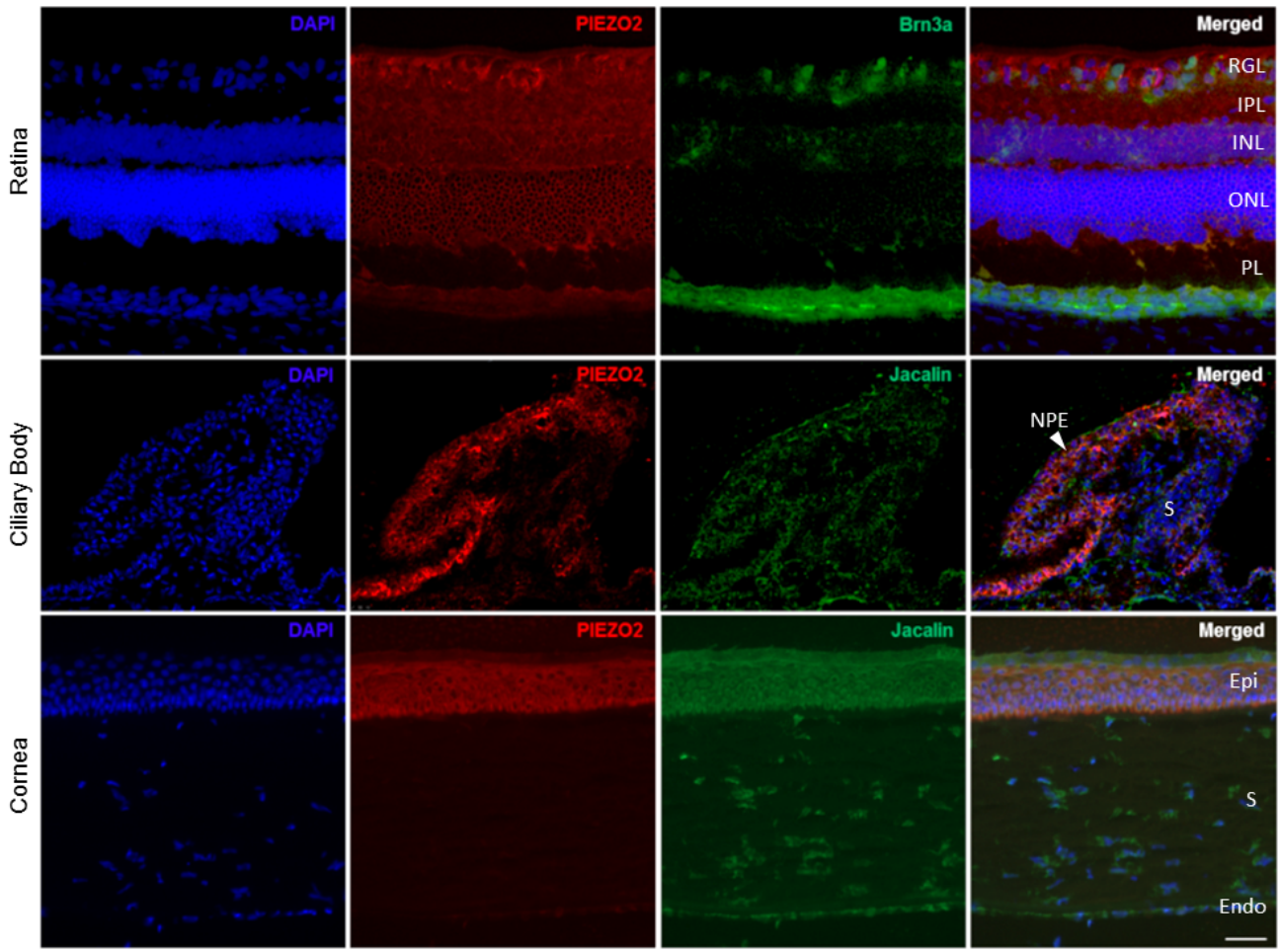

Figure 11. Localization of PIEZO2 in rat eye tissue. PIEZO2 was found distributed in the rat retina, ciliary body and cornea. PIEZO2 antibody (red); Brn3a antibody (green); Jacalin-FITC (green); DAPI (blue). Scale bar: 50μm, n > 20 sections. GCL, ganglion cell layer; IPL, inner plexiform layer; INL, inner nuclear layer; ONL, outer nuclear layer; PL, and photoreceptor layer; NPE, non-pigmented epithelium; Epi, epithelium; Endo, endothelium; S, stroma.

Further western blot analysis using anti-PIEZO2 antibody showed a clear ~80kDa band (the same as expected molecular weight for full length PIEZO2) in both kidney tissue lysate and ocular tissue lysate. The expression level of PIEZO2 in different eye tissue was calculated by using kidney cell lysate as a reference control. The highest expression of PIEZO2 was in CB (0.08 ± 0.01) (PIEZO2 CB / PIEZO2 kidney). Relative lower expression level as found in retina (0.04 ± 0.01), cornea (0.02 ± 0.00), and sclera (0.02 ± 0.00), while ON showed the lowest expression of PIEZO2 with the exception of the lens, where no PIEZO2 expression was detected (Figure 12A and 12B). RT-PCR analysis results high PIEZO2 mRNA level in the CB (20.46 ± 5.73) and sclera (311.20 ± 3.56), when using

PIEZO2 mRNA level in all the tissues lysate as reference control. A lower PIEZO2 mRNA level was observed in retina (3.42 ± 1.30), ON (3.36 ± 1.38) and cornea (0.42 ± 0.09) (Figure 12C).

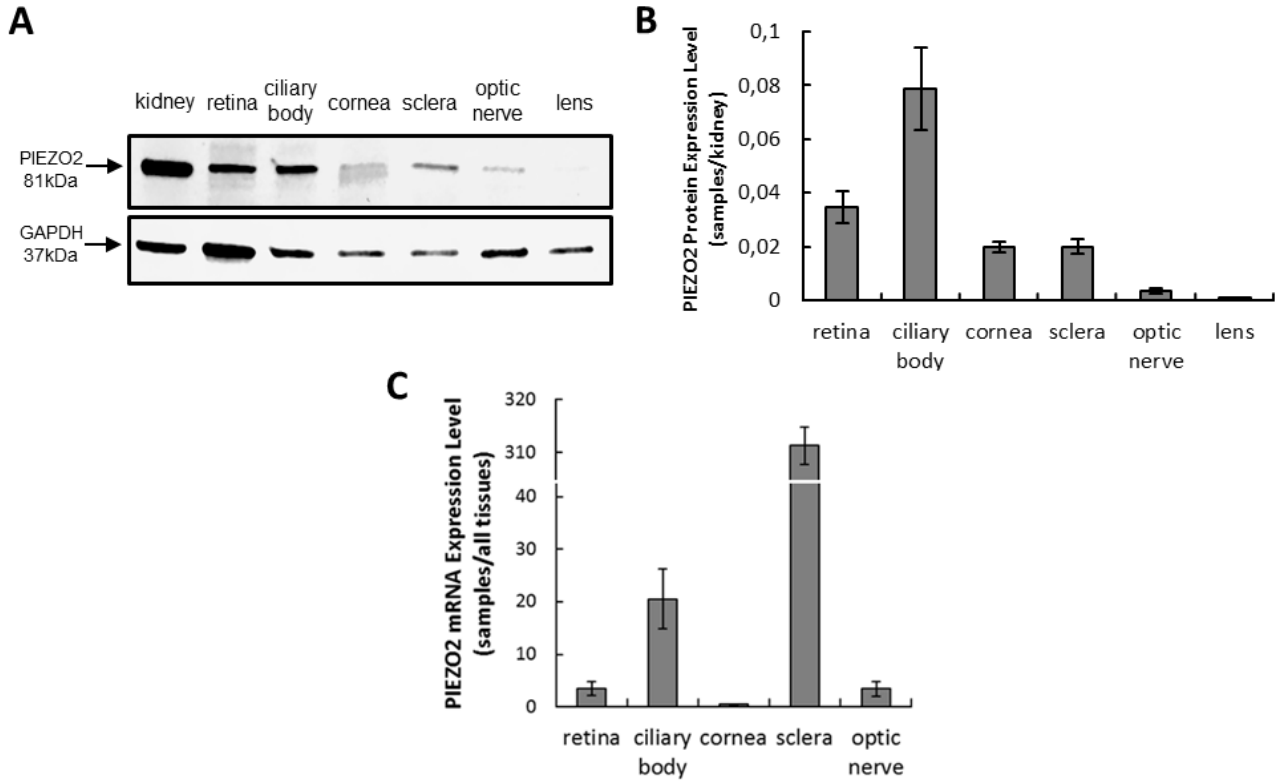

Figure 12. Localization of PIEZO2 in rat eye tissue. (A) Western blot analysis showed the protein expression level of PIEZO2 in different tissues of a rat eye(n=3). (B) Quantitative analysis of three different forms of PIEZO2 protein in different tissue. The expression of PIEZO2 was normalized to GAPDH. (C) Quantitative real-time PCR demonstrated the mRNA expression level of PIEZO2 in different tissues of rat eye. Three replications were done (n=3).

Immunohistochemistry staining showed the expression of PIEZO2 in non-pigmented as well as pigmented cells of the human eye (Figure 13A). In agreement with the results of immunohistochemistry staining of human ciliary body, western blot (Figure 13B) and PCR (Figure 13C), all confirmed the expression of PIEZO2 in HNPCE. Reverse transcription PCR showed a 422bp band which represents the PCR product of PIEZO2 (Figure 13C).

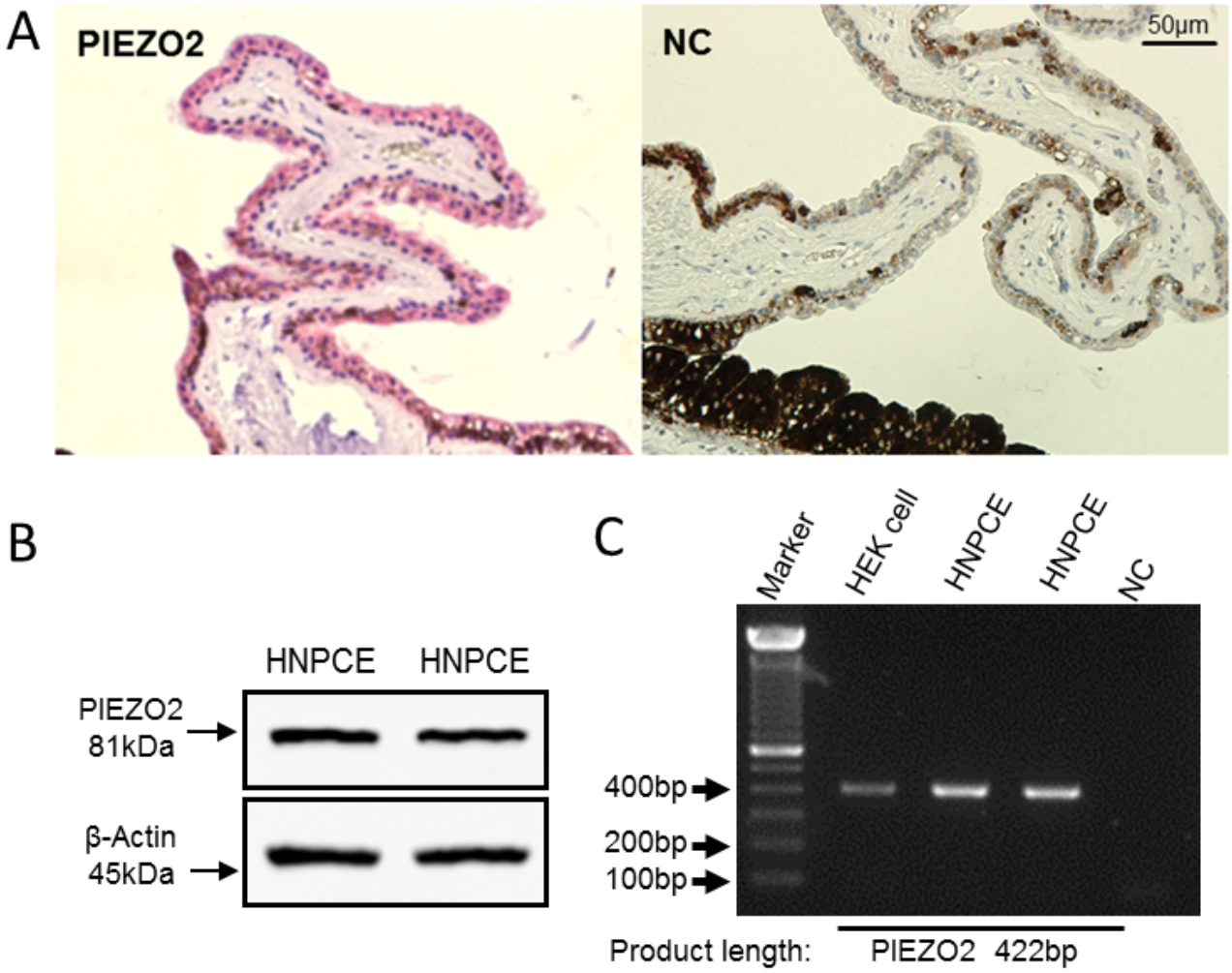

Figure 13. The expression of PIEZO2 in human ciliary body and HNPCE cells. (A) PIEZO2 is expressed in the human ciliary body epithelium. PIEZO2 antibody (red); nuclei (blue). Scale bar: 50μm (n=3). (B) Western blot analysis showed the expression of PIEZO2 in HNPCE cells, β-actin was used as loading control. (C) PIEZO1 mRNA expression was detected by reverse transcript PCR.

3.1.2 Expression and localization of TRP family candidates in eye tissues

3.1.2.1 TRPA1

Immunofluorescence staining showed positive TRPA1 signal in the rat retina, CB and cornea. In the retina, TRPA1 signal was higher in GCL, INL and ONL, but weak in IPL, OPL, and PL. TRPA1 was mainly located in cytoplasm of RGCs. TRPA1 protein expressed highly in NPE and PE of CB compared to other cells in CB. The epithelium of cornea has TRPA1 expression as well (Figure 14).

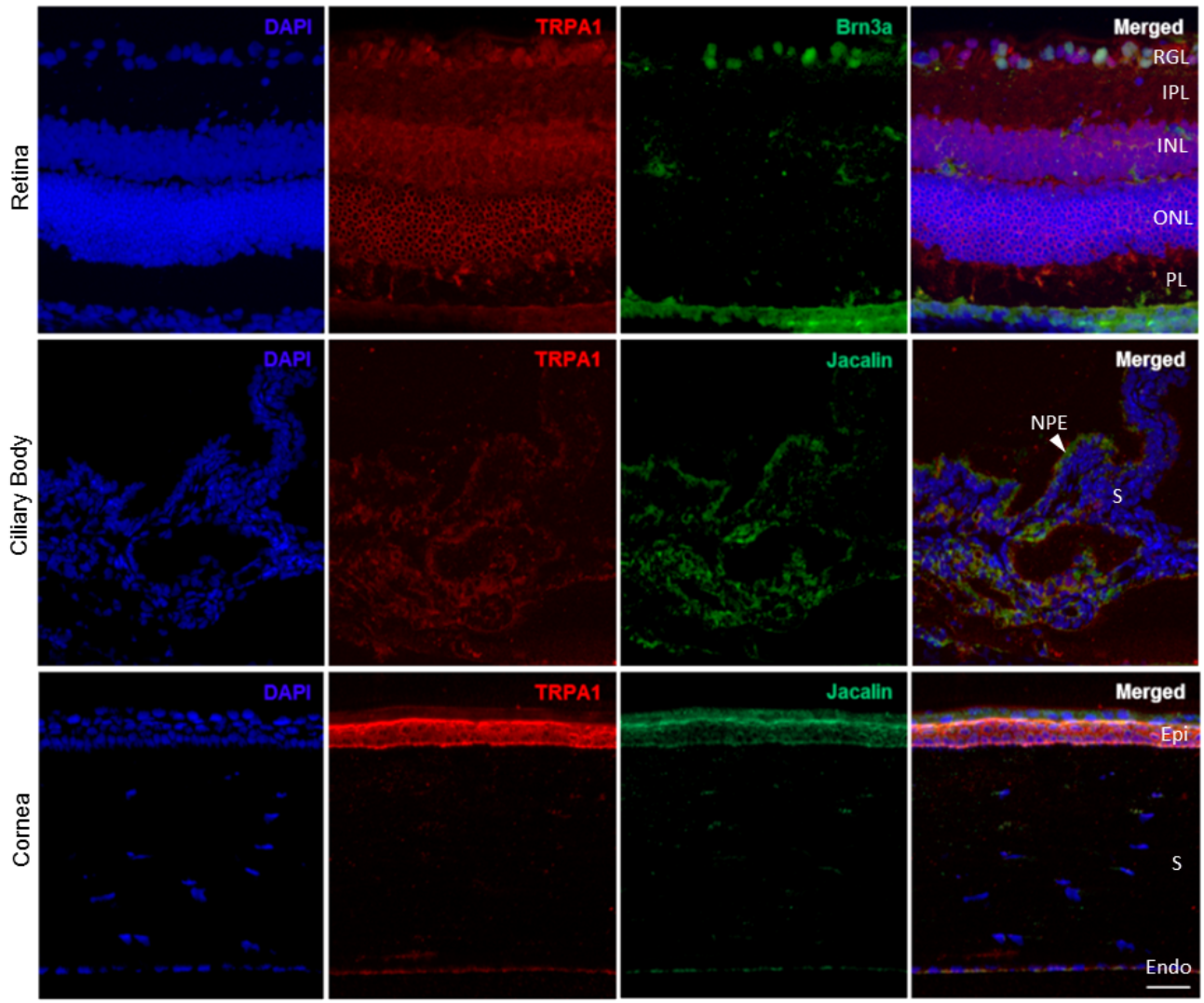

Figure 14. Localization of TRPA1 in rat eye tissue. TRPA1 was found distributed in the rat retina, ciliary body and cornea. TRPA1 antibody (red); Brn3a antibody (green); Jacalin-FITC (green); DAPI (blue). Scale bar: 50μm, n > 20 sections. GCL, ganglion cell layer; IPL, inner plexiform layer; INL, inner nuclear layer; ONL, outer nuclear layer; PL, and photoreceptor layer; NPE, non-pigmented epithelium; Epi, epithelium; Endo, endothelium; S, stroma.

Western blot analysis revealed three different TRPA1 bands. The largest band (~250kDa) is the dimer form of TRPA1, while the 150kDa and 130kDa bands represent two different isoforms of TRPA1 proteins. The dimer of TRPA1 was highly expressed in sclera (19.47 ± 2.13) and ON (8.14 ± 0.71) but weakly expressed in retina (1.85 ± 1.05), CB (8.39 ± 1.04), and cornea (6.94 ± 1.96) (the expression of TRPA1 in kidney was used as reference control). The 150kDa isoform was highly expressed in ON (153.95 ± 3.14), but weakly expressed in retina (4.94 ± 0.75), CB (6.83 ± 0.37) and sclera (16.20 ± 4.32). No

TRPA1 protein was detected in cornea. The 130kDa isoform was highly expressed in retina (6.63 ± 0.80), but weakly expressed in CB (1.43 ± 0.61), sclera (2.34 ± 0.29) and ON (1.39 ± 0.77). No TRPA1 130kDa isoform was detected in cornea, similar to the TRPA1 150kDa isoform. (Figure 15A and 15B).

RT-PCR revealed that TRPA1 mRNA was highly expressed in the sclera (7.69 ± 1.91), but less expressed in retina (2.24 ± 0.33), CB (0.95 ± 0.12), cornea (0.78 ± 0.07), and ON (0.12 ± 0.06) (Figure 15C).

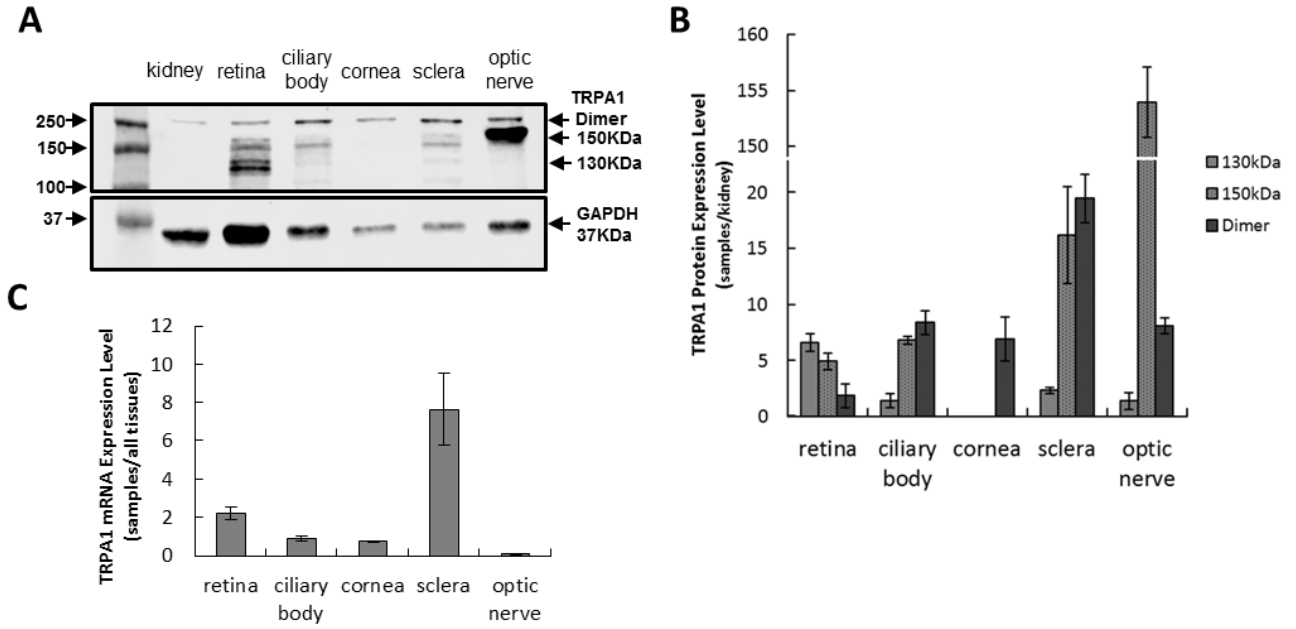

Figure 15. Localization of TRPA1 in rat eye tissue. (A) Western blot analysis showed the protein expression level of TRPA1 in different tissues of a rat eye(n=3). (B) Quantitative analysis of three different forms of TRPA1 protein in different tissue. The expression of TRPA1 was normalized to GAPDH. (C) Quantitative real-time PCR demonstrated the mRNA expression level of TRPA1 in different tissues of rat eye. Three replications were done (n=3).

Immunohistochemistry staining revealed the expression of TRPA1 in non-pigmented as well as pigmented cells of the human CB (Figure 16A). In agreement with the result of immunohistochemistry staining, western blot (Figure 16B) also confirmed the expression of TRPA1 in HNPCE. In western blot analysis, two bands were observed, a ~250kDa TRPA1 dimer band and the monomer TRPA1 band (~150kDa). The ~130kDa TRPA1 isoform was not detected in HNPCE cells (Figure 16B).

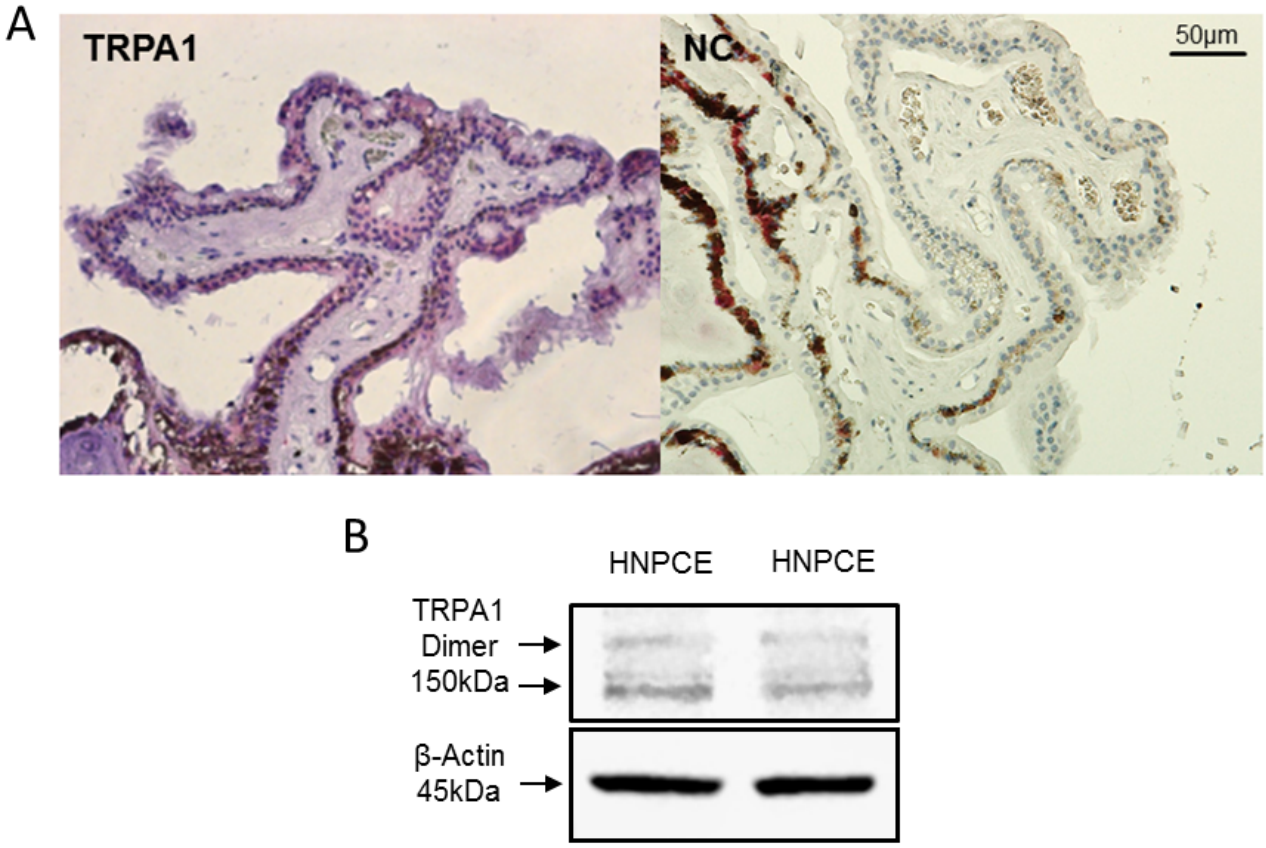

Figure 16. The expression of TRPA1 in human ciliary body and HNPCE cells. (A) TRPA1 is expressed in the human ciliary body epithelium. TRPA1 antibody (red); nuclei (blue). Scale bar: 50μm (n=3). (B) Western blot analysis showed the expression of TRPA1 in HNPCE cells, β-actin was used as loading control.

3.1.2.2 TRPM3

TRPM3 was detected in rat retina, CB and cornea by using immunofluorescence staining. TRPM3 was detected only in GCL and IPL of retina, but not in other layers. TRPM3 protein abundantly expressed in NPE, PE and stroma of CB. The expression of TRPM3 was also observed in the epithelium of cornea (Figure 17).

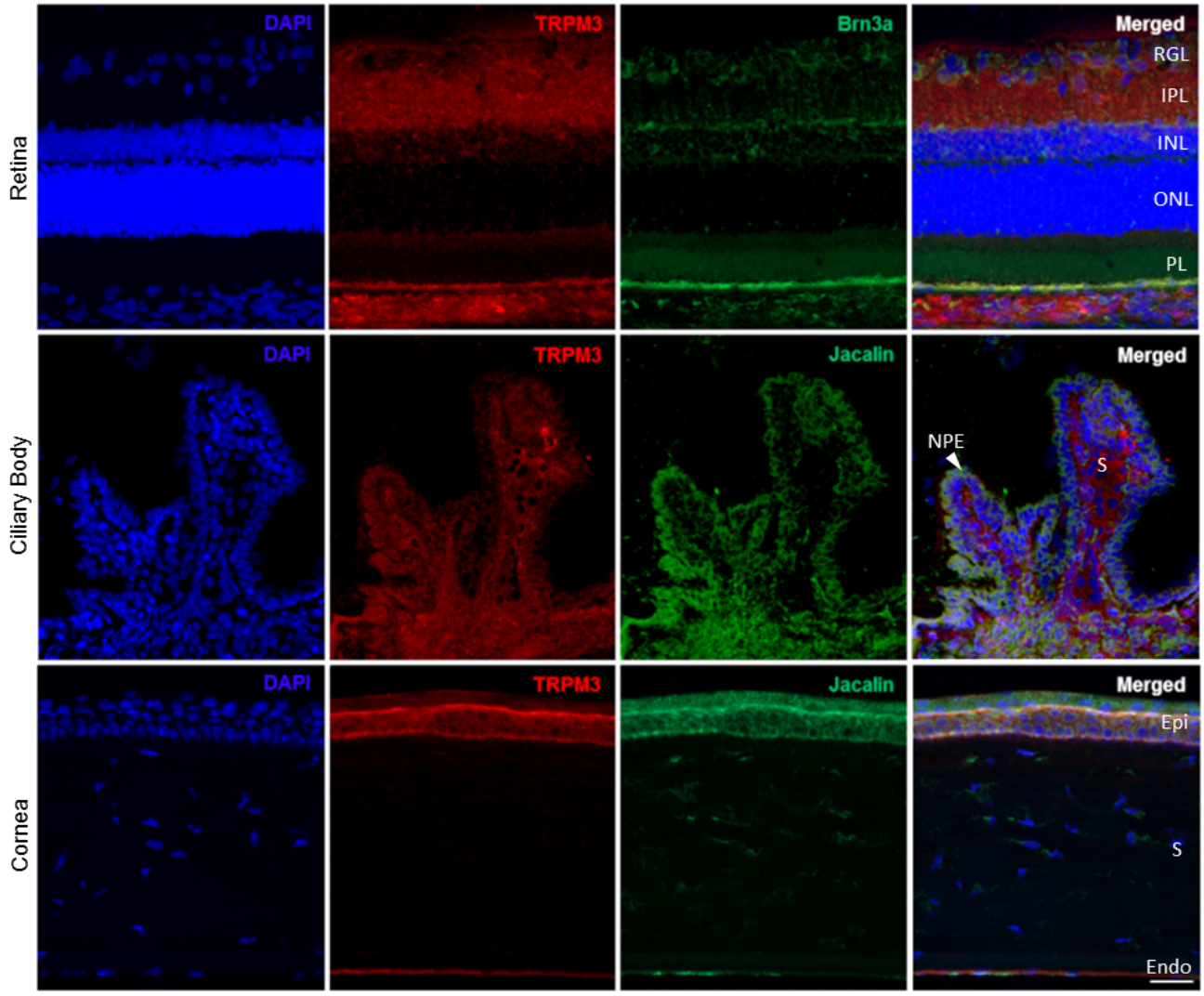

Figure 17. Localization of TRPM3 in rat eye tissue. TRPM3 was found distributed in the rat retina, ciliary body and cornea. TRPM3 antibody (red); Brn3a antibody (green); Jacalin-FITC (green); DAPI (blue). Scale bar: 50μm, n > 20 sections. GCL, ganglion cell layer; IPL, inner plexiform layer; INL, inner nuclear layer; ONL, outer nuclear layer; PL, and photoreceptor layer; NPE, non-pigmented epithelium; Epi, epithelium; Endo, endothelium; S, stroma.

Western blot analysis showed a protein band at ~200kDa (the same as expected molecular weight of full length TRPM3). High expression of TRPM3 was found in CB (1.83 ± 0.07), cornea (2.87 ± 0.23), and sclera (4.57 ± 0.24), but weak expression of TRPM3 was observed in retina (0.06 ± 0.02), ON (0.32 ± 0.05) and lens (0.17 ± 0.11) (Figure 18A and 18B) (The calculation was done by comparing their expression levels to kidney TRPM3). Quantitative RT-PCR revealed higher mRNA levels in the retina (5.43 ± 0.09), CB (1.95 ±

0.44), sclera (6.74 ± 4.72) and ON (2.94 ± 1.63), but lower levels in cornea (0.28 ± 0.14) (Figure 18C).

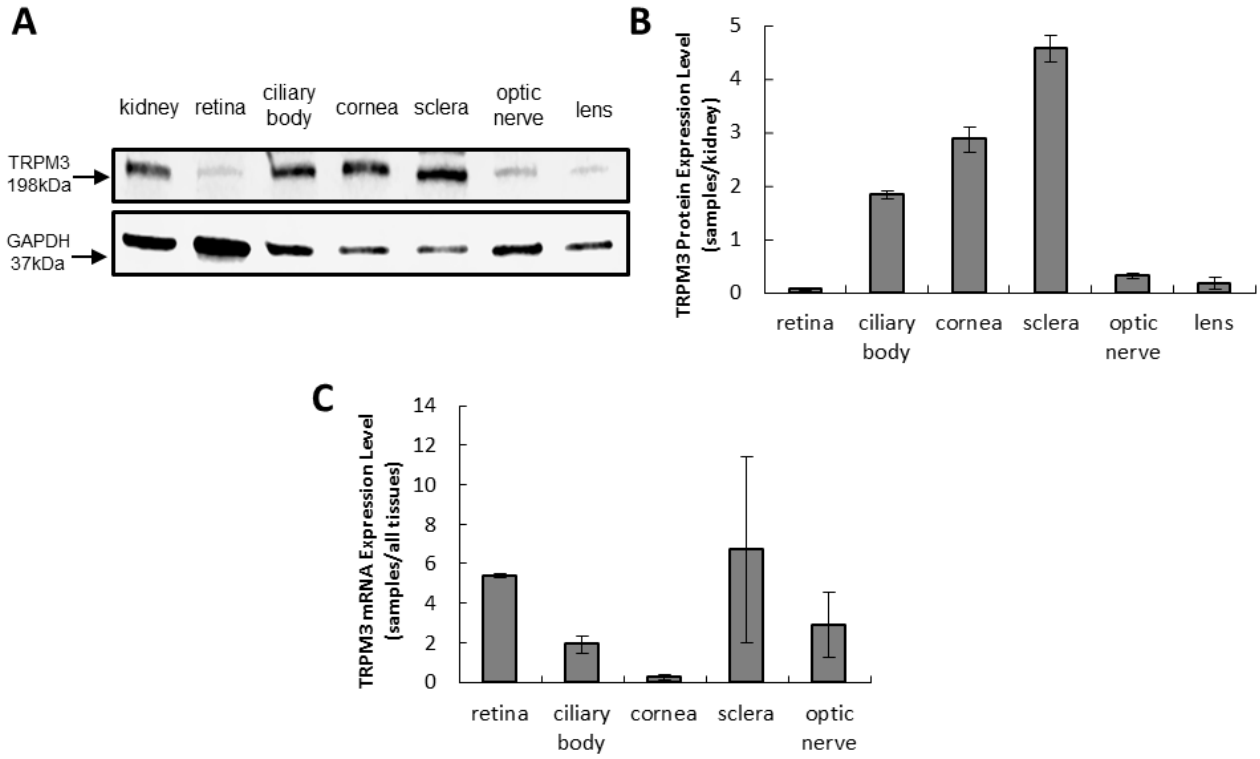

Figure 18. Localization of TRPM3 in rat eye tissue. (A) Western blot analysis showed the protein expression level of TRPM3 in different tissues of a rat eye(n=3). (B) Quantitative analysis of three different forms of TRPM3 protein in different tissue. The expression of TRPM3 was normalized to GAPDH. (C) Quantitative real-time PCR demonstrated the mRNA expression level of TRPM3 in different tissues of rat eye. Three replications were done (n=3).

Immunohistochemistry staining confirmed the expression of TRPM3 in non-pigmented as well as pigmented cells of the human CB (Figure 19A). Furthermore, the expression of TRPM3 in HNPCE cell culture was observed in HNPCE cells by using western blot (Figure 19B).

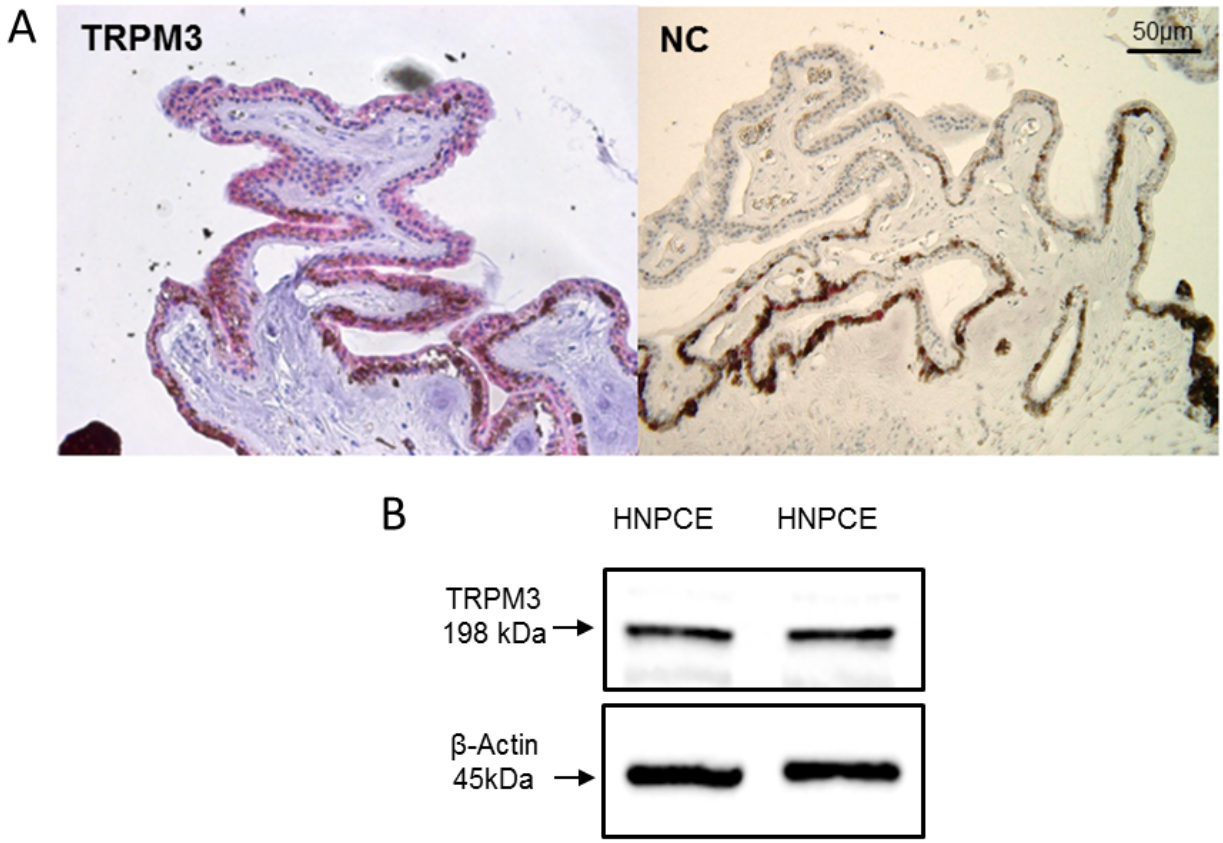

Figure 19. The expression of TRPM3 in human ciliary body and HNPCE cells. (A) TRPM3 is expressed in the human ciliary body epithelium. TRPM3 antibody (red); nuclei (blue). Scale bar: 50μm (n=3). (B) Western blot analysis showed the expression of TRPM3 in HNPCE cells, β-actin was used as loading control.

3.1.2.3 TRPV4

Immunofluorescence staining showed positive TRPV4 signal in rat retina, CB and cornea. TRPV4 was observed as highly expressed in GCL, INL and PL, but weakly expressed in IPL, OPL and ONL of retina. TRPV4 protein mainly expressed in NPE and PE of CB. The expression of TRPV4 was also observed in the epithelium of cornea (Figure 20).

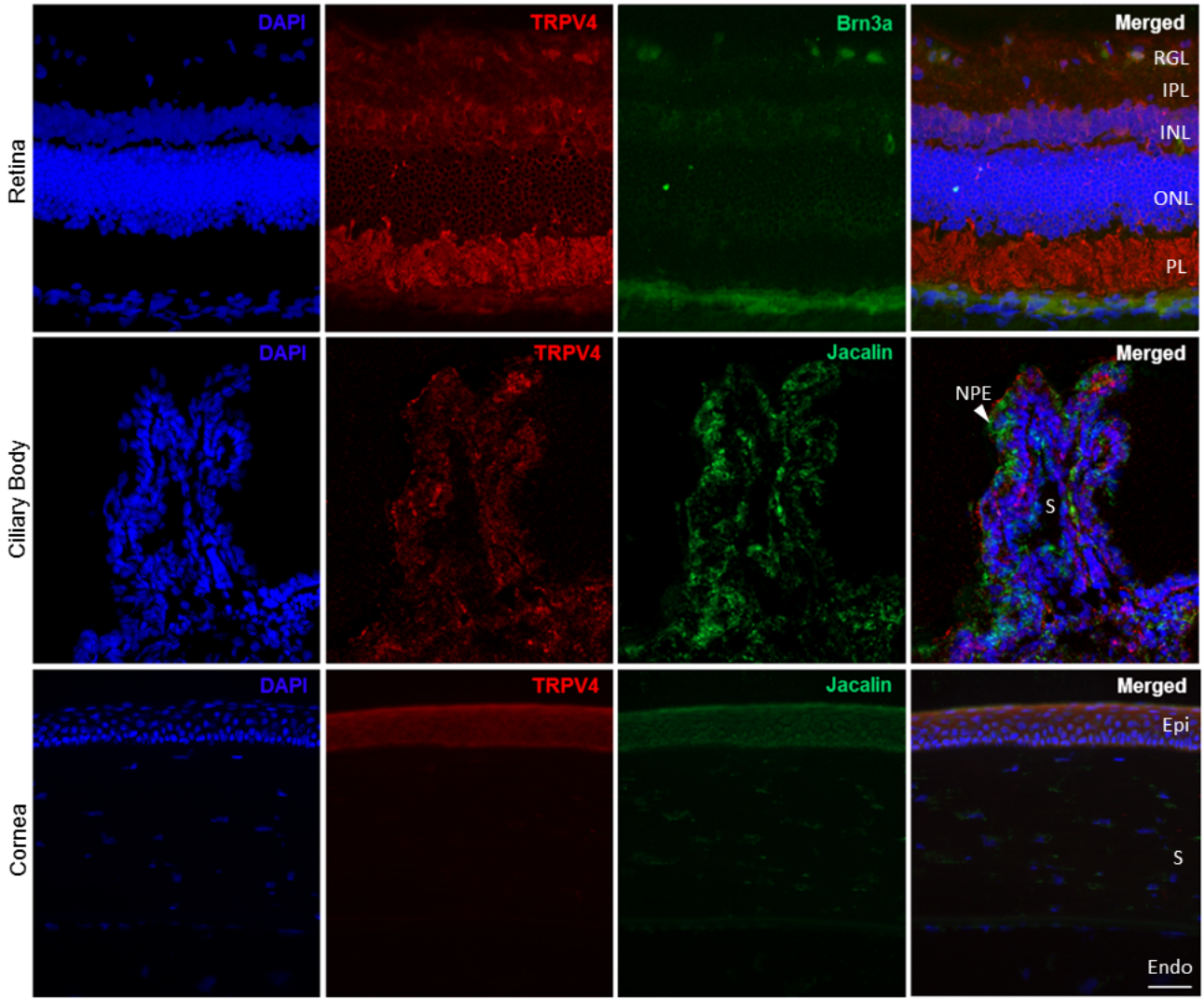

Figure 20. Localization of TRPV4 in rat eye tissue. TRPV4 was found distributed in the rat retina, ciliary body and cornea. TRPV4 antibody (red); Brn3a antibody (green); Jacalin-FITC (green); DAPI (blue). Scale bar: 50μm, n > 20 sections. GCL, ganglion cell layer; IPL, inner plexiform layer; INL, inner nuclear layer; ONL, outer nuclear layer; PL, and photoreceptor layer; NPE, non-pigmented epithelium; Epi, epithelium; Endo, endothelium; S, stroma.

Western blot analysis detected a ~75kDa protein band (the same as expected molecular weight of full length TRPV4). While highly expressed in CB (6.12 ± 1.02) and cornea (11.55 ± 3.25), retina (4.22 ± 0.60) and sclera (4.33 ± 2.20), no expression was observed in ON (Figure 21A and 21B). RT-PCR analysis revealed that TRPV4 mRNA was expressed at higher levels in the CB (2.03 ± 0.40) and sclera (5.26 ± 1.95), but lower in retina (0.71 ± 0.04), cornea (1.04 ± 0.07) and ON (0.53 ± 0.05) (Figure 21C).

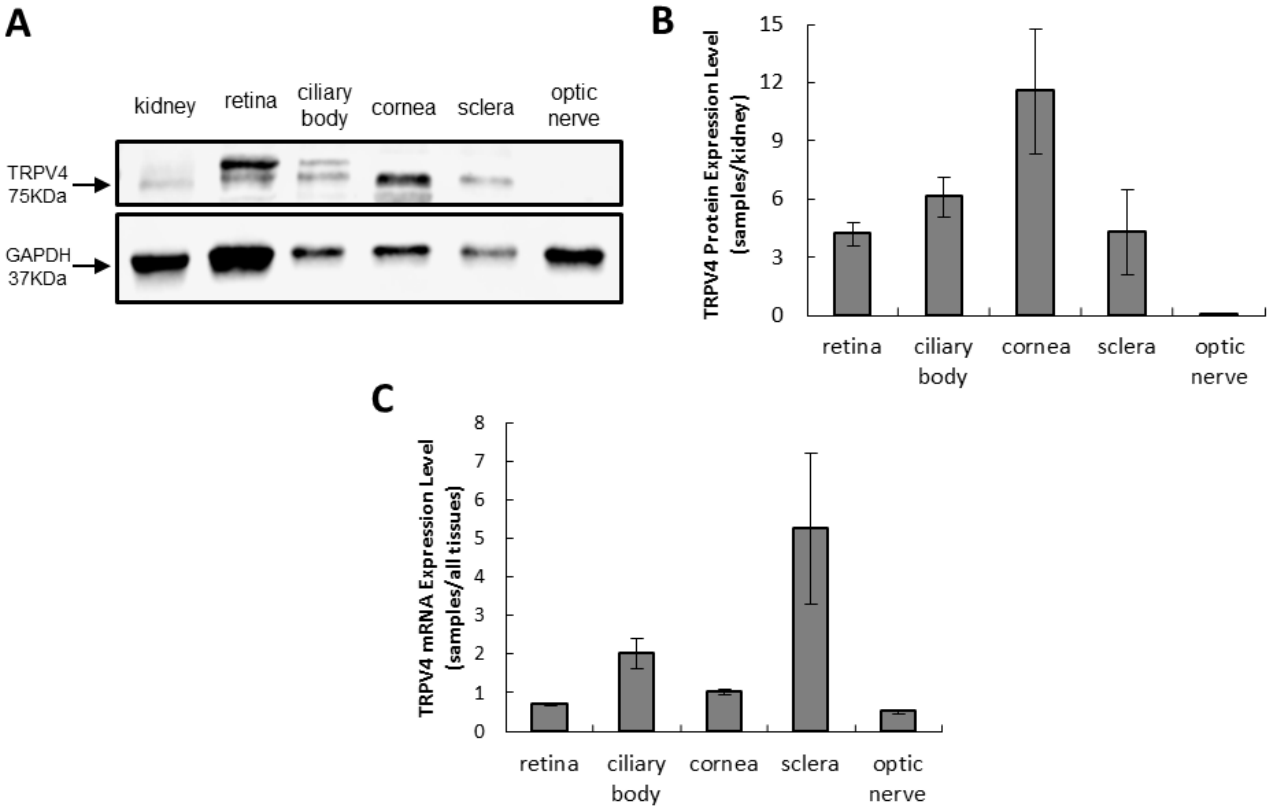

Figure 21 Localization of TRPV4 in rat eye tissue. (A) Western blot analysis showed the protein expression level of TRPV4 in different tissues of a rat eye(n=3). (B) Quantitative analysis of three different forms of TRPV4 protein in different tissue. The expression of TRPV4 was normalized to GAPDH. (C) Quantitative real-time PCR demonstrated the mRNA expression level of TRPV4 in different tissues of rat eye. Three replications were done (n=3).

Immunohistochemistry staining detected the expression of TRPV4 in non-pigmented as well as pigmented cells of the human CB (Figure 22A). Furthermore, in agreement with the results of immunohistochemistry staining of human CB, western blot (Figure 22B) also confirmed the expression of TRPV4 in HNPCE.

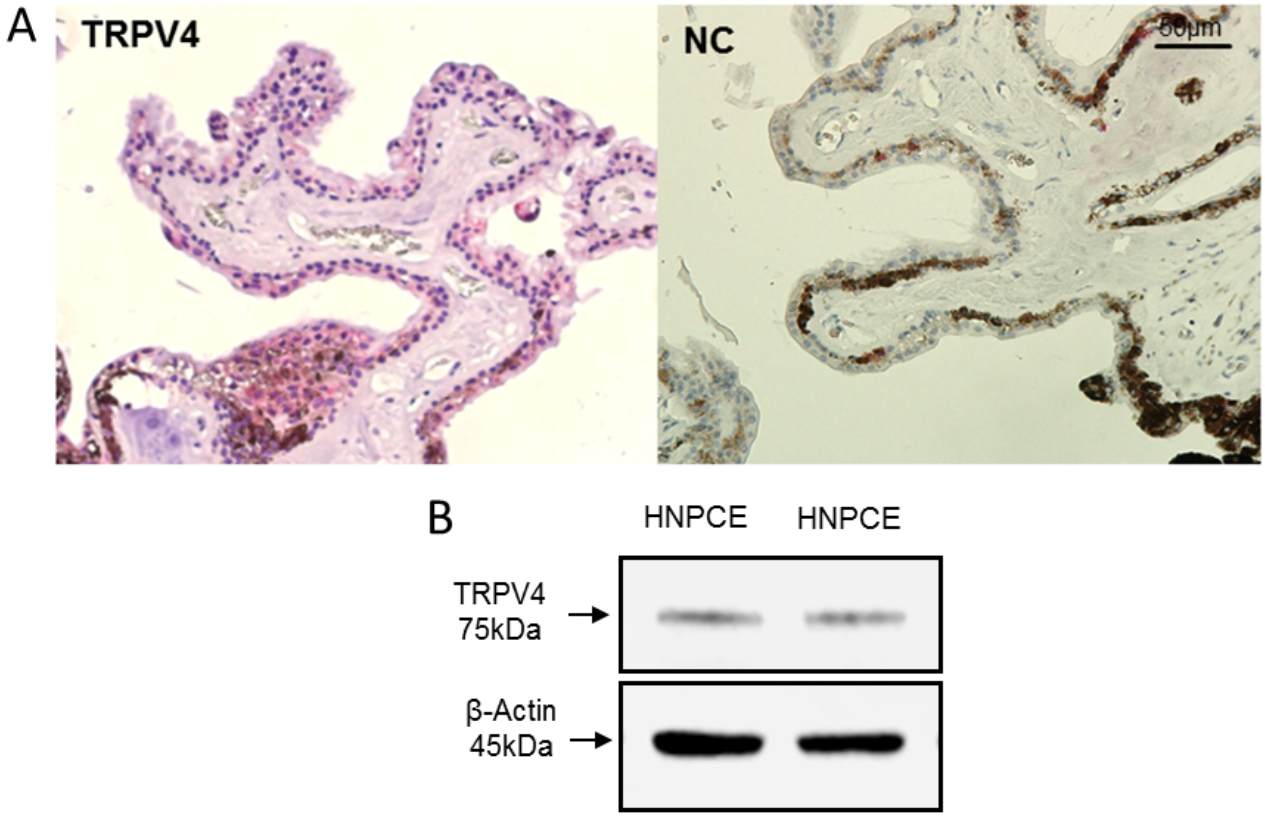

Figure 22. The expression of TRPV4 in human ciliary body and HNPCE cells. (A) TRPV4 is expressed in the human ciliary body epithelium. TRPV4 antibody (red); nuclei (blue). Scale bar: 50μm (n=3). (B) Western blot analysis showed the expression of TRPV4 in HNPCE cells, β-actin was used as loading control.

3.1.2.4 TRPP2

Immunofluorescence staining showed that TRPP2 expressed in rat retina, CB and cornea. TRPP2 expression was highly observed in GCL, INL and OPL, but weakly in IPL, ONL and PL of retina. TRPP2 was also highly expressed in NPE, PE and stroma of CB. In the corneal epithelium, the expression of TRPP2 was detected (Figure 23).

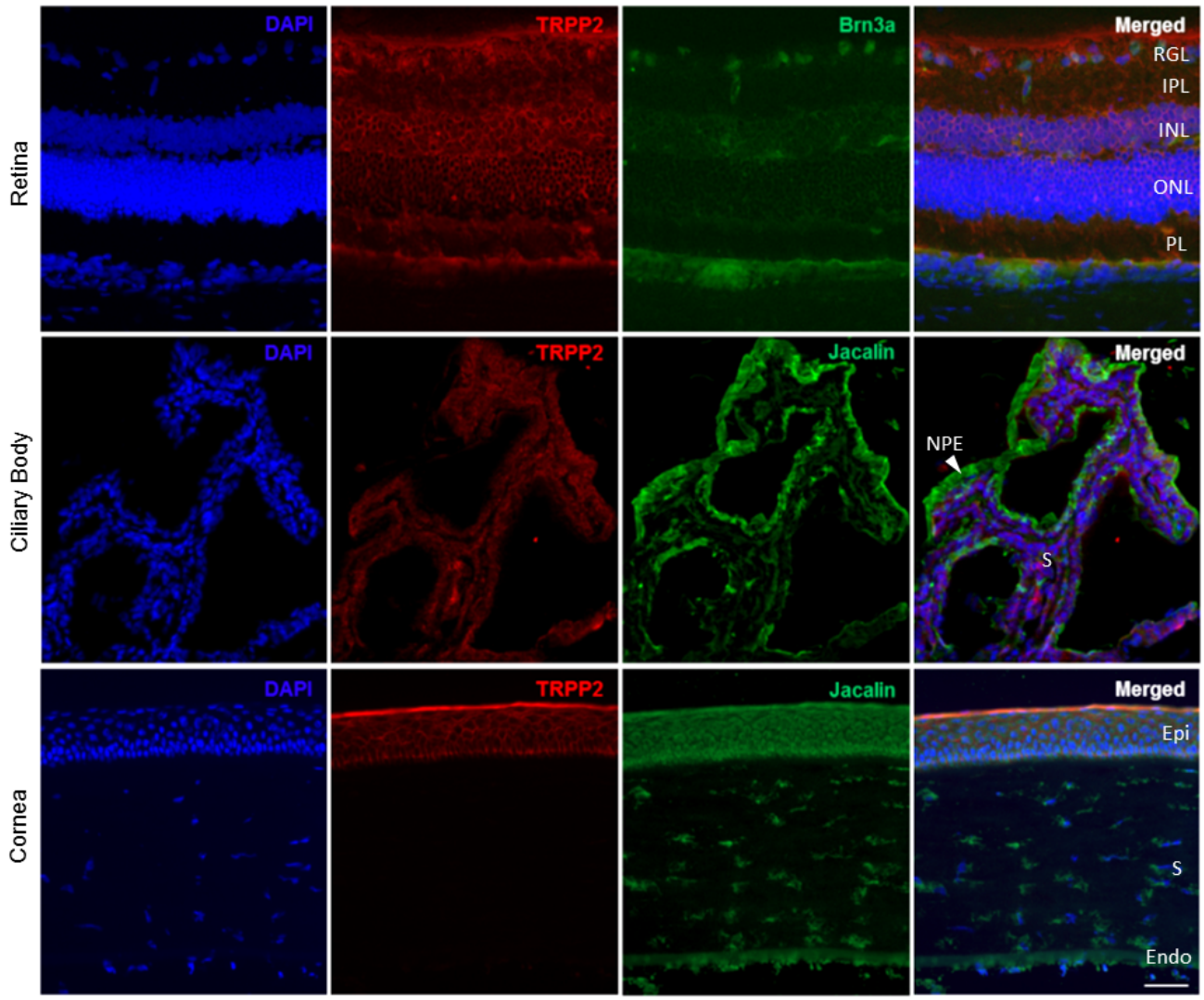

Figure 23. Localization of TRPP2 in rat eye tissue. TRPP2 was found distributed in the rat retina, ciliary body and cornea. TRPV4 antibody (red); Brn3a antibody (green); Jacalin-FITC (green); DAPI (blue). Scale bar: 50μm, n > 20 sections. GCL, ganglion cell layer; IPL, inner plexiform layer; INL, inner nuclear layer; ONL, outer nuclear layer; PL, and photoreceptor layer; NPE, non-pigmented epithelium; Epi, epithelium; Endo, endothelium; S, stroma.

Western blotting was performed to analyze the expression of TRPP2 in different structures of the rat eye. Western blot detected three TRPP2 bandy. The largest band (220kDa) is the dimer form of TRPP2, while the 110kDa and 85kDa bands represent two different isoforms of TRPP2. The dimer form of TRPP2 was highly expressed in cornea (14.76 ± 1.65), CB (3.03 ± 1.30), and lens (2.10 ± 1.15), but not in other regions. The 110kDa isoform was expressed in retina (0.62 ± 0.27), sclera (0.32 ± 0.16), CB (0.19 ± 0.06) and iris (0.18 ± 0.05) only. The 85kDa Isoform was highly expressed in CB (2.06 ± 0.90),

cornea (15.28 ± 1.61), sclera (2.51 ± 0.42), ON (1.46 ± 0.70) and lens (1.23 ± 0.43), but weakly expressed in retina (0.37 ± 0.04) and iris (0.67 ± 0.13) (Figure 24A and 24B).

Reverse transcription PCR showed the mRNA expression level of TRPP2 in different tissues of rat eye, as 344bp TRPP2 PCR products were detected in all the tissues of eye (Figure 24C), further sanger sequencing confirmed the sequences of PCR product (Figure 24E). RT-PCR analysis revealed that TRPP2 mRNA was expressed higher in the retina (4.45 ± 1.98), CB (2.54 ± 1.02), sclera (3.62 ± 0.65), ON (3.82 ± 1.93) and iris (6.94 ± 2.19), but lower in cornea (0,1 ± 0.06) (Figure 24D).

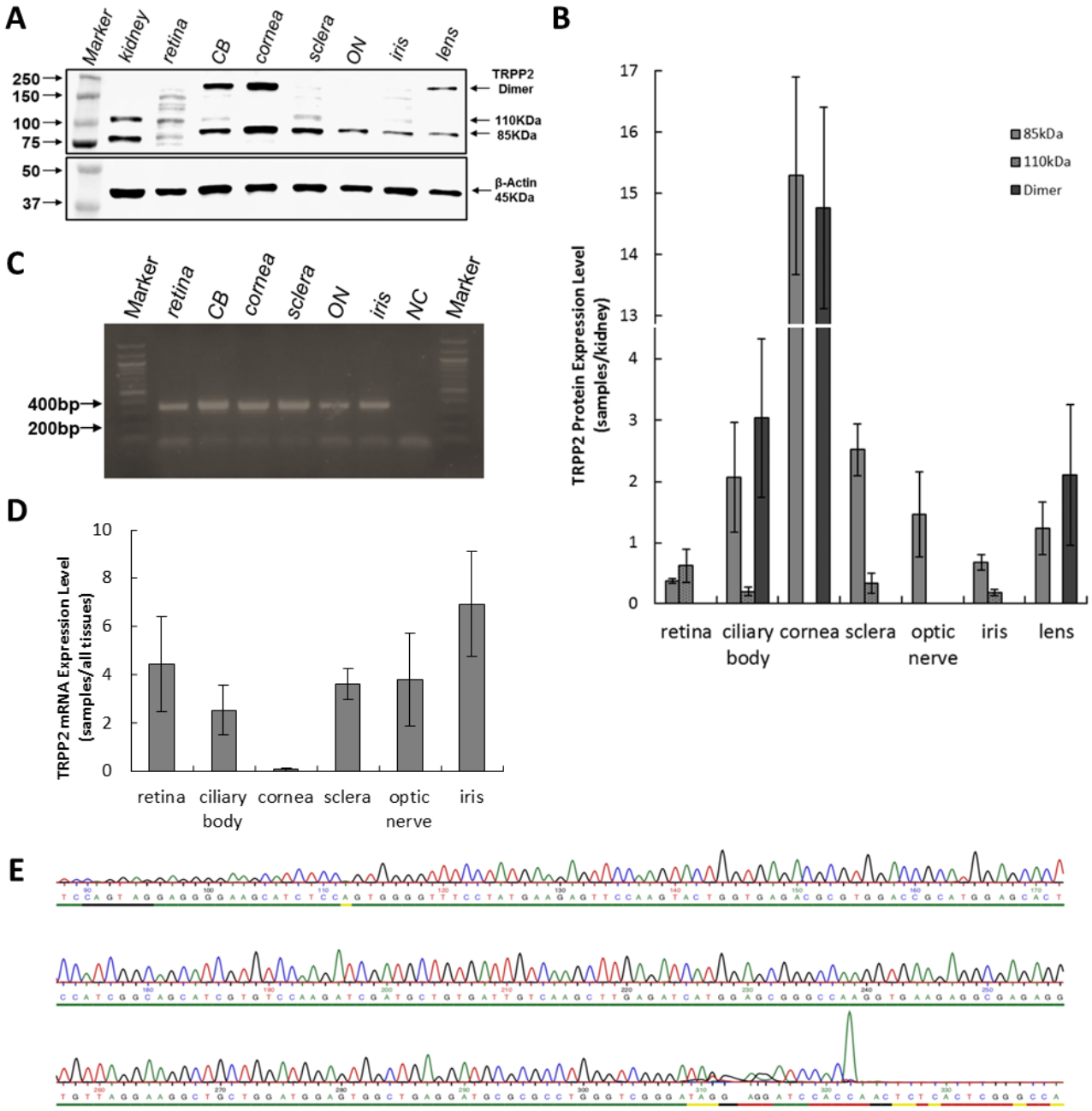

Figure 24. Localization of TRPP2 in rat eye tissue. (A) Western blot analysis showed the protein expression level of TRPP2 in different tissues of a rat eye. The largest band (220kDa) is the dimer of TRPP2, the 110kDa and 85kDa bands represent two different isoforms of TRPP2. (B) Quantitative analysis of three different forms of TRPP2 protein in different tissue. The expression of TRPP2 was normalized to β-actin. Three times of replications were done (n=3). (C) Reverse transcription PCR (showed the mRNA expression level of TRPP2 in different tissues of rat eye. A 344bp band represents the PCR product of TRPP2. CB (ciliary body), ON (optic nerve), NC (negative control). (D) Quantitative real-time PCR demonstrated the mRNA expression level of TRPV4 in different tissues of rat eye. Three times of replications were done (n=3). (E) Sanger sequencing confirmed the PCR product of TRPP2.

The expression of TRPP2 was observed in human retina (A), both PE and NPE of ciliary body (B), cornea (C), TM (D), lens (E) using immunohistochemistry staining, similar to the results found in rats (Figure 25).

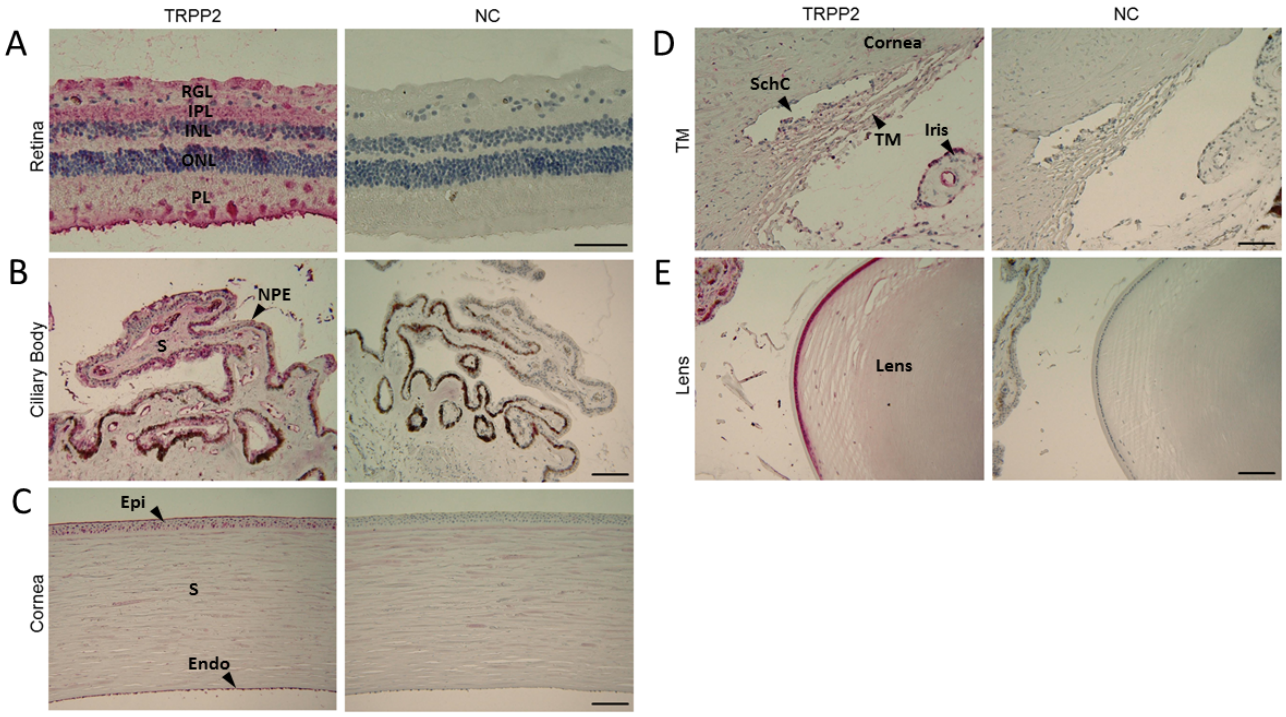

Figure 25. Localization of TRPP2 in human eye tissue. TRPP2 is expressed in the human retina (A), CB (B), cornea (C), TM (D), lens (E). TRPP2 antibody (red); nuclei(blue). Scale bar: 50μm (n=3). GCL, ganglion cell layer; IPL, inner plexiform layer; INL, inner nuclear layer; ONL, outer nuclear layer; PL, and photoreceptor layer; NPE, non-pigmented epithelium; Epi, epithelium; Endo, endothelium; S, stroma; TM, trabecular meshwork; SchC, Schlemm's canal.

Furthermore, the expression of TRPP2 in HNPCE cell culture was tested by immunostaining, western blot analysis and PCR. Immunostaining (Figure 26A), western blot (Figure 26B) and PCR (Figure 26C) results all confirmed the expression of TRPP2 in HNPCE. The TRPP2 was mainly located in nuclei and showed punctated distribution in cytoplasm of HNPCE cells (Figure 26A).

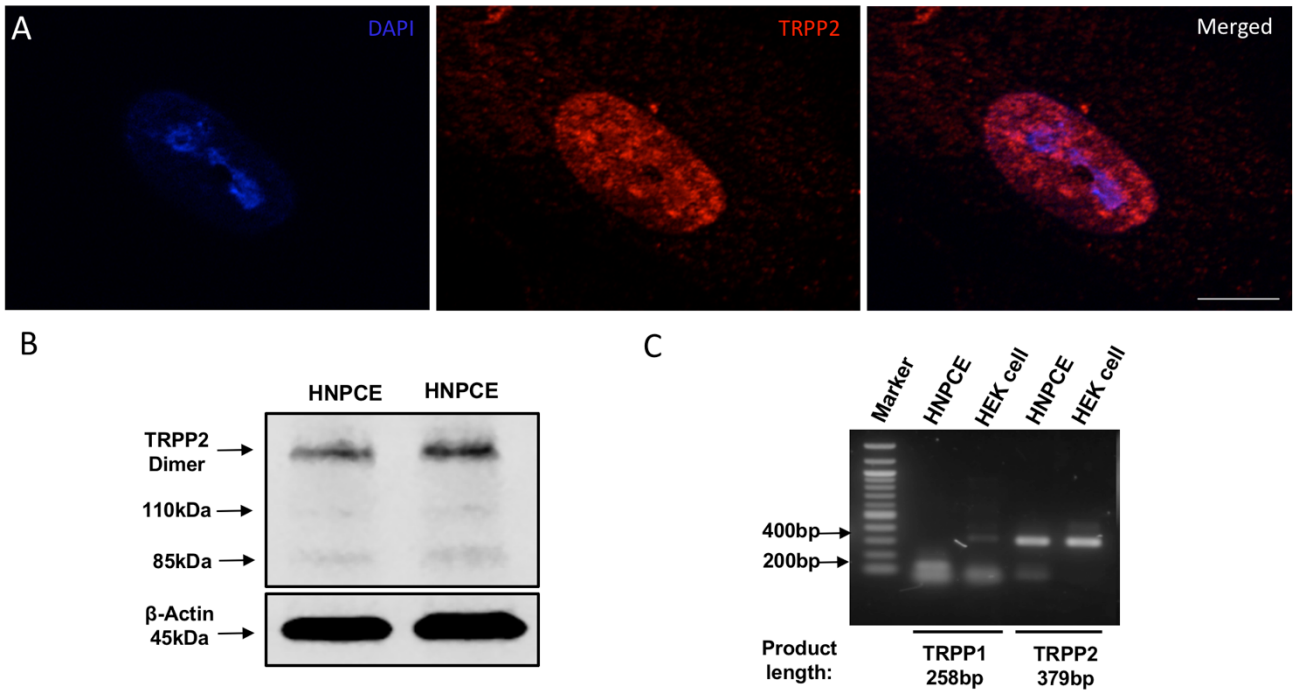

Figure 26. The expression of TRPP2 in HNPCE cells. (A) Immunoflurescence staining displays that the TRPP2 (red) localized in nuclei (via DAPI staining; blue) and partly in cytoplasm of HNPCE cells. Scale bar: 10μm. (B) Western blot analysis showed the expression of TRPP2 in HNPCE cells, β-actin was used as loading control. (C) TRPP2 mRNA expression was detected by reverse transcript PCR.

3.1.3 Expression and localization of TREK1 in eye tissue

Immunofluorescence staining showed positive TREK1 signal in rat retina, CB and cornea. TRPV4 was broadly expressed in different layers of retina, including GCL, IPL, IN L, OPL, ONL and PL. TREK1 protein was abundant in NPE and PE of CB. The expression of TREK1 was also detected in the epithelium of cornea (Figure 27).

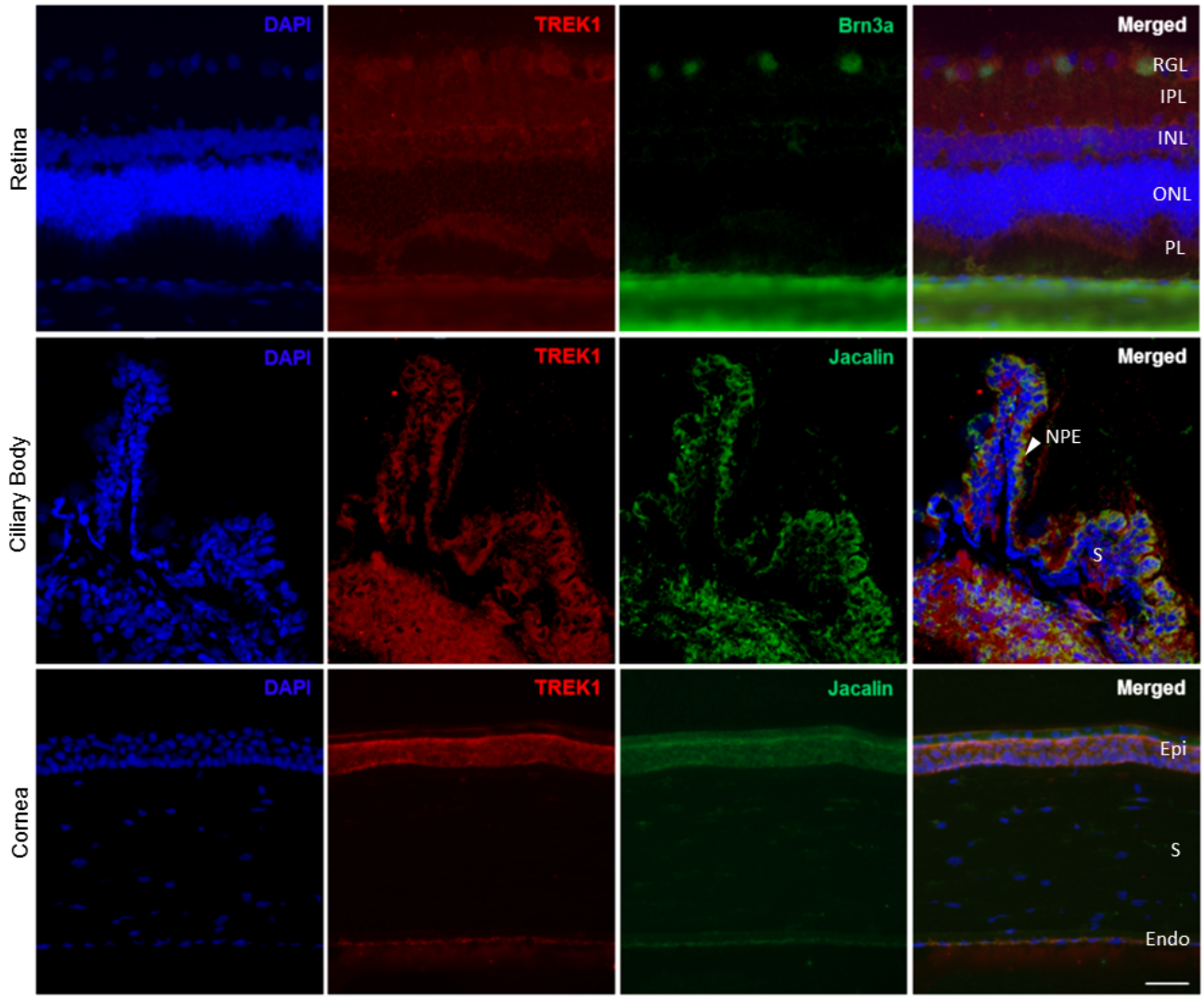

Figure 27. Localization of TREK1 in rat eye tissue. TREK1 was found distributed in the rat retina, ciliary body and cornea. TREK1 antibody (red); Brn3a antibody (green); Jacalin-FITC (green); DAPI (blue). Scale bar: 50μm, n > 20 sections. GCL, ganglion cell layer; IPL, inner plexiform layer; INL, inner nuclear layer; ONL, outer nuclear layer; PL, and photoreceptor layer; NPE, non-pigmented epithelium; Epi, epithelium; Endo, endothelium; S, stroma.

Western blot analysis using anti-TREK1 antibody revealed a ~47kDa protein band (the same as expected molecular weight for full length TREK1) eye tissues. Quantitative analysis using kidney as reference showed high expression level of TREK1 in cornea (7.03 ± 1.50), while showing a low expression level in retina (1.16 ± 0.40), CB (1.61 ± 1.11), sclera (1.98 ± 1.09) and ON (2.54 ± 1.51) (Figure 28A and 28B). Quantitative RT-PCR analysis revealed that the expression of TREK1 mRNA was higher in retina (5.91 ± 1.28)

and ON (5.98 ± 0.92), but lower in CB (0.57 ± 0.27), cornea (0.03 ± 0,02) and sclera (1.50 ± 0.68) (Figure 28C).

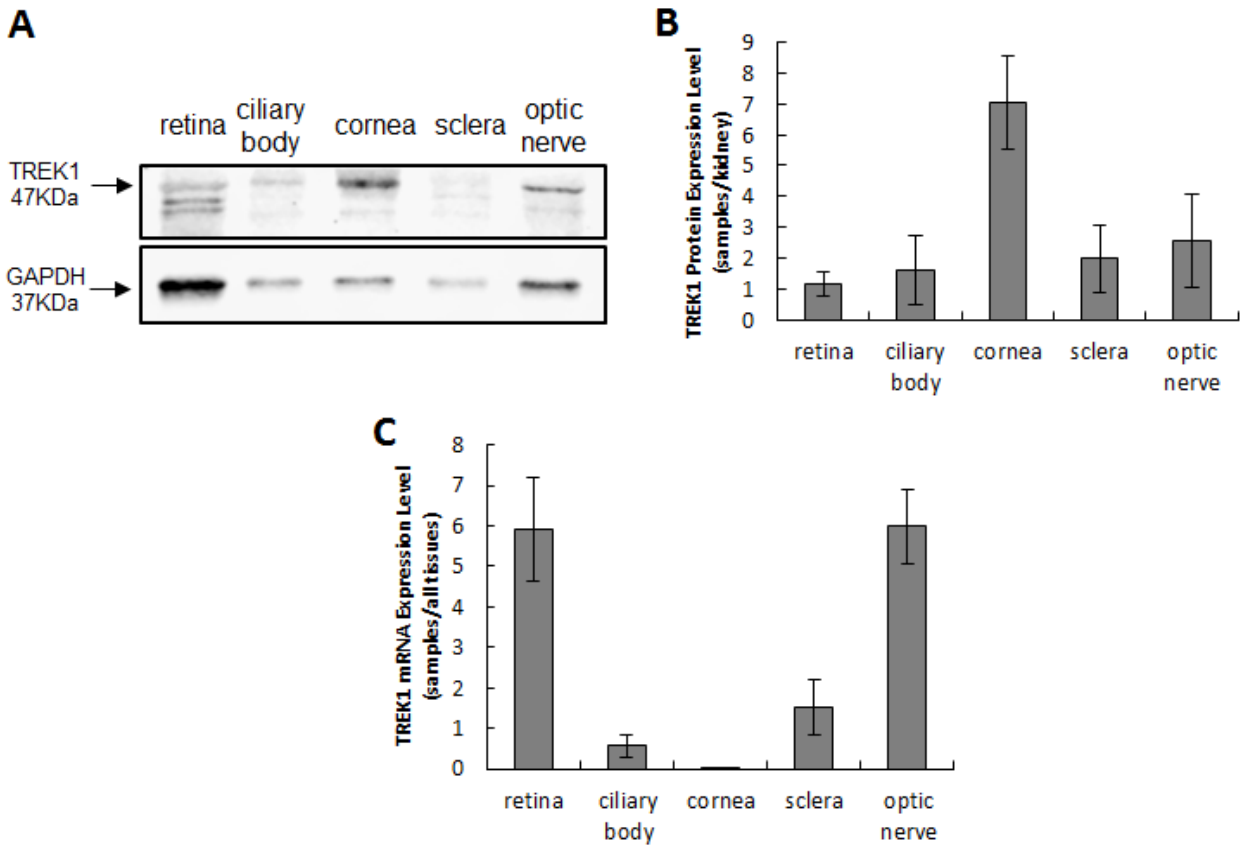

Figure 28. Localization of TREK1 in rat eye tissue. (A) Western blot analysis showed the protein expression level of TREK1 in different tissues of a rat eye(n=3). (B) Quantitative analysis of three different forms of TREK1 protein in different tissue. The expression of TREK1 was normalized to GAPDH. (C) Quantitative real-time PCR demonstrated the mRNA expression level of TREK1 in different tissues of rat eye. Three replications were done (n=3).

Using immunohistochemistry staining, the expression of TREK1 was observed in non-pigmented as well as pigmented cells of the human CB (Figure 29A). Furthermore, the expression of TREK1 in HNPCE cell culture was detected by western blot (Figure 29B) and confirmed the expression of TREK1 in HNPCE.

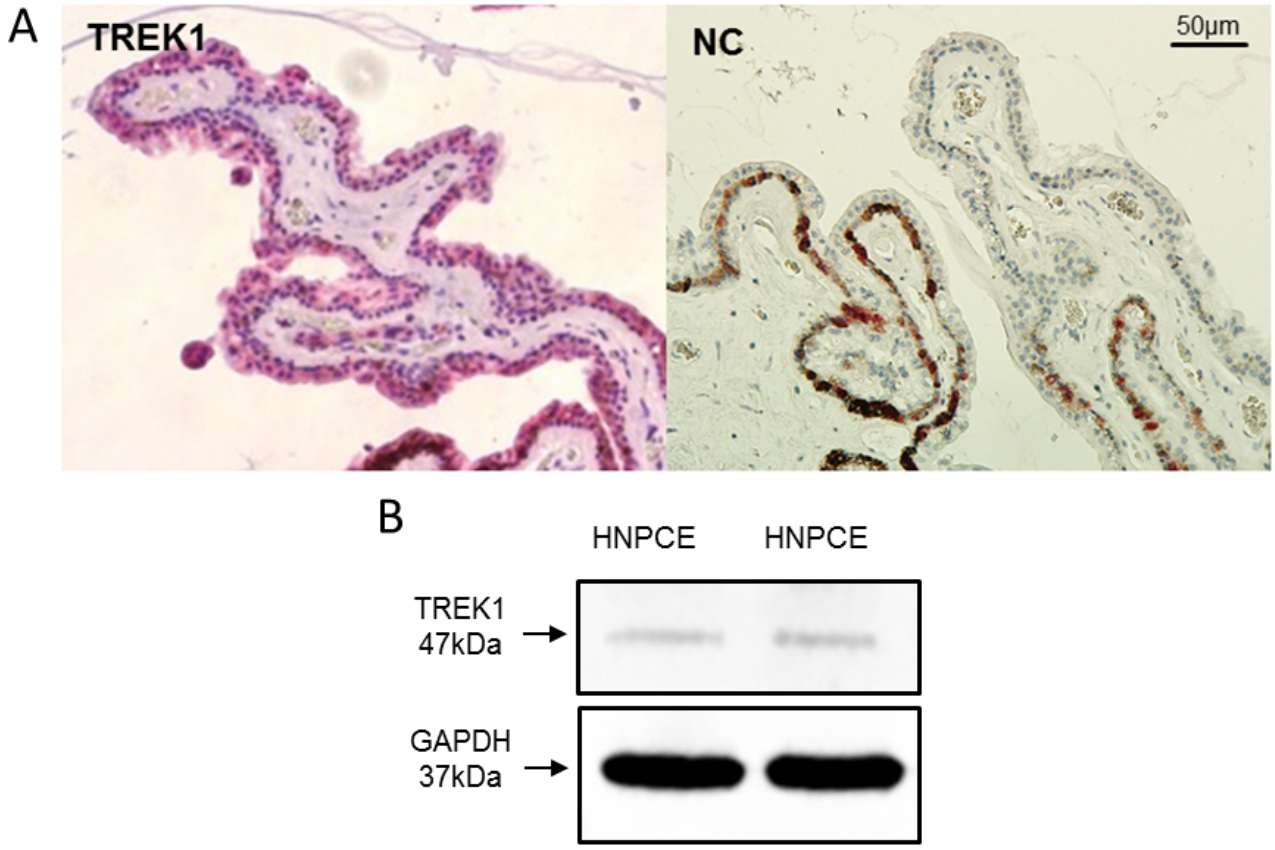

Figure 29. The expression of TREK1 in human ciliary body and HNPCE cells. (A) TREK1 is expressed in the human ciliary body epithelium. TREK1 antibody (red); nuclei (blue). Scale bar: 50μm (n=3). (B) Western blot analysis showed the expression of TREK1 in HNPCE cells, GAPDH was used as a loading control.

3.2 Characterization the primary cilia in human ciliary body and HNPCE cells

3.2.1 Serum starvation induced the formation of primary cilia in HNPCE cells

By using immunofluorescence staining, primary cilia were observed in cultured HNPCE cells (Figure 30A). The length of primary cilia was measured at different time points after serum starvation directly on the Axio (Version 4.8). Extension of the starvation time to 24 hours, 48 hours, 72 hours, respectively, did not affect the length of primary cilia. Twenty-four hours after serum starvation, HNPCE cells formed on average 4.4 μm (4.4 ± 1.4 μm) primary cilia in length. After 48 hours of starvation, the length of primary cilia did not change largely (4.8 ± 1.0 μm). After 72 hours of starvation, the average length of the primary cilia was 5.1 μm (5.1 ± 0.9 μm). No significant difference was seen at different time points (Figure 30B). And the number cells were counted with primary cilia at different time points of serum starvation. Interestingly, our results showed that extension of the time of serum

starvation could induce the formation of primary cilia in HNPCE cells. Without serum starvation (at 0 hours) only 26% of cells can form primary cilia (26.0 ± 5.6%). After serum starvation for 24 hours, the percentage of cells with primary cilia increased to 65% (65.0 ± 4.9 %). Extended serum starvation time to 48 or 72 hours caused almost all of HNPCE cells to form primary cilia (93.9 ± 6.1 % at 48 hour and 96.4 ± 4.7 % at 72 h) (Figure 30C).

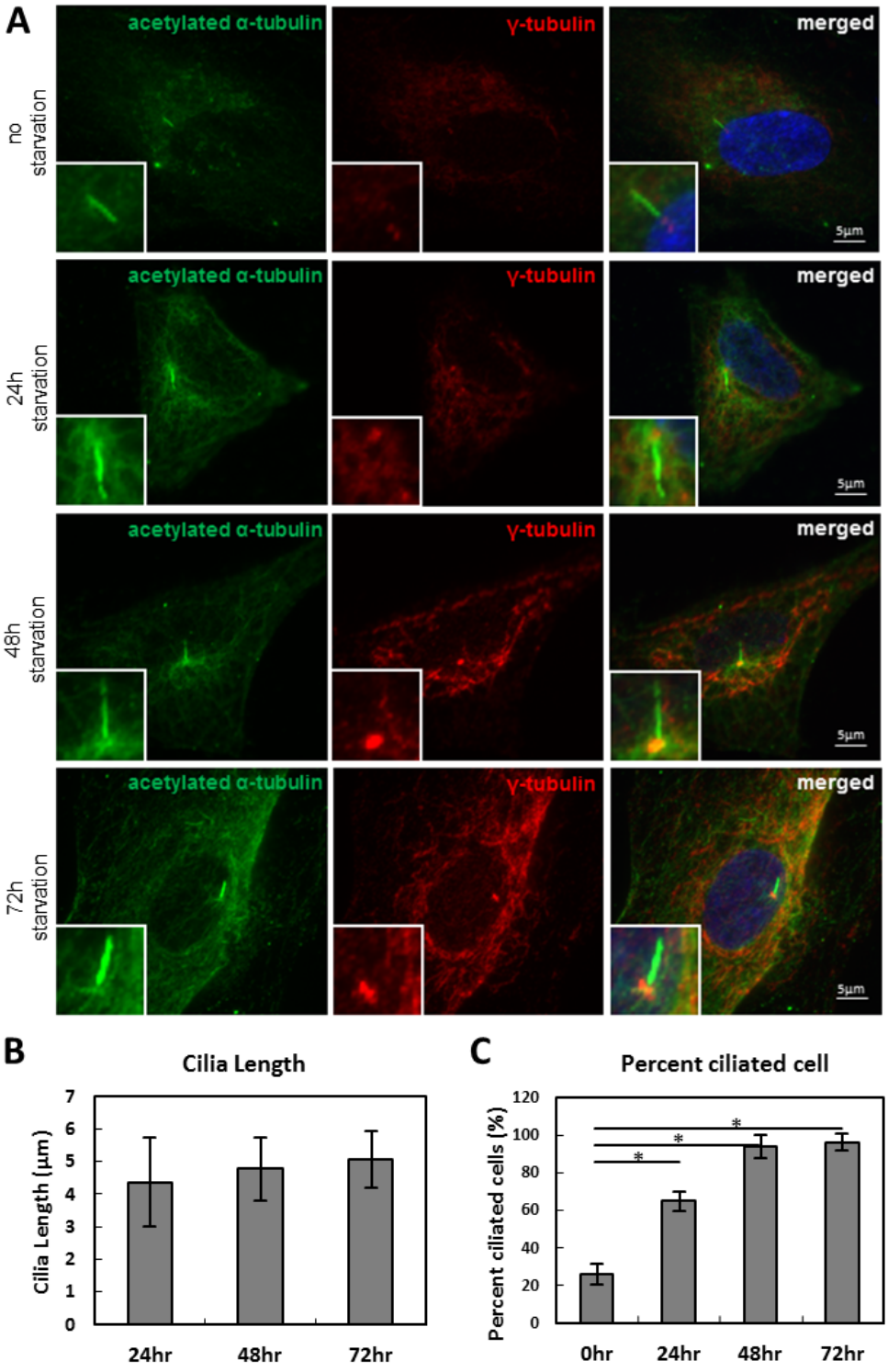

Figure 30. Formation of primary cilia in HNPCE cell culture. (A) Serum-starvation of HNPCE cells was performed at 0, 24, 48, and 72 h. Representative immunofluorescence photomicrographs showing cilia formation with anti-acetylated α-tubulin (green) antibody and γ-tubulin (green) antibody (DAPI, blue). Cilia length (B) and ciliation rate (C) are shown. Error bars represent SD (SD). n > 50 cilia, three independent replicates, ANOVA, *p<0.05. (Scale bar, 5μm.)

3.2.2 Primary cilia in HNPCE cells of human CB

3.2.2.1 Primary cilia in HNPE cells

In HNPCE cell culture, the typical sign of primary cilia, a “9+0” arrangement, was also observed by electron microscopy (Figure 31A). Thus, this data further supports the formation of primary cilia in HNPCE cells.

3.2.2.2 Primary cilia in human CB

The primary cilia structure was observed in the NPE of human ciliary body on human eye tissue sections (Figure 31B). Thus, *in vitro* and *in vivo* data support the existence of primary cilia in the HNPCE cells.

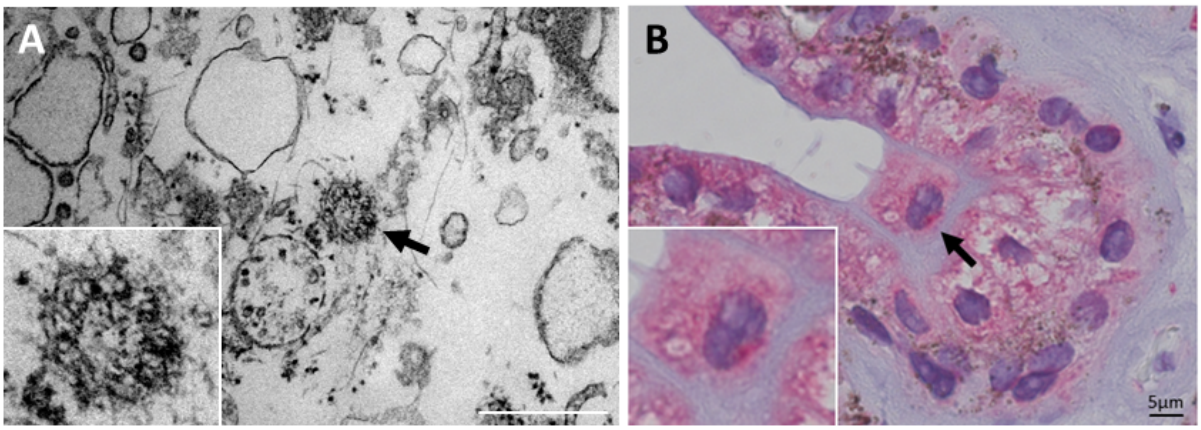

Figure 31. Formation of primary cilia in HNPCE cell culture and human ciliary body epithelium. (A) Electron micrograph showed a primary cilium in HNPCE. Arrow shows crossing section of primary cilium. (Scale bar, 500 nm.) (B) Immunohistochemical staining detected a primary cilium in HNPCE of human eye. Arrow shows primary cilium. (Scale bar, 5μm.)

3.2.3 Colocalization of primary cilia and MSCs candidate

TRPP2 was observed distributed on the axoneme and the basal body of primary cilia in HNPCE cells with 48 hours serum-starvation (Figure 32F). But the similar co-localization

results were not observed on other MSCs candidates studied in this study (Figure 32A~E, G).

As Immunofluorescence staining showed, PIEZO1, TRPM3 and TRPV4 were observed mainly located in nuclei and diffusely distributed in cytoplasm of HNPCE cells (Figure 32A, D, E). PIEZO2 was located in nuclei but presented cord-like distribution in the cytoplasm of HNPCE cells (Figure 32B). TRPA1 was mainly located in nuclei and had punctuated distributed in cytoplasm of HNPCE cells (Figure 32C). TREK1 had punctated distributed in cytoplasm of HNPCE cells (Figure 32G).

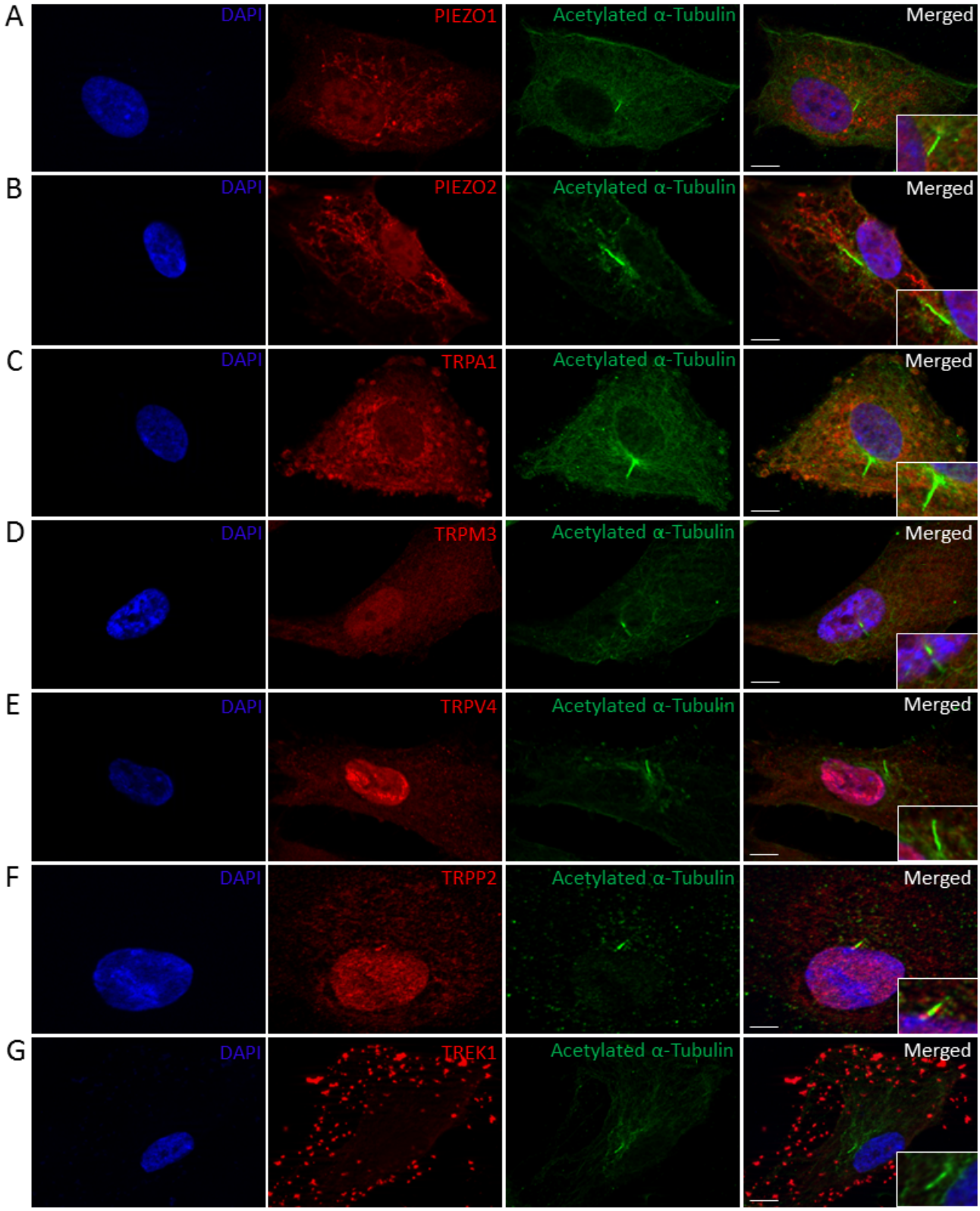

Figure 32. Immunostaining for MSCs candidates co-localizes to primary cilia in HNPCE cells. Double immunostaining was performed on HNPCE cells after serum-starved for 48h. (A) PIEZO1, (B) PIEZO2, (C) TRPA1, (D) TRPM3, (E) TRPV4, (F) TRPP2 and (G) TREK1. MSCs antibodies (red); acetylated α-tubulin (green); DAPI (blue). (n > 20 cells, Scale bar, 5μm.)

3.3 MSCs expression under different pressure level

The level of PIEZO1 protein in HNPCE did not significant changed after exposing in 60 mmHg hydrostatic pressures for 24 hours. The qPCR result, however, showed that PIEZO1 mRNA level decreased 30% and 40% at 12 hours and 24 hours, respectively (Figure 33A, Table 14). The level of PIEZO2 protein in HNPCE significantly dropped to nearly 50% compared to control group after applying 60mmHg hydrostatic pressure for 24 hours. Consistently, the PIEZO2 mRNA level reduced about 70% and 90% after applying 60 mmHg hydrostatic pressure for 12 hours to 24 hours, respectively (Figure 33B, Table 14). However, there was no significant change of TRPA1 protein level (both isoform and dimer) after applying 24 hours of 60 mmHg hydrostatic pressure. On the contrary, the TRPA1 mRNA level increased significantly at 24 hours under high pressure, as almost four times the amount of TRPA1 was observed at 24 hours with high hydrostatic pressure, compared to control group (Figure 33C, Table 14). The protein level of TRPM3 significantly decreased TRPM3 mRNA level at 12 hours (TRPM3 mRNA reduced to 26%) and 24 hours (TRPM3 mRNA reduced to 22%) (Figure 33D, Table 14). The TRPV4 protein remained unchanged at 24 hours, while its mRNA level increased around 10% at 12 hours. However, the TRPV4 mRNA level returned to normal level at 24 hours (Figure 33E, Table 14). TRPP2 protein level doubled, both the dimer and the ~85kDa isoforms band, while the level of the ~110kDa isoforms band quadrupled. On the contrary, the TRPP2 mRNA level decreased to 57% after 24 hours of loaded hydrostatic pressure (Figure 33F, Table 14). After 24 hours of induced hydrostatic pressure, the protein level of TREK1 in HNPCE raised about 60%, while the TREK1 mRNA level did not significantly change after being exposed to 60 mmHg hydrostatic pressure for 24 hours (Figure 33G, Table 14).

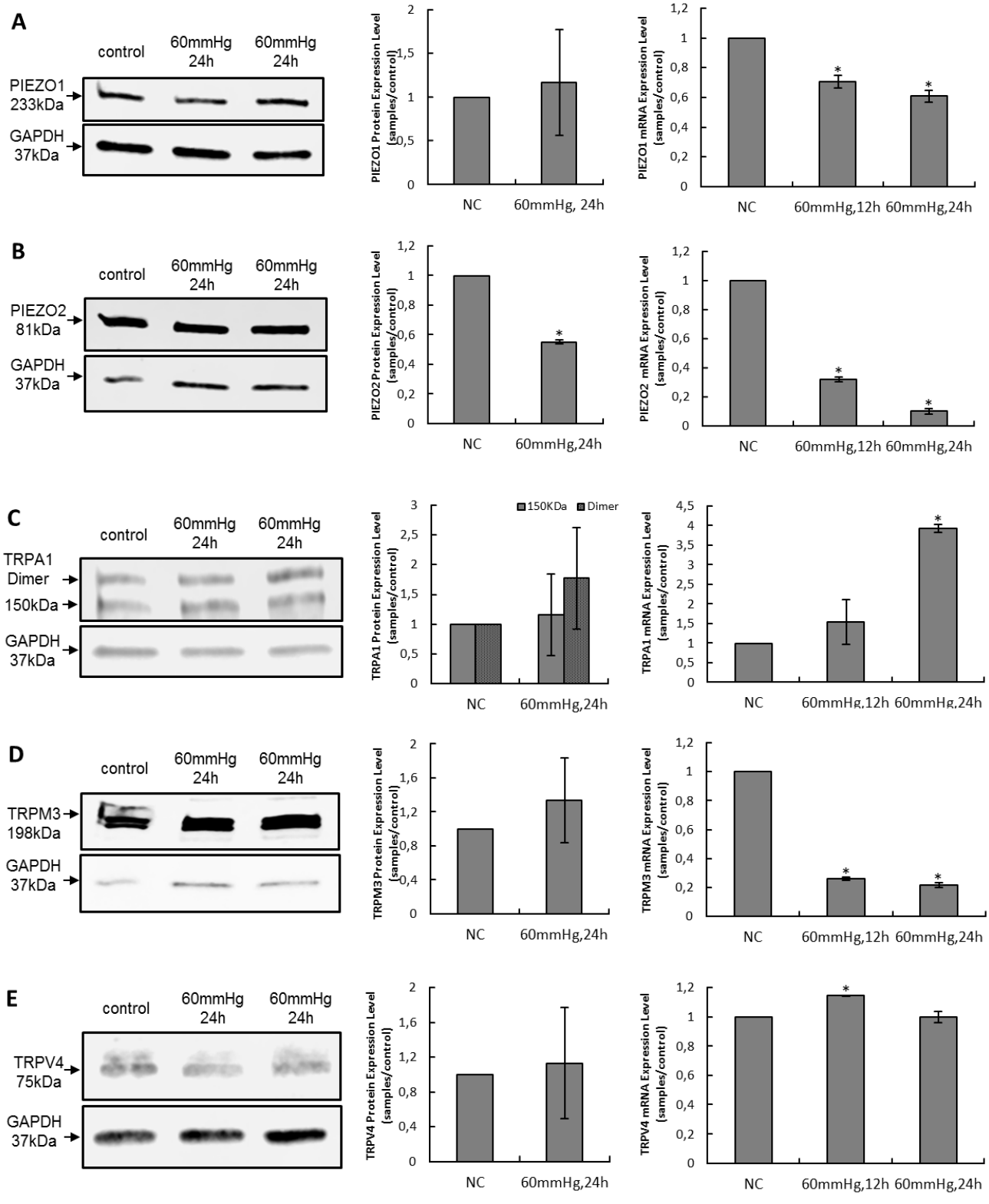
A
control
60mmHg 24h
60mmHg 24h
PIEZO1 233kDa
GAPDH 37kDa
PIEZO1 Protein Expression Level (samples/control)
NC
60mmHg, 24h
PIEZO1 mRNA Expression Level (samples/control)
NC
60mmHg,12h
60mmHg,24h
B
control
60mmHg 24h
60mmHg 24h
PIEZO2 81kDa
GAPDH 37kDa
PIEZO2 Protein Expression Level (samples/control)
NC
60mmHg,24h
PIEZO2 mRNA Expression Level (samples/control)
NC
60mmHg,12h
60mmHg,24h
C
control
60mmHg 24h
60mmHg 24h
TRPA1 Dimer
150kDa
GAPDH 37kDa
150KDa
Dimer
TRPA1 Protein Expression Level (samples/control)
NC
60mmHg,24h
TRPA1 mRNA Expression Level (samples/control)
NC
60mmHg,12h
60mmHg,24h
D
control
60mmHg 24h
60mmHg 24h
TRPM3 198kDa
GAPDH 37kDa
TRPM3 Protein Expression Level (samples/control)
NC
60mmHg,24h
TRPM3 mRNA Expression Level (samples/control)
NC
60mmHg,12h
60mmHg,24h
E
control
60mmHg 24h
60mmHg 24h
TRPV4 75kDa
GAPDH 37kDa
TRPV4 Protein Expression Level (samples/control)
NC
60mmHg,24h
TRPV4 mRNA Expression Level (samples/control)
NC
60mmHg,12h
60mmHg,24h

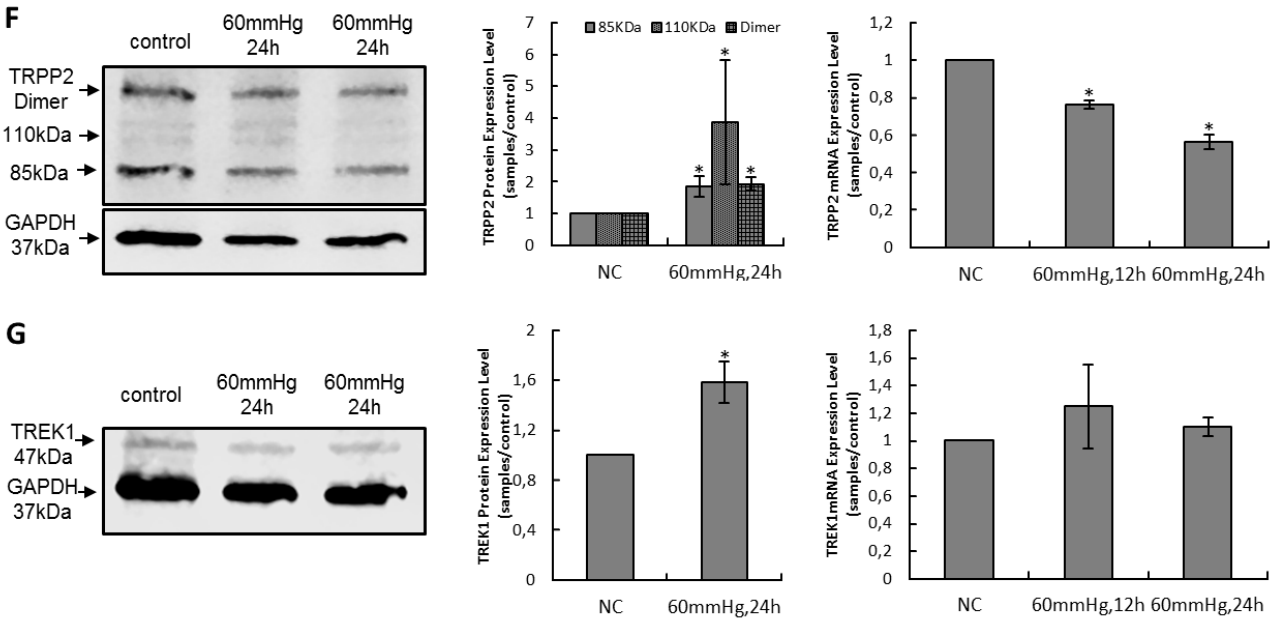

Figure 33. Analysis protein (left and middle) and mRNA (right) expression level of (A) PIEZO1, (B) PIEZO2, (C) TRPA1, (D) TRPM3, (E) TRPV4, (F) TRPP2 and (G) TREK1 in HNPCE after high hydrostatic pressure. (treated groups vs. control group: * $p < 0.05$).

Table 14. List of relative value of protein and mRNA level in the HNPCE after pressure

MSCs	Time	Relative Protein Level (P)	Relative mRNA Level (P)
PIEZO1	NC	1.00 ± 0.00 (-)	1.00 ± 0.00 (-)
	12 h	-	0.71 ± 0.04 (<0.0001)*
	24 h	1.17 ± 0.60 (0.5253)	0.61 ± 0.04 (<0.0001)*
PIEZO2	NC	1.00 ± 0.00 (-)	1.00 ± 0.00 (-)
	12 h	-	0.32 ± 0.02 (<0.0001)*
	24 h	0.55 ± 0.01 (<0.0001)*	0.10 ± 0.02 (<0.0001)*
TRPA1	NC	1.00 ± 0.00 (-)	1.00 ± 0.00 (-)
	12 h	-	1.54 ± 0.57 (0.084)
	24 h	1.15 ± 0.69(150kDa) (0.6108) 1.77 ± 0.86(Dimer) (0.0928)	3.94 ± 0.10 (<0.0001)*
TRPM3	NC	1.00 ± 0.00 (-)	1.00 ± 0.00 (-)
	12 h	-	0.26 ± 0.01 (<0.0001)*
	24 h	1.34 ± 0.50 (0.1735)	0.22 ± 0.02 (<0.0001)*
TRPV4	NC	1.00 ± 0.00 (-)	1.00 ± 0.00 (-)
	12 h	-	1.15 ± 0.01 (<0.0001)*
	24 h	1.13 ± 0.64 (0.6921)	1.00 ± 0.04 (0.9608)
TRPP2	NC	1.00 ± 0.00 (-)	1.00 ± 0.00 (-)
	12 h	-	0.76 ± 0.02 (<0.0001)*
	24 h	1.85 ± 0.32(85kDa) (0.0029) * 3.86 ± 1.95(110kDa) (0.0228) * 1,93 ± 0.20(Dimer) (0.0003) *	0.57 ± 0.04 (<0.0001)*
TREK1	NC	1.00 ± 0.00 (-)	1.00 ± 0.00 (-)
	12 h	-	1.25 ± 0.30 (0.1163)
	24 h	1.58 ± 0.17 (0.001) *	1.10 ± 0.06 (0.091)

Data are the mean ± SD; relative values were calculated as ratio pressure group (60 mm Hg) to control group (NAP). P values were calculated versus control (NAP) by Student's t-test. NC, negative control. * P < 0.05.

3.4 TRPP2 expression under different pressure level

3.4.1 TRPP2 siRNA treated in HNPCE cells

TRPP2 siRNA treated HNPCE cells expressed significantly low level of TRPP2 protein compared to either wild type un-transfected cells or scramble siRNA treated cells (Figure 34, 35).

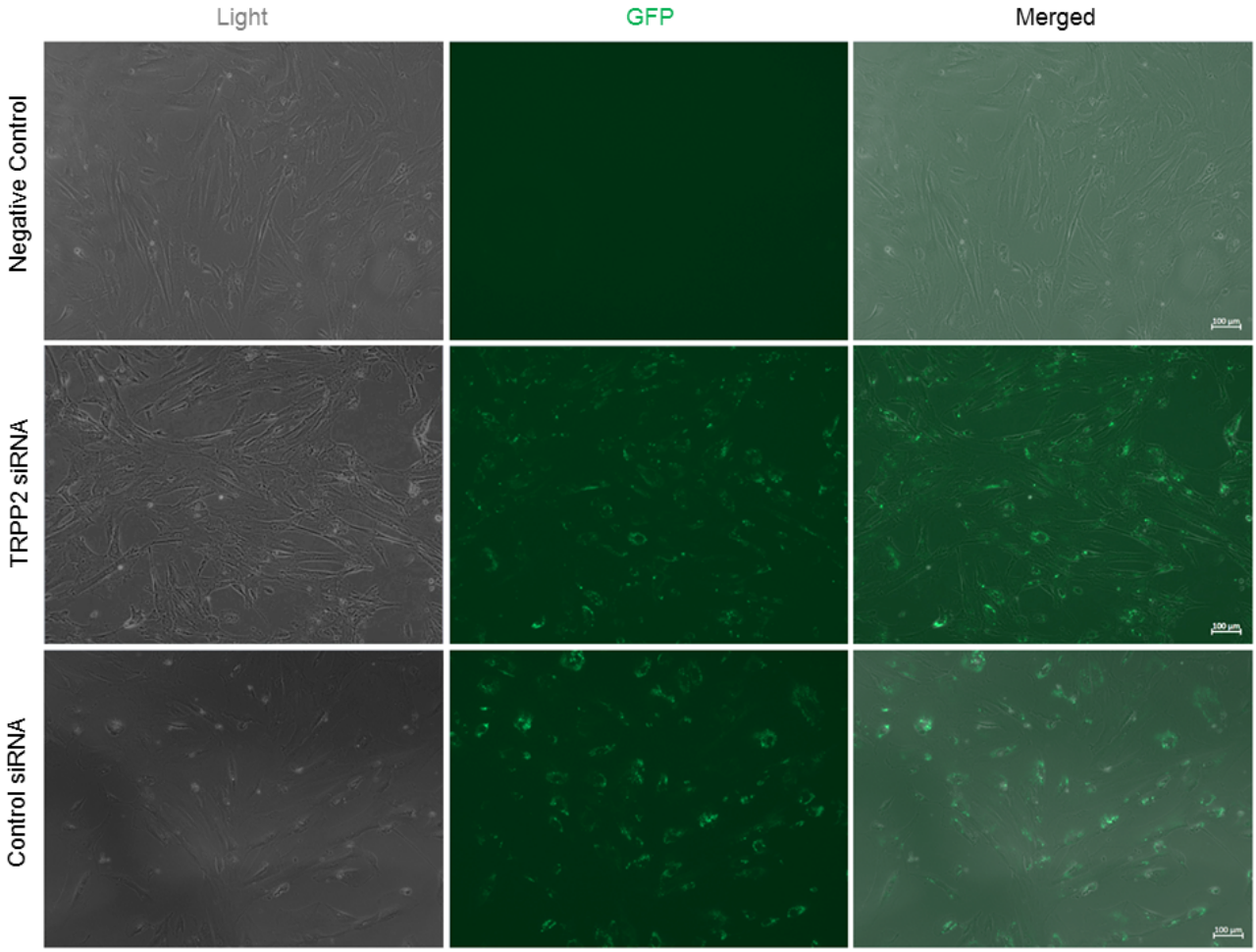

Figure 34. The expression of TRPP2 protein and siRNA in TRPP2-siRNA HNPCE cells. The transfection efficiency was estimated two days after transfection. The total cells and green fluorescent protein (GFP) expressed cells were observed under light and fluorescence microscopy, respectively. Light micrograph (left); Fluorescent micrograph (middle); Merged (right) (× 100).

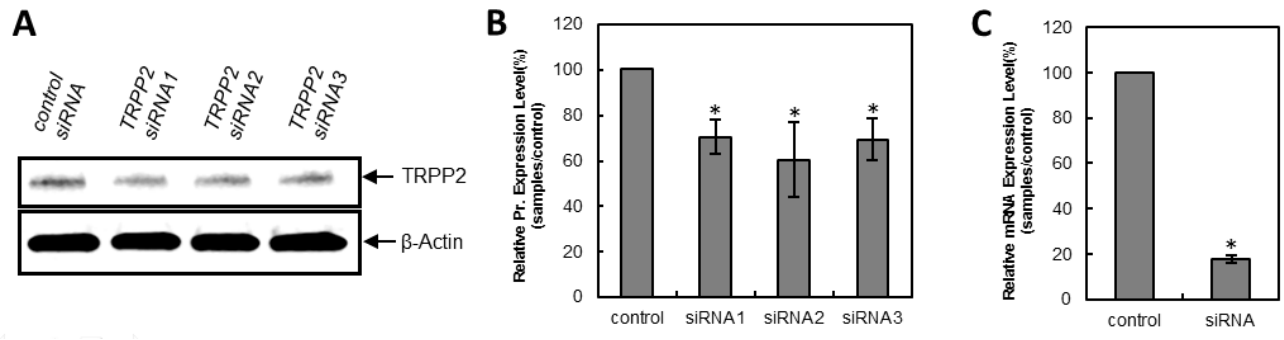

Figure 35. The expression of TRPP2 protein and siRNA in TRPP2-siRNA HNPCE cells. (A) Total cellular protein was extracted two days after infection and the protein level of TRPP2 was determined by western blot analysis using anti-TRPP2 antibody. (B) Quantitative analysis of TRPP2 level. TRPP2 siRNA showed significant effect in repressing TRPP2 expression, which repressed TRPP2 to 60 percent in protein level. values were calculated as ratio between the band intensity of TRPP2 and β-actin. (C) Bar graph represents the values of TRPP2 (mean ± standard deviation), which is calculated as ratio between TRPP2 levels of different siRNA samples and the average of those obtained from control siRNA, scramble sequences. Total RNA was extracted two days after infection. Actin expression was used as a control. Data are expressed as mean ± standard deviation calculated from three different experiments. *p<0,05 TRPP2 siRNA vs. Control siRNA.

3.4.2 Expression of TRPP2 with high hydrostatic pressure in HNPCE cells and siRNA-TRPP2 treated HNPCE cells

The expression of TRPP2 protein was measured 24 hours after being exposed to pressure, while the cell was simultaneously transfected with TRPP2-siRNA or control siRNA. The three bands of TRPP2 protein (~85kDa, ~110kDa and its dimer) were observed and quantified by western blot analysis.

In the control siRNA group, the 85kDa TRPP2 isoform increased about 50% after exposure to 60 mmHg hydrostatic pressure for 24 hours as compared to the NAP group. The 110kDa TRPP2 isoform in control siRNA group decreased about 60% after being treated with high pressure as compared to the NAP group. However, no significant changes of TRPP2 dimer was detected in high pressure group compared to NAP group.

Under NAP TRPP2-siRNA group, the expression of two TRPP2 isoforms (~85kDa and ~110kDa) in TRPP2 siRNA group were reduced about 70% more than the control siRNA group, while the expression of TRPP2 dimer did not show significant differences compared to control siRNA group.

However, after being induced by hydrostatic pressure for 24 hours, the expression of TRPP2 110kDa isoform and the dimer form TRPP2 silenced group were significantly reduced, 60% more than control siRNA group at NAP. The ~85kDa TRPP2 isoform, however, remained unchanged (Figure 36, Table 15).

Under hydrostatic pressure at 60 mmHg for 24 hours, the expression of 85kDa TRPP2 isoform decreased significantly; 50% in TRPP2-siRNA treated HNPCE cells comparing with the control siRNA treated HNPCE cells. No significant differences of 85kDa TRPP2 isoform and the dimer were detected after treated with hydrostatic pressure and siRNA.

In TRPP2 siRNA treated cells, hydrostatic pressure treated group did not show significant differences compared to the NAP group (Figure 36, Table 16).

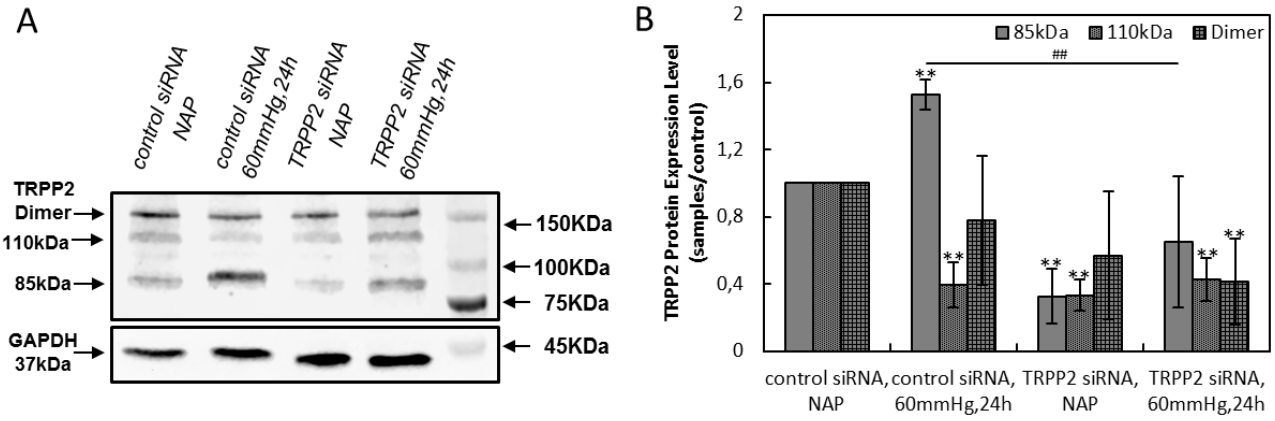

Figure 36. Elevated pressure on HNPCE cells increase TRPP2 expression. (A) Total cellular protein was extracted two days after pressure on HNPCE cells and determined by western blot analysis using anti-TRPP2 antibody. GAPDH was used as an internal control. (B) Quantitative analysis of TRPP2 protein expression of western blot. TRPP2 values were calculated as ratio between the band intensity of TRPP2 and GAPDH. Bars represent the values of TRPP2 (mean ± standard deviation), which is calculated as ratio between TRPP2 protein levels of treated group (TRPP2 siRNA or/and 60mmHg) and control group (control siRNA, NAP). Data are expressed as mean ± standard deviation calculated from two different experiments in duplicate. Group 2/ Group 3/Group 4 vs Group 1, *p<0,05, **p<0,01; Group 2 vs Group 4, $^{\#}$ P < 0.05, $^{\#\#}$ P < 0.01; Group 3 vs Group 4, $^{+}$ P < 0.05, $^{++}$ P < 0.01.

3.4.3 Analysis of expression changed of other MSCs candidate in siRNA-TRPP2 treated HNPCE cells under high pressure

Western blot analysis showed that after 24 hours hydrostatic pressure incubation the PIEZO1 protein level decreased significantly, about 8% in comparison to NAP. However,

when treated with TRPP2 siRNA, neither NAP nor 60mmHg high pressure for 24 hours did affected the expression of PIEZO1 in HNPCE cells significantly compared to control siRNA group (Figure 37A, Table 15).

The PIEZO2 protein level reduced nearly 50% when treated HNPCE cells with a pressure of only 60 mmHg high. TRPP2 siRNA treated cells showed decreased PIEZO2 protein level (reduced 30%) compared to control siRNA group in NAP. However, combined high pressure and TRPP2 siRNA did not significantly affect the expression of PIEZO2 when compared to NAP and control siRNA treated HNPCE cells (Figure 37B, Table 15).

Western blot analysis detected the dimer form and 150kDa isoform of TRPA1 proteins in HNPCE cells. Under NAP, TRPP2 siRNA treated HNPCE cells showed 50% less of 150kDa TRPA1 isoform when compared to control siRNA treated HNPCE cells. Under high pressure, treated HNPCE cells with TRPP2-siRNA did not affect the 150kDa TRPA1 isoform level compared to control siRNA group. Interestingly, incubated HNPCE cells under 60mmHg hydrostatic pressure for 24 hours significantly increased the TRPA1 dimer level. TRPA1 dimer in control siRNA treated group increased five times and TRPA1 dimer in TRPP2-siRNA treated group increased nine times. Treated HNPCE cells with TRPP2-siRNA only could also induce the TRPA1 dimer level for twofold in NAP (Figure 37C, Table 15).

Under high pressure conditions, the TRPM3 protein level decreased significantly about 37% and 14% when treated HNPCE cells with control siRNA and TRPP2-siRNA cells, respectively. No significant difference of TRPM3 protein level was observed between control siRNA and TRPP2-siRNA under NAP (Figure 37D, Table 15).

After transfection of TRPP2-siRNA cells, the TRPV4 protein level deceased 50% compared to control siRNA HNPCE cells under NAP. When treated HNPCE cells with control siRNA only, high pressure incubation led to decreased expression of TRPV4 protein to 40% compared to NAP group. However, when cells were treated with both TRPP2-siRNA and hydrostatic pressure, no expression change of TRPV4 was observed compared to treated cells with control siRNA and NAP (Figure 37E, Table 15).

After incubation under 60mmHg hydrostatic pressure 24 hours, the TREK1 protein decreased about 45% and 50% in control siRNA and TRPP2-siRNA groups, respectively. No significantly differences of TREK1 protein level were observed when treated cell with TRPP2-siRNA or control siRNA under NAP (Figure 37F, Table 15).

Taking this into account, after hydrostatic pressure at 60mmHg treatment for 24 hours, transfection HNPCE cells with TRPP2-siRNA led to a 50% increased expression of TRPA1 dimer and increased expression of TRPM3 of 20%, when compared to control siRNA transfected cells (Figure 37C, D, Table 16). The same change could not be replicated with the other MSCs candidates.

In TRPP2-siRNA transfected cells, hydrostatic pressure treatment led to reduced TRPA1 ~150kDa isoform and dimer form levels compared to NAP treatment (Figure 37C, Table 16). There were no significant changes in other MSCs candidates under the same situation.

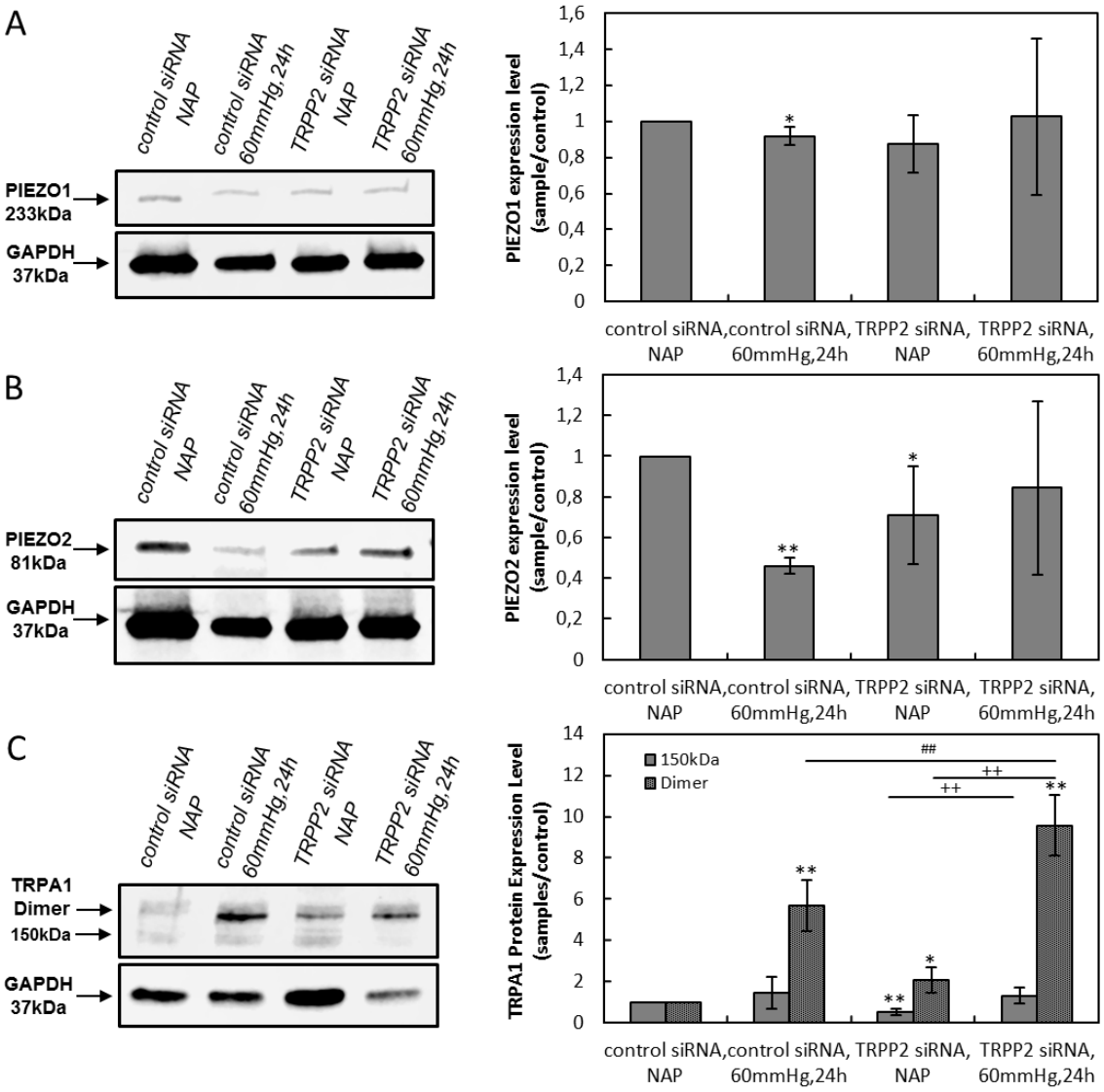
A
control siRNA NAP
control siRNA 60mmHg,24h
TRPP2 siRNA NAP
TRPP2 siRNA 60mmHg,24h
PIEZO1 233kDa
GAPDH 37kDa
PIEZO1 expression level (sample/control)
1,6
1,4
1,2
1
0,8
0,6
0,4
0,2
0
control siRNA, NAP
control siRNA, 60mmHg,24h
TRPP2 siRNA, NAP
TRPP2 siRNA, 60mmHg,24h
B
control siRNA NAP
control siRNA 60mmHg,24h
TRPP2 siRNA NAP
TRPP2 siRNA 60mmHg,24h
PIEZO2 81kDa
GAPDH 37kDa
PIEZO2 expression level (sample/control)
1,4
1,2
1
0,8
0,6
0,4
0,2
0
control siRNA, NAP
control siRNA, 60mmHg,24h
TRPP2 siRNA, NAP
TRPP2 siRNA, 60mmHg,24h
C
control siRNA NAP
control siRNA 60mmHg,24h
TRPP2 siRNA NAP
TRPP2 siRNA 60mmHg,24h
TRPA1 Dimer 150kDa
GAPDH 37kDa
TRPA1 Protein Expression Level (samples/control)
150kDa
Dimer
##
++
++
14
12
10
8
6
4
2
0
control siRNA, NAP
control siRNA, 60mmHg,24h
TRPP2 siRNA, NAP
TRPP2 siRNA, 60mmHg,24h

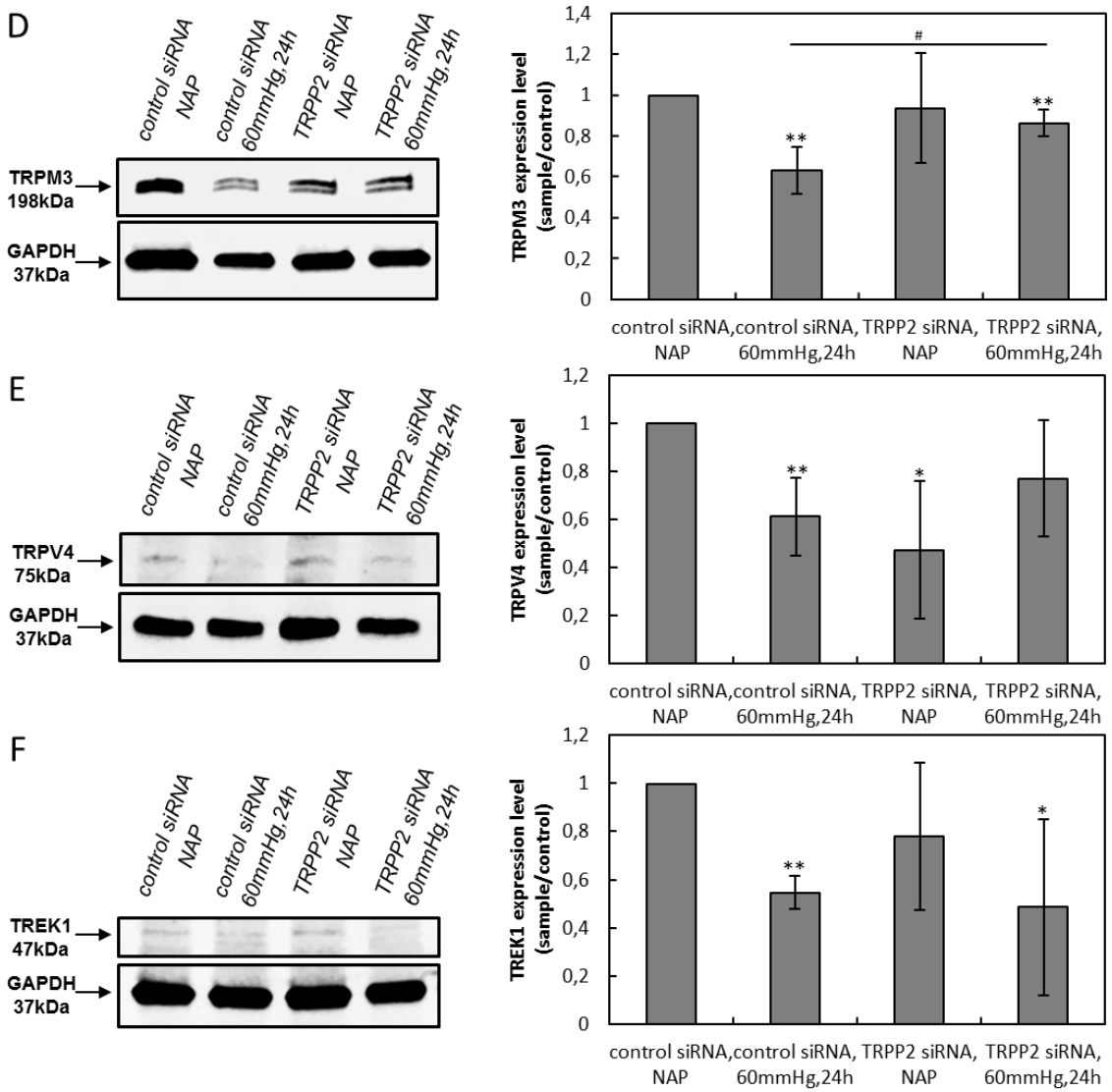

Figure 37. Analysis of PIEZO1(A), PIEZO2(B), TRPA1(C), TRPM3(D), TRPV4(E) and TREK1(F) expression in TRPP2 knockdown HNPCE after high pressure. The protein expression levels were calculated as the ratio between band intensity of the treated group and control group, while the expression of treated group was calculated as ratio among the band relative to these proteins and GAPDH. Data are expressed as mean ± standard deviation calculated from at least two different experiments in duplicate. Group 2/ Group 3/Group 4 vs Group 1, *p<0,05, **p<0,01; Group 2 vs Group 4, $^{\#}$ P < 0.05, $^{\#\#}$ P < 0.01; Group 3 vs Group 4, $^{+}$ P < 0.05, $^{++}$ P < 0.01.

Table 15. List of relative value of protein level in TRPP2 siRNA HNPCE after pressure

MSCs	Group	Relative Protein Level (P)
PIEZO1	control siRNA, NAP	1.00 ± 0.00 (-)
	control siRNA, 60mmHg	0.92 ± 0.05 (0.015)*
	TRPP2 siRNA, NAP	0.87 ± 0.16 (0.1245)
	TRPP2 siRNA, 60mmHg	1.02 ± 0.43 (0.8952)
PIEZO2	control siRNA, NAP	1.00 ± 0.00 (-)
	control siRNA, 60mmHg	0.46 ± 0.04 (<0.0001)**
	TRPP2 siRNA, NAP	0.71 ± 0.24 (0.0429)*
	TRPP2 siRNA, 60mmHg	0.85 ± 0.43 (0.4281)

TRPA1	control siRNA, NAP	1.00 ± 0.00(150kDa) (-) 1.00 ± 0.00(Dimer) (-)
	control siRNA, 60mmHg	1.47 ± 0.77(150kDa) (0.2075) 5.68 ± 1.23(Dimer) (0.0007)**
	TRPP2 siRNA, NAP	0.51 ± 0.16(150kDa) (0.0016)** 2.07 ± 0.62(Dimer) (0.0138)*
	TRPP2 siRNA, 60mmHg	1.32 ± 0.37(150kDa) (0.0992) 9.56 ± 1.46(Dimer) (0.0001) **
TRPM3	control siRNA, NAP	1.00 ± 0.00 (-)
	control siRNA, 60mmHg	0.63 ± 0.11 (0.0014)**
	TRPP2 siRNA, NAP	0.94 ± 0.27 (0.5966)
	TRPP2 siRNA, 60mmHg	0.86 ± 0.06 (0.0065)**
TRPV4	control siRNA, NAP	1.00 ± 0.00 (-)
	control siRNA, 60mmHg	0.61 ± 0.16 (0.0042)**
	TRPP2 siRNA, NAP	0.47 ± 0.29 (0.0106)*
	TRPP2 siRNA, 60mmHg	0.77 ± 0.24 (0.0812)
TRPP2	control siRNA, NAP	1.00 ± 0.00(85kDa) (-) 1.00 ± 0.00(110kDa) (-) 1.00 ± 0.00(Dimer) (-)
	control siRNA, 60mmHg	1.53 ± 0.08(85kDa) (<0.0001)** 0.39 ± 0.14(110kDa) (0.0004)** 0.78 ± 0.38(Dimer) (0.2246)
	TRPP2 siRNA, NAP	0.33 ± 0.16(85kDa) (0.0005)** 0.33 ± 0.09(110kDa) (<0.0001)** 0.57 ± 0.38(Dimer) (0.0504)
	TRPP2 siRNA, 60mmHg	0.65 ± 0.39(85kDa) (0.0923) 0.43 ± 0.13(110kDa) (0.0004)** 0.41 ± 0.26(Dimer) (0.0049)**
TREK1	control siRNA, NAP	1.00 ± 0.00 (-)
	control siRNA, 60mmHg	0.55 ± 0.07 (<0.0001)**
	TRPP2 siRNA, NAP	0.78 ± 0.31 (0.1518)
	TRPP2 siRNA, 60mmHg	0.49 ± 0.36 (0.0262)*

Data are the mean ± SD; relative values were calculated as ratio Group 2/ Group 3/Group 4 to Group 1. P values were calculated versus control siRNA (NAP) by Student's t-test. * $P < 0.05$, ** $P < 0.01$.

Table 16. List of relative value of protein level in TRPP2 siRNA HNPCE after pressure

MSCs	Group 2 vs Group 4 (60mmHg: control siRNA vs TRPP2 siRNA)	Group 3 vs Group 4 (TRPP2 siRNA: NAP vs 60mmHg)
PIEZO1	0.5736	0.4647
PIEZO2	0.0929	0.5362
TRPA1	0.688 (150kDa) $0.0076^{\#\#}$ (Dimer)	0.0078^{++} (150kDa) 0.0003^{++} (Dimer)
TRPM3	$0.0125^{\#}$	0.5493
TRPV4	0.2546	0.124

TRPP2	0.0057## (85kDa) 0.6792 (110kDa) 0.1266 (Dimer)	0.1318 (85kDa) 0.2194 (110kDa) 0.4506 (Dimer)
TREK1	0.7069	0.2064

P values were calculated Student's t-test. # P < 0.05, ## P < 0.01, ++ P < 0.01.

3.5 PIEZO2 expression under different pressure level

3.5.1 Selection of PIEZO2 siRNA

Four different PIEZO2 siRNA were transfected them into primary cultured HNPCE cells separately. qRT-PCR analysis was performed to analysis the PIEZO2 mRNA level after transfection of siRNA. One siRNA (siRNA1) showed strongest effect in repressing the mRNA level of PIEZO2. PIEZO2 siRNA1 transfection in primary cultured HNPCE cells could reduce the expression of PIEZO2 protein to 35% compared to wild type cells or control siRNA transfected cells (Figure 38).

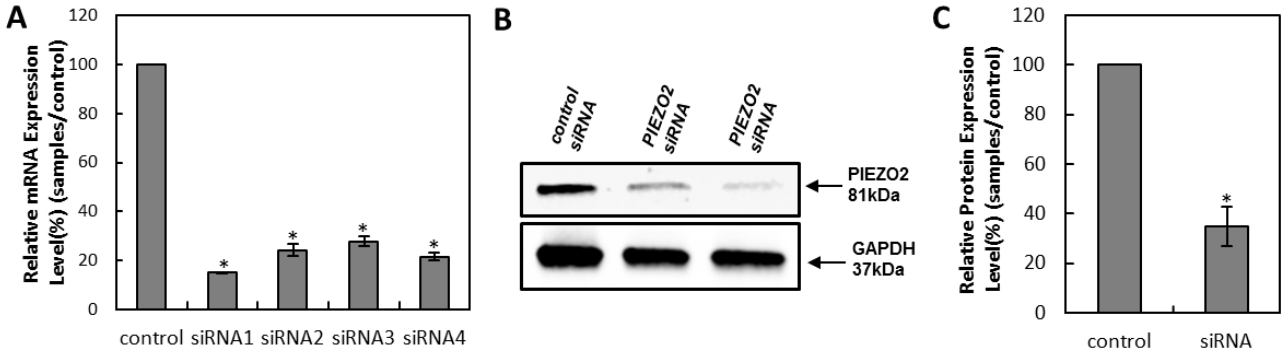

Figure 38. The expression of PIEZO2 protein and siRNA in PIEZO2-siRNA HNPCE cells. (A) qRT-PCR analysis the effect of PIEZO2 siRNA. Total RNA was extracted two days after infection, and relative PIEZO2 mRNA expression was determined by qRT-PCR. Actin expression was used as a loading control. Data are presented as mean ± SD of three independent experiments. *p<0,05 PIEZO2 siRNA vs. Control siRNA; (B) Total cellular protein was extracted two days after infection and the protein level of TRPP2 was determined by western blot analysis using anti-PIEZO2 antibody. GAPDH was used as an internal control; (C) Quantitative analysis of PIEZO2 level. PIEZO2-siRNA cells showed significant effect in repressing PIEZO2 protein expression, which repressed PIEZO2 to 40% in protein level. Values were calculated as ratio between the band intensity of PIEZO2 and GAPDH. *p<0,05 PIEZO2 siRNA vs. Control siRNA.

3.5.2 Expression of PIEZO2 with high hydrostatic pressure in HNPCE cells and siRNA-PIEZO2 treated HNPCE cells

The expression of PIEZO2 protein were measured 24 hours after being exposed to pressure, the cells were simultaneously transfected with PIEZO2-siRNA or control siRNA. The bands of PIEZO2 protein (~81kDa) were observed and quantified by western blot analysis.

In control siRNA group, the protein expression of PIEZO2 decreased significantly by about 50% after 60 mmHg hydrostatic pressure for 24 hours when compared to NAP group. In PIEZO2-siRNA group, the PIEZO2 protein level decreased significantly, about 48% and 39% of control siRNA in NAP group and hydrostatic pressure loaded group, respectively (Figure 39, Table 17).

There was no significant difference between PIEZO2-siRNA group and control siRNA group when incubate under hydrostatic pressure at 60 mmHg for 24 hours.

In PIEZO2-siRNA treated cells, the expression of PIEZO2 protein decreased significantly by about 20% in the hydrostatic pressure loaded group comparing with NAP group (Figure 39, Table 18).

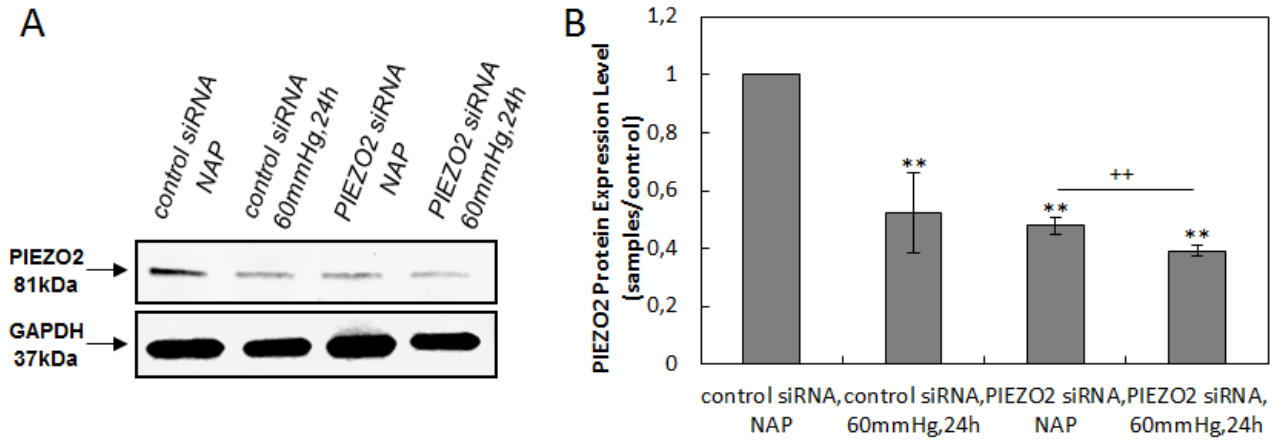

Figure 39. Elevated pressure on HNPCE cells increase PIEZO2 expression. (A) Total cellular protein was extracted two days after pressure on HNPCE cells and determined by western blot analysis using anti-PIEZO2 antibody. GAPDH was used as an internal control. (B) Quantitative analysis of PIEZO2 protein expression of western blot. PIEZO2 values were calculated as ratio between the band intensity of PIEZO2 and GAPDH. Bars represent the values of PIEZO2 (mean ± standard deviation), which is calculated as ratio between PIEZO2 levels of treated group (PIEZO siRNA or/and 60mmHg) and control group (control siRNA, NAP). Data are expressed as mean ± standard deviation calculated from two different experiments in

duplicate. Group 2/ Group 3/Group 4 vs Group 1, *p<0,05, **p<0,01; Group 2 vs Group 4, # P < 0.05, ## P < 0.01; Group 3 vs Group 4, + P < 0.05, ++ P < 0.01.

3.5.3 Analysis of expression changed of other MSCs candidate in siRNA-PIEZO2 treated HNPCE cells after high pressure

Western blot analysis showed that after 24 hours hydrostatic pressure incubation the PIEZO1 protein level significantly increased by about 10% compared with NAP. When cells were treated with PIEZO2-siRNA, PIEZO1 protein expression level were 70% and 200% higher than control group, in NAP and hydrostatic pressure group respectively (Figure 40A, Table 17).

The high-pressure incubation only led the 150kDa isoform and dimer of TRPA1 raise 40% and 76%, respectively. Under NAP, treated HNPCE cells with PIEZO2-siRNA did not affect the level of TRPA1 150kDa isoform compared to control siRNA group, while the TRPA1 dimer form expression significantly increased 60% compared to NAP and control siRNA group. High pressure and PIEZO2-siRNA treated HNPCE cells showed 50% less of 150kDa TRPA1 isoform than NAP control siRNA treated HNPCE cells. However, the dimer form raised five times in high pressure PIEZO2-siRNA treated cells for 24 hours (Figure 40B, Table 17).

Under NAP conditions, transfection of PIEZO2-siRNA into HNPCE cells, the TRPM3 protein level significantly increased, 30% compared to control siRNA transfected HNPCE cells. When treated HNPCE cells with high pressure and control siRNA, the expression of TRPM3 protein decreased to 50% compared to NAP and control siRNA group. However, when treated cells with both PIEZO2-siRNA and hydrostatic high pressure, the expression of TRPM3 significantly increased about 50% compared to treated cells with NAP and control siRNA and group (Figure 40C, Table 17).

Under high pressure condition, the TRPV4 protein level significantly decreased to 52% and 54% when HNPCE cells were treated with control siRNA or PIEZO2-siRNA cells, respectively. Under NAP condition, TRPP2-siRNA treated cells led to significantly

decreased TRPV4 protein levels to 60% when transfected cells with PIEZO2-siRNA compared to treated cells with control siRNA (Figure 40D, Table 17).

The TRPP2 isoform (~85kDa) and dimer form apparently by using western blot analysis, but the TRPP2 isoform (~110kDa) was very weak. After hydrostatic pressure-incubation for 24 hours, TRPP2 both the two isoforms and the dimer form levels were two times more than NAP treated group. However, in NAP, treated HNPCE cells with PIEZO2-siRNA or control siRNA did not show difference of TRPP2 protein level. The 85kDa isoform of TRPP2 protein level increased 50% in high pressure and PIEZO2-siRNA treated HNPCE cells compared to NAP and PIEZO2-siRNA treated HNPCE cells, while no significant differences were observed with either the 110kDa TRPP2 isoform or the dimer form (Figure 40E, Table 17).

After incubation under 60mmHg hydrostatic high pressure for 24 hours, the TREK1 protein level was not significantly different from NAP. However, in PIEZO2-siRNA treated cells, the TREK1 protein increased about two times and 69%, respectively, when treated cell under NAP or hydrostatic pressure for 24 hours (Figure 40F, Table 17).

Taking this into account, after treated cells with hydrostatic high pressure at 60 mmHg treatment for 24 hours, transfection HNPCE cells with PIEZO2-siRNA led to a doubled expression of PIEZO1, tripled expression of TRPA1 dimer, 70% increased expression of TRPM3 and 30% increased expression of TREK1, when compared to high pressure treated but control siRNA transfected cells (Figure 40A, B, C, F, Table 18). The expression of the 150kDa isoform of TRPA1 and the 85kDa, 110kDa isoform and dimer of TRPP2 significantly decreased about 70%, 20%, 50% and 40% separately (Figure 40B, E, Table 16). No significant differences were found in the change of TRPV4 protein expression (Figure 40D, Table 18).

In PIEZO2-siRNA transfected cells, hydrostatic high-pressure treatment led to reduction of half of TRPA1 (~150kDa) isoform and 20% of TREK1 protein levels compared to NAP treatment in HNPCE cells (Figure 40B, F, Table 18). However, an increase of 40% of PIEZO1, threefold of TRPA1 dimer, twice of TRPM3, 35% of TRPV4 and 70% of TRPP2

isoform (~85kDa) protein were observed, separately (Figure 40A, B, C, D, E, Table 18). There were no significant changes in the protein expression change of TRPP2 isoform (~110kDa) and dimer form (Figure 40E, Table 18).

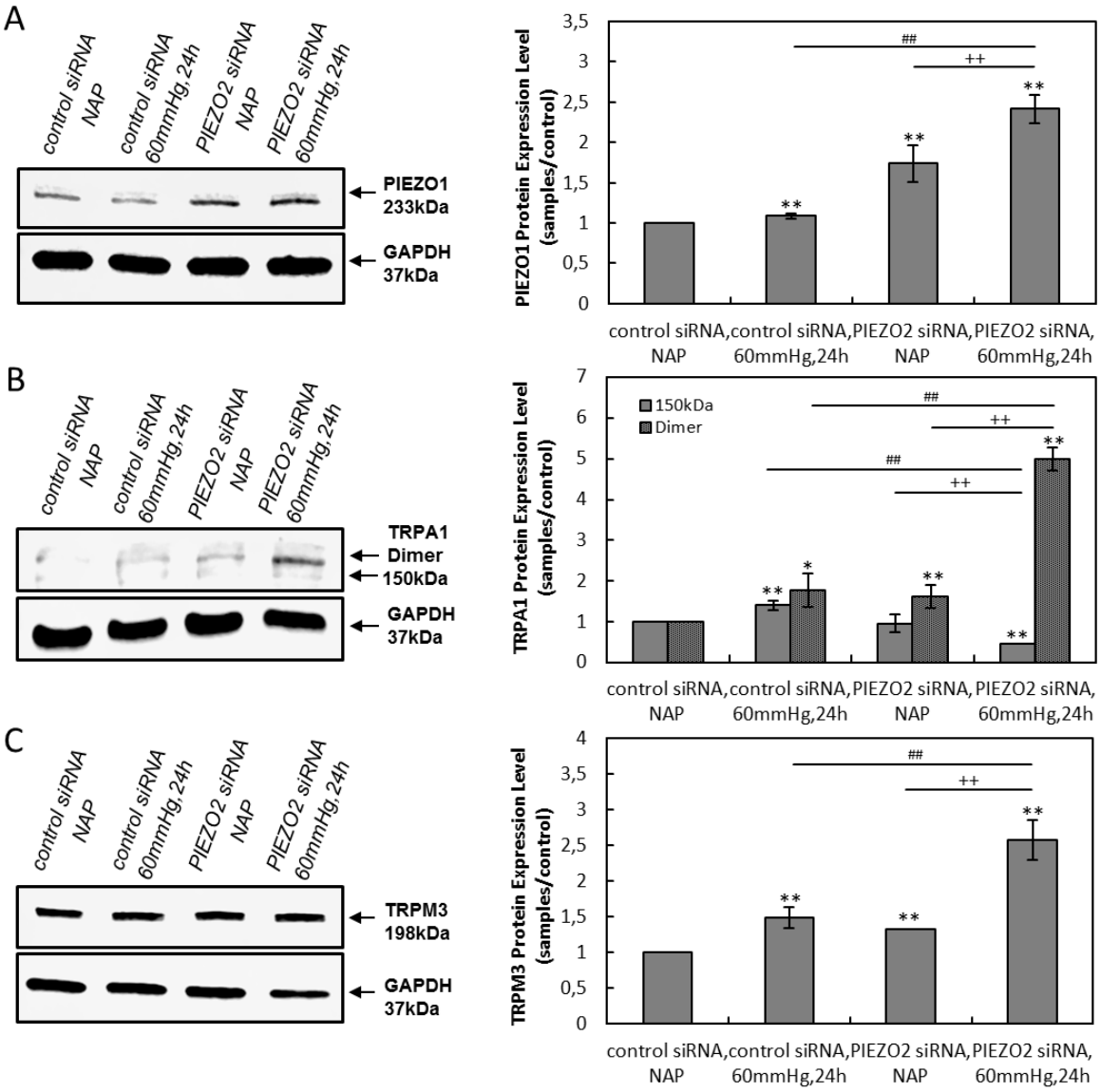

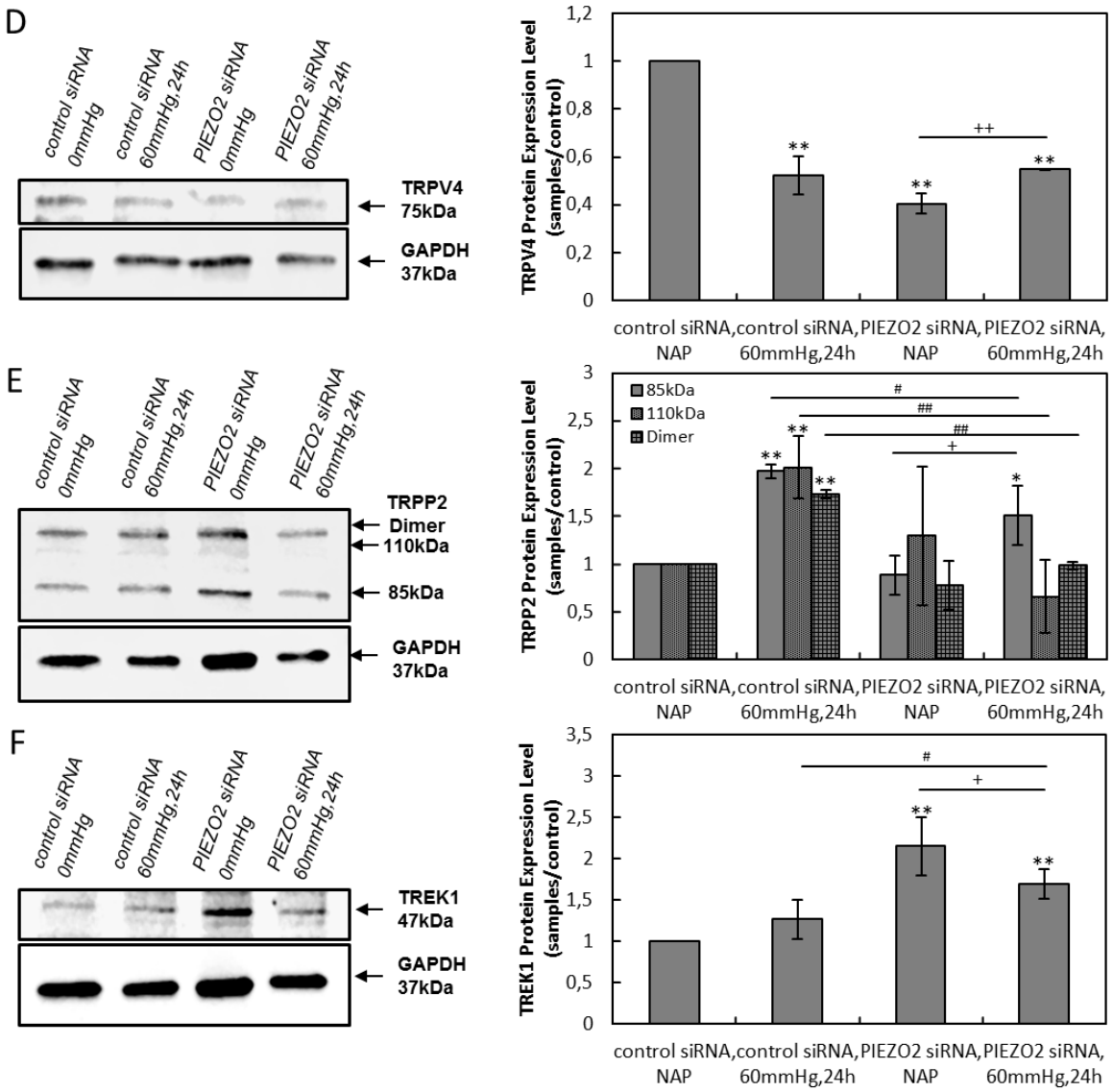

Figure 40. Analysis of PIEZO1(A), TRPA1(B), TRPM3(C), TRPV4(D), TRPP2(E) and TREK1(F) expression in PIEZO2 knockdown HNPCE after high pressure. The protein expression levels were calculated as the ratio between band intensity of the treated group and control group, while the expression of treated group was calculated as ratio among the band relative to these proteins and GAPDH. Data are expressed as mean ± standard deviation calculated from at least two different experiments in duplicate. Group 2/ Group 3/Group 4 vs Group 1, *p<0,05, **p<0,01; Group 2 vs Group 4, $^{\#}$ P < 0.05, $^{\#\#}$ P < 0.01; Group 3 vs Group 4, $^{+}$ P < 0.05, $^{++}$ P < 0.01.

Table 17. List of relative value of protein level in PIEZO2 siRNA HNPCE after pressure

MSCs	Group	Relative Protein Level (P)
PIEZO1	control siRNA, NAP	1.00 ± 0.00 (-)
	control siRNA, 60mmHg	1.09 ± 0.03 (0.002)**
	PIEZO2 siRNA, NAP	1.74 ± 0.23 (0.0013)**
	PIEZO2 siRNA, 60mmHg	2.42 ± 0.18 (<0.0001)**
PIEZO2	control siRNA, NAP	1.00 ± 0.00 (-)
	control siRNA, 60mmHg	0.52 ± 0.14 (0.0011)**

	PIEZO2 siRNA, NAP	0.48 ± 0.03 (<0.0001)**
	PIEZO2 siRNA, 60mmHg	0.39 ± 0.02 (<0.0001)**
TRPA1	control siRNA, NAP	1.00 ± 0.00(150kDa) (-) 1.00 ± 0.00(Dimer) (-)
	control siRNA, 60mmHg	1.40 ± 0.11(150kDa) (0.001)** 1.76 ± 0.41(Dimer) (0.0105)*
	PIEZO2 siRNA, NAP	0.96 ± 0.22(150kDa) (0.6646) 1.61 ± 0.28(Dimer) (0.0059)**
	PIEZO2 siRNA, 60mmHg	0.46 ± 0.01(150kDa) (<0.0001)** 4.99 ± 0.27(Dimer) (<0.0001)**
TRPM3	control siRNA, NAP	1.00 ± 0.00 (-)
	control siRNA, 60mmHg	1.49 ± 0.15 (0.0013)**
	PIEZO2 siRNA, NAP	1.32 ± 0.01 (<0.0001)**
	PIEZO2 siRNA, 60mmHg	2.58 ± 0.28 (0.0002)**
TRPV4	control siRNA, NAP	1.00 ± 0.00 (-)
	control siRNA, 60mmHg	0.52 ± 0.08 (0.0001)**
	PIEZO2 siRNA, NAP	0.40 ± 0.04 (<0.0001)**
	PIEZO2 siRNA, 60mmHg	0.54 ± 0.01 (<0.0001)**
TRPP2	control siRNA, NAP	1.00 ± 0.00(85kDa) (-) 1.00 ± 0.00(110kDa) (-) 1.00 ± 0.00(Dimer) (-)
	control siRNA, 60mmHg	1.97 ± 0.08(85kDa) (<0.0001)** 2.01 ± 0.33(110kDa) (0.0016)** 1.73 ± 0.04(Dimer) (<0.0001)**
	PIEZO2 siRNA, NAP	0.89 ± 0.21(85kDa) (0.2582) 1.30 ± 0.72(110kDa) (0.3732) 0.78 ± 0.25(Dimer) (0.0979)
	PIEZO2 siRNA, 60mmHg	1.51 ± 0.31(85kDa) (0.0148)* 0.99 ± 0.04(110kDa) (0.0997) 0.99 ± 0.04(Dimer) (0.4684)
TREK1	control siRNA, NAP	1.00 ± 0.00 (-)
	control siRNA, 60mmHg	1.26 ± 0.24 (0.0543)
	PIEZO2 siRNA, NAP	2.15 ± 0.36 (0.0014)**
	PIEZO2 siRNA, 60mmHg	1.69 ± 0.18(0.0007)**

Data are the mean ± SD; relative values were calculated as ratio Group 2/ Group 3/Group 4 to Group 1. P values were calculated versus control siRNA (NAP) by Student's t-test. * P < 0.05, ** P < 0.01.

Table 18. List of relative value of protein level in PIEZO2 siRNA HNPCE after pressure

MSCs	Group 2 vs Group 4 (60mmHg: control siRNA vs PIEZO2 siRNA)	Group 3 vs Group 4 (PIEZO2 siRNA: NAP vs 60mmHg)
PIEZO1	$<0.0001^{\#\#}$	0.0043^{++}
PIEZO2	0.0791	0.0029^{++}
TRPA1	$<0.0001^{\#\#}$ (150kDa) $<0.0001^{\#\#}$ (Dimer)	0.0052^{++} (150kDa) $<0.0001^{++}$ (Dimer)
TRPM3	$0.0011^{\#\#}$	0.0004^{++}

TRPV4	0.4975	0.0011^{++}
TRPP2	$0.0235^{\#}$ (85kDa) $0.0028^{\#\#}$ (110kDa) $<0.0001^{\#\#}$ (Dimer)	0.0143^{+} (85kDa) 0.1319 (110kDa) 0.1164 (Dimer)
TREK1	$0.0255^{\#}$	0.0477^{+}

P values were calculated Student's t-test. $^{\#}$ $P < 0.05$, $^{\#\#}$ $P < 0.01$, $^{+}$ $P < 0.05$, $^{++}$ $P < 0.01$.

4. Discussion

In this study, the expression and localization of the seven MSCs candidates (PIEZO1, PIEZO2, TRPA1, TRPM3, TRPV4, TRPP2 and TREK1) were analyzed in the rat eye. Furthermore, the expression pattern was studied analogously in human specimen, focusing on the CB. The expression of MSCs as candidates of pressure sensors in the HNPCE cells was analyzed. The co-localization of MSCs candidates with primary cilia in HNPCE cells was characterized as well. In addition, an assessment of the interaction or potential role of TRPP2 and PIEZO2 in the sensation of hydrostatic pressure was investigated by examining the expression of the proteins in relation to different time of hydrostatic pressure conditions.

4.1 Expression and localization of MSCs in tissue types of the eye

In order to characterize the potential function of MSCs in sensing the IOP, the expression of putative MSCs in the eyes was determined by using immunostaining, western blotting, conventional PCR and quantitative real-time PCR method. The PIEZO channels (PIEZO1 and PIEZO2), four TRP members and TREK1 were selected as the candidate genes because they are related to mechanosensing in many tissues (Coste et al., 2010; Delmas et al., 2011).

4.1.1 PIEZO family

The PIEZO proteins are essential component of mechanotransduction and widely expressed in mammalian tissues, which may indicate that PIEZO involved in mechanical transduction in various organs (Coste et al., 2010). There are two members in the PIEZO family, PIEZO1 and PIEZO2. The expression of PIEZO1 was found in the bladder, colon, kidney, lung, and skin, while PIEZO2 was expressed in the bladder, colon, and lung, as well as in dorsal root ganglia, but low expressed in kidney or in skin (Coste et al., 2010). Many studies have showed that PIEZO family plays a critical role in sensing blood pressure. For example, PIEZO1 has the function of regulating of pressure-induced hyperpermeability in endothelial cells of the lung vascular via disruption of the adherens junctions (Friedrich et

al., 2019). PIEZO1 mediates fluid shear stress–induced releasing of adrenomedullin and ATP in endothelial cells in blood vascular, through which to regulate vascular tone and blood pressure (Iring et al., 2019; Wang et al., 2016). PIEZO channels were also detected in the carotid sensory neurons and were considered as the long-sought baroreceptor, which is critical in controlling acute blood pressure (Zeng et al., 2018). As PIEZO channel has mechanosensitive function in vascular system, it may indicate that it has similar functions in regulating aqueous humor of ocular tissues.

Recent studies have shown that PIEZO1 was robustly expressed in primary cultured human TM cells, as well as in the ciliary body and cornea of normotensive mice (Yarishkin et al., 2021). It can also regulate the trabecular components of aqueous humor outflow (Yarishkin et al., 2021). Another study using immunostaining and western blot analysis also detected the expression of PIEZO1 in human and mouse TM (Zhu et al., 2021). As PIEZO1 was found in TM cells, it may have a potential function in regulating aqueous humor. PIEZO1 has been identified as the key TM mechanosensor for stretch, shear flow and pressure detection, as its activation causes intracellular signals to change the cytoskeleton and cell-extracellular matrix contact tissues.

Patch clamp recording showed that mechanical stimulation can activate Piezo1 currents in TM cells in human and mouse (Zhu et al., 2021). Similar to our studies and other reports all found that PIEZO1 was expressed on the plasma membrane and in the cytoplasm (near the nucleus) in HNPCE cells (Figure 8 and 10A) (Coste et al., 2010; McHugh et al., 2010; Miyamoto et al., 2014). In urothelial cell cultures, the expression of PIEZO1 in the plasma membrane may indicate its function as a stretch-activated channel, through which to mediate Ca^{2+} influx and ATP release (Miyamoto et al., 2014). In human red blood cells, similar function of Piezo1 in regulating Ca^{2+} influx was found as well (Cinar et al., 2015). In this study, the expression of PIEZO1 in HNPCE cells may indicate the same role in regulatory Ca^{2+} flux in HNPCE cells. Nevertheless, the role of the PIEZO1 in HNPCE cells is unclear so far and needs further characterization.

Another PIEZO protein, PIEZO2, showed several similarities to PIEZO1. For example, PIEZO1 and PIEZO2 showed very similar expression pattern in eyes. Tran and colleagues found that PIEZO1 and PIEZO2 are two of the 11 MSCs found in the TM of the human eye (Tran et al., 2014). Astrocytes in the ON head also express both PIEZO1 and PIEZO2 (Choi et al., 2015). In the present study, PIEZO1 and PIEZO2 were found widely expressed in both human and rat eyes with the highest expression level in the CB and retina.

PIEZO1 and PIEZO2 also showed many differences as well. For instance, PIEZO1 mainly expressed in non-sensory tissues, while PIEZO2 in sensory neurons (Wu et al., 2017).

In the eye, PIEZO2 expressed in a subpopulation of corneal afferent neurons, like pure mechanical nociceptors which can sense harmful mechanical stimuli of the cornea (Bron et al., 2014). Recently report showed that PIEZO2 has an important role in regulating mechanically activated currents of different dynamics in corneal trigeminal neurons and can also transduce mechanical force through corneal nociceptors (Fernández-Trillo et al., 2020). The current study showed that the PIEZO2 is not only distributed in normotensive rat corneas, but also in TM and CB of rat eyes and in human CB and HNPCE cells.

A poor correlation between mRNA (Figure 9C; Figure 12C) and protein (Figure 9A, B; Figure 12A, B) level was found both in PIEZO1 and PIEZO2. The reasons might be that: (1) the process of translating mRNA into protein involves many complexes and diverse post transcriptional modifications to occur, (2) the half-lives of proteins in vivo may differ substantially, (3) there are errors and noise during protein and mRNA expression analysis. Therefore, mRNA level sometimes cannot directly represent protein level (Greenbaum et al., 2003).

Table 19. Expression of PIEZO1 in ocular tissues and cell types and the methods of their detection

Tissue/cell type	Method	Literature
cornea	IHC	(Yarishkin et al., 2021)
	IF, WB, qPCR	**present study**
lens	**WB**	**present study**
TM	IHC	(Yarishkin et al., 2021)
	IHC, WB	(Zhu et al., 2021)

	IF	(Tran et al., 2014)
TM cells	ICC, qPCR	(Yarishkin et al., 2021)
	IHC, WB	(Zhu et al., 2021)
	ICC, WB, proteomic analysis	(Tran et al., 2014)
Ciliary body	IHC	(Yarishkin et al., 2021)
	IF, WB, qPCR, IHC	**present study**
NPE cells	IHC	(Zhu et al., 2021)
	ICC, WB, RT-PCR	**present study**
retina	**IF, WB, qPCR**	**present study**
ONH	PCR	(Choi et al., 2015)
	WB, qPCR	**present study**
ONH astrocytes	single-cell PCR	(Choi et al., 2015)

Table 20. Expression of PIEZO2 in ocular tissues and cell types and the methods of their detection

Tissue/cell type	Method	Literature
corneal trigeminal neurons	ISH	(Bron et al., 2014)
	ICC	(Fernández-Trillo et al., 2020)
cornea	**IF, WB**	**present study**
TM	IF	(Tran et al., 2014)
TM cells	ICC, WB, proteomic analysis	(Tran et al., 2014)
	qPCR	(Yarishkin et al., 2021)
Ciliary body	**IF, WB, qPCR, IHC**	**present study**
NPE cells	**ICC, WB, RT-PCR**	**present study**
retina	**IF, WB, qPCR**	**present study**
ONH	PCR	(Choi et al., 2015)
	WB, qPCR	**present study**
ONH astrocytes	single-cell PCR	(Choi et al., 2015)

4.1.2 Transient receptor potential (TRP) family

4.1.2.1 TRPA1

TRPA1 was first considered to be involved in mechanical sensation when it was found in inner-ear hair cells (Corey et al., 2004). Although the mechanical sensing function of TRPA1 in the inner-hair is still controversial (Corey, 2006), the role of TRPA1 proteins in different structure of the eye has been extensively studied already (Hirt and Liton, 2016; Reinach et al., 2015). For example, LC-MS/MS-based proteomic analysis revealed that TRPA1 was expressed in the CB of normal human eyes (Goel et al., 2013). Another study showed that TRPA1 was expressed in the basal epithelial cell layer of mouse cornea, as well as in both regenerated epithelium and the stroma of corneas after an alkali burn, suggesting that the alkali burn could upregulate TRPA1 expression in stromal cell (Okada

et al., 2014). The expression of TRPA1 was also detected by IHC staining in human uvea at high level (Mergler et al., 2014). In our study, both western blotting and RT-PCR analysis demonstrated that TRPA1 was expressed in many different structures of rat eyes, including retina, CB, cornea, sclera and ON (Figure 15), while immunofluorescence staining suggested the expression of TRPA1 in retina, cornea, and CB of rat eyes (Figure 14).

Using western blot analysis, three different TRPA1 protein bands were observed, which could be the two isoforms of TRPA1 bands and the TRPA1 dimer band (Figure 15A). The two TRPA1 isoforms were also found in another study. Zhou and colleagues observed two splice forms of TRPA1 proteins and named as TRPA1a and TRPA1b (Zhou et al., 2013). Western blot showed that these two isoforms have a difference in size of 30 amino acids, but there is no effective antibody to detect them separately (Zhou et al., 2013). The largest band (~250kDa) was observed and defined as the dimer form of TRPA1, as the observed molecular weight of this bands was twice as large as the molecular weight of TRPA1 monomer band. TRPA1, like many other MSCs, plays an important role in transducing mechanical stimuli into mechanosensitive currents in trigeminal ganglion (TG) nerve endings (Meng et al., 2015). Although there are mechanoreceptive TG nerve endings in the inner wall of the anterior chamber, the roles of mechanoreceptive TRPA1 and TG nerve endings in intraocular pressure perception need to be studied further (Meng et al., 2015).

Table 21. Expression of TRPA1 in ocular tissues and cell types and the methods of their detection

Tissue/cell type	Method	Literature
cornea	IHC **IF, WB, qPCR**	(Okada et al., 2014) **present study**
TG neurons of anterior chambers	IF	(Meng et al., 2015)
Ciliary body	proteomic analysis **IF, WB, qPCR, IHC**	(Goel et al., 2013) **present study**
NPE cells	**ICC, WB**	**present study**
TM	IF	(Tran et al., 2014)
TM cells	ICC, WB, proteomic analysis	(Tran et al., 2014)
uvea	RT-PCR	(Mergler et al., 2014)
retina	RT-PCR **IF, WB, qPCR**	(Gilliam and Wensel, 2011) **present study**
ONH	**WB, qPCR**	**present study**
ONH astrocytes	single-cell PCR	(Choi et al., 2015)

4.1.2.2 TRPM3

The expression of TRPM3 at mRNA level has been extensively studied in different tissues of mammalian eyes by using in-situ hybridization and RT-PCR. Its expression was detected in the lens (Bennett et al., 2014; Karali et al., 2007), CB (Li et al., 2007; Shaham et al., 2013), retina (Gilliam and Wensel, 2011; Karali et al., 2007), RPE (Gilliam and Wensel, 2011; Wang et al., 2010), astrocytes and oligodendrocytes of the optic nerve head (Choi et al., 2015; Papanikolaou et al., 2017). In addition, the NEIBank sequence database also showed the expressed sequence tag of TRPM3 in the human iris, lens, retina, and retinal pigment epithelium (Wistow et al., 2002; Wistow et al., 2008). However, the expression of TRPM3 at protein level in the mammalian ocular tissues has not been systematically investigated. Therefore, to identify the expression of TRPM3 at both mRNA and protein levels in the rat eye was detected by utilizing IF, WB and RT-PCR analysis. Finally, higher expression of TRPM3 was observed in rat CB, cornea and sclera, and lower expression in retina, ON, and lens (Figure 18A, B). Further WB and IF analysis showed the expression of TRPM3 in HNPEC (Figure 19). In rat retina, IF staining showed that the TRPM3 is strongly immunolabeled in the GCL and IPL, but weakly labeled in the INL and OPL (Figure 17), which is similar to the results of another study (Brown et al., 2015). The expression of TRPM3 in CB was also observed by using IF and WB analysis. Similar results were found in several other studies (Hughes et al., 2012; Li et al., 2007). In human eyes, the expression of TRPM3 were detected by using different research methods as well, for example, direct proteomic analysis proved the expression of TRPM3 in the CB of normal human eyes (Goel et al., 2013). In-situ hybridization (ISH) analysis detected the expression of TRPM3 mRNA expression in the RPE, INL, and GCL of the neural retina, as well as in the CB and epithelial cells of the lens (Karali et al., 2007). Nevertheless, our study showed the expression of TRPM3 in the cornea and the sclera at both mRNA and protein level for the first time. Furthermore, the TRPM3 protein was also detected in the lens (Figure 18).

The exact role of TRPM3 in the eye is still unclear. However, in the epithelium of the lens and RPE, TRPM3 could maintain the intracellular Ca^{2+} and preserve lens transparency (Rhodes and Sanderson, 2009; Wimmers et al., 2007). Patients with TRPM3 gene mutation presented hereditary cataracts with hypertensive glaucoma and variable anterior segment defects (Bennett et al., 2014), which also links the TRPM3 mutation to glaucoma. Interestingly, mutation in microRNA-204 (miR-204), a micro RNA is located in intron-9 of TRPM3 gene, causes inherited retinal dystrophy and ocular coloboma (Conte et al., 2015). As miR-204 and TRPM3 are co-expressed in the same ocular tissues at the same developmental stages (Karali et al., 2007), miR-204 was proposed as a post-transcription regulator of TRPM3 during eye development (Shiels, 2020). Nevertheless, further experiments need to be performed to explore the function of TRPM3 in the pathogenesis of hereditary cataracts and glaucoma.

Table 22. Expression of TRPM3 in ocular tissues and cell types and the methods of their detection

Tissue/cell type	Method	Literature
cornea	**IF, WB**	**present study**
Iris	cDNA library	(Wistow et al., 2002)
Lens	ISH	(Karali et al., 2007)
	cDNA library	(Wistow et al., 2008)
	ISH	(Shaham et al., 2013)
	RT-qPCR	(Xie et al., 2013)
	RT-PCR	(Bennett et al., 2014)
	RT-PCR, Microarrays	(Terrell et al., 2015)
	WB	**present study**
Ciliary body	ISH	(Karali et al., 2007)
	RT-qPCR	(Li et al., 2007)
	ISH	(Gilliam and Wensel, 2011)
	IF	(Hughes et al., 2012)
	ISH	(Shaham et al., 2013)
	proteomic analysis	(Goel et al., 2013)
	IF, WB, qPCR, IHC	**present study**
NPE cells	**ICC, WB**	**present study**
Retina	ISH	(Karali et al., 2007)
	cDNA library	(Wistow et al., 2008)
	RT-qPCR	(Hackler et al., 2010)
	RT-qPCR	(Krol et al., 2010)
	RT-PCR, Northern, ISH	(Gilliam and Wensel, 2011)
	IF	(Brown et al., 2015)
	IF, WB, qPCR	**present study**
Müller cell	IF	(Hughes et al., 2012)
RPE	cDNA library	(Schulz et al., 2004)
	ISH	(Karali et al., 2007)

	cDNA library	(Wistow et al., 2008)
	RT-qPCR	(Wang et al., 2010)
	ISH	(Gilliam and Wensel, 2011)
	RT-qPCR	(Adijanto et al., 2012)
	ISH	(Shaham et al., 2013)
	RT-qPCR,WB	(Zhao et al., 2015)
	qPCR	(Samuel et al., 2017)
ONH	**WB, qPCR**	**present study**
ONH astrocytes	single-cell PCR	(Choi et al., 2015)
	RT-qPCR, IF	(Papanikolaou et al., 2017)
ONH oligodendrocytes	RT-qPCR, IF	(Papanikolaou et al., 2017)

4.1.2.3 TRPV4

TRPV4 belongs to transient receptor potential vanilloid subfamily and expresse in almost the whole ocular structure, including conjunctiva (Mergler et al., 2012), corneal epithelial (Martínez-Rendón et al., 2017; Mergler et al., 2011a; Okada et al., 2016; Pan et al., 2008), corneal endothelial (Mergler et al., 2011b), lens (Nakazawa et al., 2019; Shahidullah et al., 2012), TM (Luo et al., 2014; Ryskamp et al., 2016a; Yarishkin et al., 2021), CB (Alkozi and Pintor, 2015; Jo et al., 2016) and retina (Gilliam and Wensel, 2011; Taylor et al., 2017). Many studies showed the expression of TRPV4 in different eye tissues, most of them analyzed the expression of TRPV4 in retina. The expression of TRPV4 was detected in several different cell-types in retina, like RGCs (Gao et al., 2019; Lakk et al., 2018; Ryskamp et al., 2016a; Ryskamp et al., 2011a), bipolar cells (BCs) (Gao et al., 2019), Müller cells (Jo et al., 2015; Matsumoto et al., 2018; Ryskamp et al., 2014) and retinal pigment epithelial cells (RPE) (Cordeiro et al., 2010; Zhao et al., 2015). In the study by using IF, WB and RT-PCR methods we demonstrated that TRPV4 is expressed in the rat retina, CB and cornea, which is similar to many previous studies (Table 23).

TRPV4 has been shown to have multiple functions reacting different stimulation, e.g. TRPV4 can be activated by heat, cell swelling, mechanical stress and chemical compounds (White et al., 2016). TRPV4 expressed in the cornea could theoretically confer temperature sensitivity to the cornea (Mergler et al., 2011a) and sense hypotonic stimulation (Pan et al., 2008) to protect against the effects of such stresses. In porcine lens epithelium TRPV4 regulates hemi-channel-mediated ATP release and Na^+-K^+-ATPase activity (Shahidullah et

al., 2012), while in mouse RGCs TRPV4 play a function in modulating calcium flux, spiking rate, and apoptosis (Ryskamp et al., 2011b).

The TRPV4 channel plays critical role in secreting aqueous fluid and regulating intraocular pressure in CB and TM. For example, studies have revealed that TRPV4 is expressed in HNPCE cells, while activation of TRPV4 can trigger melatonin releasing from HNPCE cells (Alkozi and Pintor, 2015) through up-regulation of Arylalkymine N-acetyltransferase (AANAT), the first rate-limiting enzyme for melatonin synthesis (Alkozi et al., 2017). The melatonin is a neurohormone produced by the pineal gland during the night to regulate the circadian rhythm; it may also regulate the aqueous humor production (Osbourne, 1994) and reduce IOP by activating melatonin MT3 receptors (Pintor et al., 2003). Moreover, another report also showed that the TRPV4 channel is important osmosensor in mouse NPE cells and may participate in IOP regulation (Jo et al., 2016). Due to the critical role of TRPV4 in IOP regulation, it has been used as a treatment target of glaucoma as well. For example, the selective TRPV4 antagonist (HC-067047) can reduce the IOP in mice with glaucoma through regulating Ca^{2+} outflow (Ryskamp et al., 2016b). However, evidence from another study showed opposite results. Mutation in OCRL, an inositol polyphosphate 5-phosphatase, causes Lowe syndrome, in which glaucoma is a typical syndrome. OCRL is an interaction partner of TRPV4, and both proteins are localized within the primary cilia of human TM and may be involved in IOP regulation by increasing Ca^{2+} influx rather than out flux. Further experiments showed that TRPV4 agonist, GSK 1016790A, treatment led to reduced IOP in wild-type mice and knock-out of TRPV4 in mice caused the increased IOP (Luo et al., 2014), which is opposite to the results found in TRPV4 antagonist (HC-067047) treatment. Thus, the role of TRPV4 in controlling the IOP and the treatment effect by blocking or activating this channel needs to be studied further.

Table 23. Expression of TRPV4 in ocular tissues and cell types and the methods of their detection

Tissue/cell type	Method	Literature
conjunctiva	IHC	(Mergler et al., 2012)
conjunctival epithelial cells	RT-PCR, IHC	(Mergler et al., 2012)
cornea	**IF, WB, qPCR**	**present study**
corneal epithelial cells	RT-PCR, WB RT-PCR	(Pan et al., 2008) (Mergler et al., 2011a)

	IHC	(Okada et al., 2016)
	qPCR, WB, IF	(Martínez-Rendón et al., 2017)
corneal endothelial cells	RT-PCR	(Mergler et al., 2011b)
TG neurons of anterior chambers	IF	(Meng et al., 2015)
Lens	WB	(Shahidullah et al., 2012)
	WB, IF	(Nakazawa et al., 2019)
TM	IF	(Ryskamp et al., 2016b)
TM cells	qPCR	(Yarishkin et al., 2021)
	RT-PCR, WB, ICC	(Ryskamp et al., 2016b)
	ICC	(Luo et al., 2014)
Ciliary body	**IF, WB, qPCR, IHC**	**present study**
NPE cells	ICC	(Alkozi and Pintor, 2015)
	IF	(Jo et al., 2016)
	ICC, WB	**present study**
retina	RT-PCR, Northern	(Gilliam and Wensel, 2011)
	IF	(Taylor et al., 2017)
	IF, WB, qPCR	**present study**
RGCs	RT-PCR, WB, IF	(Ryskamp et al., 2011b)
	IF	(Ryskamp et al., 2014)
	IF	(Gao et al., 2019)
	qPCR, IF	(Lakk et al., 2018)
bipolar cells (BCs)	IF	(Gao et al., 2019)
Müller	IF	(Jo et al., 2015)
	IF	(Ryskamp et al., 2014)
	IF	(Matsumoto et al., 2018)
RPE	RT-PCR	(Cordeiro et al., 2010)
	RT-qPCR,WB	(Zhao et al., 2015)
ONH	**qPCR**	**present study**

4.1.2.4 TRPP2

TRPP2 is another member TRP family and being responsible for mechanotransduction. The role of TRPP2 in sensing mechanical pressure has been reported in many organs and tissues. In some reports, TRPP2 was found co-localized on primary cilia and played a function in regulating Ca^{2+} flux mainly on primary cilia. In the kidney, TRPP2 (also called polycystin 2, PKD2) interacted with its molecular chaperones polycystin 1 (PKD1) to form a polycystin complex, which co-localized with the primary cilia in kidney epithelium cells, and activation of TRPP2 induces Ca^{2+} influx into primary cilia by fluid flow (Nauli et al., 2003). In cardiovascular system, TRPP2 was also found on primary cilia of vascular endothelial cells and can regulate Ca^{2+} channel in response to shear stress in blood vessels, while TRPP2 dysfunctions caused compromised fluid sensing which further impairs the synthesis of nitric

oxide and induces the development of hypertension, especially in ADPKD patients carrying the TRPP2 mutation (AbouAlaiwi et al., 2009).

The function of TRPP2 in primary cilia has been reported in many different tissues. TRPP2 was considered as an important ion channel in the primary cilia of the renal collecting duct epithelium (Liu et al., 2018). Furthermore, PKD1 and TRPP2, both present in primary cilia of vascular smooth muscle cells, when directly stimulated with mechanical pressure by collagen or induced ciliary deflection lead to Ca^{2+} influx and this procedure depends on the presence of cilia (Lu et al., 2008). In the respiratory system, TRPP2 was expressed in primary cilia of human bronchial smooth muscle cells and might have the function in sensing and transducing extracellular mechanochemical signals. TRPP2 may have the function in maintenance and remodeling the airway wall, and its disfunction might be responsible for the bronchiectasis in ADPKD (Wu et al., 2009).

Although increased evidence supports that TRPP2 plays mechanic sensory roles in several cellular systems, its role in eyes has not been characterized so far. Evidence from a polycystic kidney disease (PKD) patient may indicate the potential role of TRPP2 in glaucoma pathogenesis. This patient suffered from polycystic kidney disease (PKD) and presented rapid loss of vision during the terminal stages of the illness, the postmortem examination revealed pathological glaucomatous changes in both eyes (Berkley, 1951). Further studies have also shown the expression of TRPP2 in the eye. TRPP2 expression has been found in different structures of eyes, like the TM (Tran et al., 2014), cornea (Obermüller et al., 1999), retina (Gallagher et al., 2006; Gilliam and Wensel, 2011) and optic nerve head (Choi et al., 2015), although different species were utilized in these studies. In our study, proved the distribution of TRPP2 in both rat and human CB (Figure 23, 24, 25), as well as in HNPCE cells for the first time (Figure 26), which may further support its role in the pathogenesis of glaucoma.

Table 24. Expression of TRPP2 in ocular tissues and cell types and the methods of their detection

Tissue/cell type	Method	Literature
cornea	IHC	(Obermüller et al., 1999)
	IF, WB, RT-PCR, IHC	**present study**
Iris	**WB, RT-PCR, qPCR, IHC**	**present study**

lens	**WB, IHC**	**present study**
TM	IF	(Tran et al., 2014)
	IHC	**present study**
TM cells	ICC, WB, proteomic analysis	(Tran et al., 2014)
Ciliary body	**IF, WB, RT-PCR, qPCR, IHC**	**present study**
NPE cells	**ICC, WB, RT-PCR**	**present study**
retina	RT-PCR, Northern, ISH, WB, IF	(Gilliam and Wensel, 2011)
	IF	(Gallagher et al., 2006)
	IF, WB, RT-PCR, qPCR, IHC	**present study**
ONH	PCR	(Choi et al., 2015)
	WB, RT-PCR, qPCR	**present study**
ONH astrocytes	single-cell PCR	(Choi et al., 2015)

4.1.3 Two-pore domain K+ (K2P) channel family

4.1.3.1 TREK1

TREK1 is a mechanosensitive stretch-activated potassium channel and belongs to the two-pore domain K+ (K2P) channel family (Chemin et al., 2005). Its expression has been demonstrated in the eyes, for example in the TM of human eyes (Tran et al., 2014) and in retina of mice eyes (Hughes et al., 2017; Zhang et al., 2019). Except of TM, our results showed that TREK1 was expressed at different expression levels in the rat retina, CB, cornea, and HNPCE cells.

The role of TREK1 in regulating IOP has been widely analyzed by some studies, specifically using TM cells as model system. TREK1 is an interaction partner of extracellular matrix (ECM) protein cochlin, they interact together to transduce the mechanosensation into TM cells, through which to remodel the cytoskeleton and finally resulted in regulation of fluid flow across cell layers (Goel et al., 2011). TREK1 could also interact with cochlin to regulate IOP, because the silencing of TREK-1 prevented increased IOP which was induced by cochlin-overexpression (Carreon et al., 2017a). TREK1 can also maintain the Ca^{2+} homeostasis in TM cells and work as regulator of TM mechanosensitivity (Yarishkin et al., 2018). TREK-1 mediates TM mechanotransduction through sensing the extra- and intracellular pH shifts which can modulate aqueous outflow and subsequently to regulate IOP (Yarishkin et al., 2019), as treatment with TRPV4 inhibitor causes residual outward conductance by TREK1 in the TM, which indicates that TRPV4 and TREK-1 channels may work together to regulate IOP (Yarishkin et al., 2018). In this study, the expression of

TREK1 in human CB and HNPCE cells were observed (Figure 29), which may also indicate that TREK1 has function in the CB like in the TM cells but needs to be investigated further.

Table 25. Expression of TREK1 in ocular tissues and cell types and the methods of their detection

Tissue/cell type	Method	Literature
cornea	**IF, WB**	**present study**
TM	IF	(Tran et al., 2014)
TM cells	ICC, WB, proteomic analysis	(Tran et al., 2014)
	ICC	(Goel et al., 2011)
	WB, IHC	(Carreon et al., 2017a)
	WB, ICC	(Yarishkin et al., 2018)
Ciliary body	**IF, WB, qPCR, IHC**	**present study**
NPE cells	**ICC, WB**	**present study**
retina	qPCR, IF	(Hughes et al., 2017)
	qPCR, WB, IHC	(Zhang et al., 2019)
	IF, WB, qPCR	**present study**
ONH	**WB, qPCR**	**present study**

4.2 TRPP2 located in primary cilia of HNPCE cells

4.2.1 Primary cilia

Primary cilia have been described as mechanosensory organelles in cholangiocytes (Masyuk et al., 2006), vascular endothelia (Iomini et al., 2004; Nauli et al., 2008), renal collecting duct epithelium (Liu et al., 2018) and chondrocytes (Wann et al., 2012). The primary cilium membrane is composed of a microtubule based axoneme and anchored through a basal body (Ishikawa and Marshall, 2011). Using immunocytochemistry staining, primary cilia in HNPCE cell culture were detected because of positive staining of anti-acetylated α-tubulin or Arl13b, a small GTPase localized in the axoneme of the cilia, and anti-γ-tubulin which stained the basal body of the cilia (Figure 30). Further electron microscopy observation showed ultra-structure of primary cilia in HNPCE cell culture (Figure 31A). The immunohistochemistry staining of paraffin section from the human eye also showed the typical primary cilia structure (Figure 31B). All those observations proved the existence of primary cilia in HNPCE cells.

In the present study, whether serum starvation could affect the formation of primary cilia was also investigated, as serum starvation is a widely described method of inducing primary cilia (Nachury et al., 2007). The average lengths of primary cilia did not change

significantly when extending the starvation time from 24 to 72 hours (Figure 30B). This result is different from a study using primary human TM cells in which the average length of cilia was increased followed by serum deprivation (Luo et al., 2014). These differences may be due to that difference cell types were used and the HNPCE cells are different from TM cells in reaction to serum starvation**.** However, similar to the TM cells (Luo et al., 2014), increasing the serum starvation time leads to increase the number of HNPCE cells with primary cilia (Figure 30C). In TM cells, primary cilia are critical in response to the change of pressure, for example, fluid flow or elevated hydrostatic pressure can shorten the length of primary cilia (Luo et al., 2014). Nevertheless, the changes of primary cilia in HNPCE following high pressure are not clear so far.

4.2.2 Co-localization of MSCs and primary cilia

Since the results showed the expression of MSCs in the human and rat CB, it was sought to know whether these MSC could co-localize with primary cilia to regulate IOP. Thus, immunofluoresence co-staining of MSCs and primary cilia was performed in primary HNPCE cell culture. The expression of all seven selected MSCs candidates (PIEZO1, PIEZO2, TRPA1, TRPM3, TRPV4, TRPP2 and TREK1) were observed on different cellular structures of HNPCE cells (Figure 32). And TRPP2 is localized on the primary cilia of HNPCE cells (Figure 32F), but PIEZO1, PIEZO2, TRPA1, TRPM3, TRPV4 and TREK1 did not show clear co-localization with primary cilia (Figure 32). The co-localization of TRPP2 and primary cilia has been found in several stress-bearing cells, like kidney cells (Nauli et al., 2003), vascular endothelial cells (AbouAlaiwi et al., 2009), vascular smooth muscle cells (Lu et al., 2008) and bronchial smooth muscle cells (Wu et al., 2009), in which TRPP2 is localized on the membrane of primary cilia. And TRPP2 can be activated and induced Ca^{2+} influx into primary cilia through sensing the bending of the primary cilia, induced by fluid flow (Nauli et al., 2003), shear stress (AbouAlaiwi et al., 2009), or extracellular matrix tension (Lu et al., 2008), which function like a mechanical stress sensor. However, the link between TRPP2 and IOP regulation warrants further investigation. It is speculated that

TRPP2 and primary cilia of HNPCE cells likely function as mechanical/pressure sensor in sensing the IOP and participate in the procedure of aqueous humor formation.

Previous reports show that TRPV4 is expressed and localized within the primary cilia of human TM (Luo et al., 2014). But in our results, the co-localization of TRPV4 on the primary cilia was not observed in HNPCE cells (Figure 32E), which might be due that: (1) primary cultured HNPCE cells are different from TM cells; (2) because there is not specific antibody for TRPV4 available, different antibodies were used in these two reports.

The HNPCE primary cells used in this study were purchased from a commercial manufacturer. The cell line was characterized by using immunocytochemical methods and further identified by pharmacological technologies (Sharif et al., 2014). In the current study, experiments were performed by using primary HNPCE cells less than four passage times, since the cells change their morphology and lose physical characterize with more manipulation. The limitation is the morphology and physical characteristic of primary cilia changed by passaging. With the living conditions changed for the live tissues, the sensation function of the primary cilia might also have been changed. Since the human eye tissue sections were obtained from patient with choroidal melanoma and not from a physiological human eye, the primary cilia in the physiological human eye still needs to be investigated further. In addition, most primary antibodies used for MSCs immuno-staining are polyclonal antibodies and may not be specific to the antigen, therefore being able to cause non-specific signals.

4.3 Pressure chamber test

In the present study, the expression of multiple MSCs were identified, but their role in regulating IOP is unclear, thus the protein and mRNA expressions of selected MSCs were investigated by using a device of hydrostatic pressure to imitate a glaucoma situation. A pressure chamber was installed by using a vertical PLL-coated T-75 flask sealed with a cap, connected to a long tube instead of the acrylic cylinder as a device to culture HNPCE cells. Pressure was applied by incubating HNPCE cells at the bottom of the flask, while the

connected tube was filled with epithelial cell culture complete medium and was maintained the height of the fluid column at 79.8cm to produce a pressure of 60mmHg. The hydrostatic pressure was adjusted to simulate conditions of the disease scenario that occurs during a severe acute glaucoma attack (60mmHg). The pressure chamber used in this study was reformed from an equipment used in other study, in which acrylic cylinder filled with artificial cerebrospinal fluid was used to simulate high pressure condition. The height of liquid column at 13.5, 47.3, and 101.2cm corresponded to the pressure of 10, 35, and 75mmHg, respectively (Ishikawa et al., 2014). A similar hydrostatic pressure device was utilized by some other studies as well, in order to study the pressure-induced calcium (Ca^{2+}) influx in cultured rat optic nerve astrocytes (Mandal et al., 2010). In that study, the astrocytes were cultured in a closed double glass window pressure chamber (Warner Instruments, Model RC30). After filling with DMEM/F12 complete medium, the chamber was connected with the fluid column at 20cm subjected increased hydrostatic pressure for 15mmHg.

Utilizing the hydrostatic pressure device can imitate a glaucoma situation. By using the device, the response of the primary cultured HNPCE cells to hydrostatic pressure can be determined through analyzing the expression of multiple MSCs candidates at both mRNA and protein level. The mRNA levels of MSCs were measured at 12 and 24 hours with HNPCE cells treated with hydrostatic pressure, while the protein levels were detected only at 24 hours. At 12 and 24 hours, the mRNA level of PIEZO1, PIEZO2, TRPM3 and TRPP2 were significantly decreased, while TRPA1 and TRPV4 mRNA expression were significantly increased, but TREK1 remained unchanged (Figure 33). The WB analysis revealed that the protein level of PIEZO2 was significantly decreased at 24 hours, while TRPP2 and TREK1 protein expression were significantly increased at 24 hours, but PIEZO1, TRPA1, TRPM3 and TRPV4 did not change significantly (Figure 33). Taking this into account, the PIEZO2 and TRPP2 were change at both mRNA and protein level, which may indicate that the expression of these two channels is more sensitive to high pressure in HNPCE compared to other candidates.

In this study, the expression changes of MSCs were not consistent at the protein level detected by WB analysis and at mRNA level detected by real-time PCR analysis. The reasons might be that the technology of real-time PCR analysis is a quite sensitive method, and any artifacts can interfere with amplification efficiency.

Due to the high expression change of TRPP2 and PIEZO2 to high hydrostatic pressure, siRNA was used to silence TRPP2 and PIEZO2 in primary cultured HNPCE cells to see the reaction of others. High transfection efficiency in HNPCE cells was detected by using Lipofectamine 2000_optimized method (Avci-Adali et al., 2014) when compared to the method recommended in the manual. The transfection complexes were performed by using 1µl, 2µl Lipofectamine 2000 and different amounts of 40, 80 and 160pmol eGFP siRNA separately. The transfection of HNPCE cells with 2µl Lipofectamine 2000 and 160pmol siRNA resulted in the highest transfection efficiency. Although it showed high transfection efficiency, siRNA is still technique where the gene of interest is silenced, rather than the gene knock-out, which completely removes the gene of interest.

In addition, the pressure analysis is limited to only high hydrostatic pressure, the effect of MSCs candidates to low pressure was not tested. And the direct connection of TRPP2 and PIEZO2 to IOP regulation also needs further characterization, like Ca^{2+} response in HNPCE cells.

4.4 TRPP2 and PIEZO2 expression under different pressure level

Previous reports showed that TRPP2 on primary cilia may function as a mechanosensitive channel by forming homo-tetramer or hetero-tetramer with other types of TRP family members. TRPP2 can be assembled as homo-tetramer (Kobori et al., 2009) or hetero-tetramer with polycystin-1(PKD1) (Zhu et al., 2011), TRPC1 (Kobori et al., 2009) and TRPV4 (Stewart et al., 2010). For example, TRPP2 interacts with popycystin-1(PKD1) to form a 3:1 ratio channel complex by using its C-terminal coiled-coil domain (Zhu et al., 2011). TRPP2 can form a hetero-tetramer with TRPC1 with a ratio of 2:2 subunits and an alternating arrangement (Kobori et al., 2009). Similarly, TRPP2 and TRPV4 also form a

hetero-tetramer with a 2:2 ratio with alternating subunit arrangement (Stewart et al., 2010). The hetero-tetramer complex could also be assembled by three different TRP subfamily members. TRPV4, TRPC1, and TRPP2 can assemble together to form a heteromeric TRPV4-C1-P2 complex heteromeric channel, while the fourth subunit in this heteromeric TRPV4-C1-P2 complex channel could be anyone of the three channels (Du et al., 2014). A recent report showed that a hetero-multimer, formed by TRPM3 and TRPP2 subunits, may also exist in primary cilia of renal epithelia cells (Kleene et al., 2019). Furthermore, TRPP2 can not only form a hetero-tetramer with TRP family members, but could also regulate the function by interacting with other MSCs. For example, TRPP2 may inhibit PIEZO1-dependent stretch-activated channels in renal tubular epithelial cells (Peyronnet et al., 2013). TRPP2 can also block TREK1 activation of by a Filamin A-mediated cytoskeletal mechanism (Li Fraine et al., 2017).

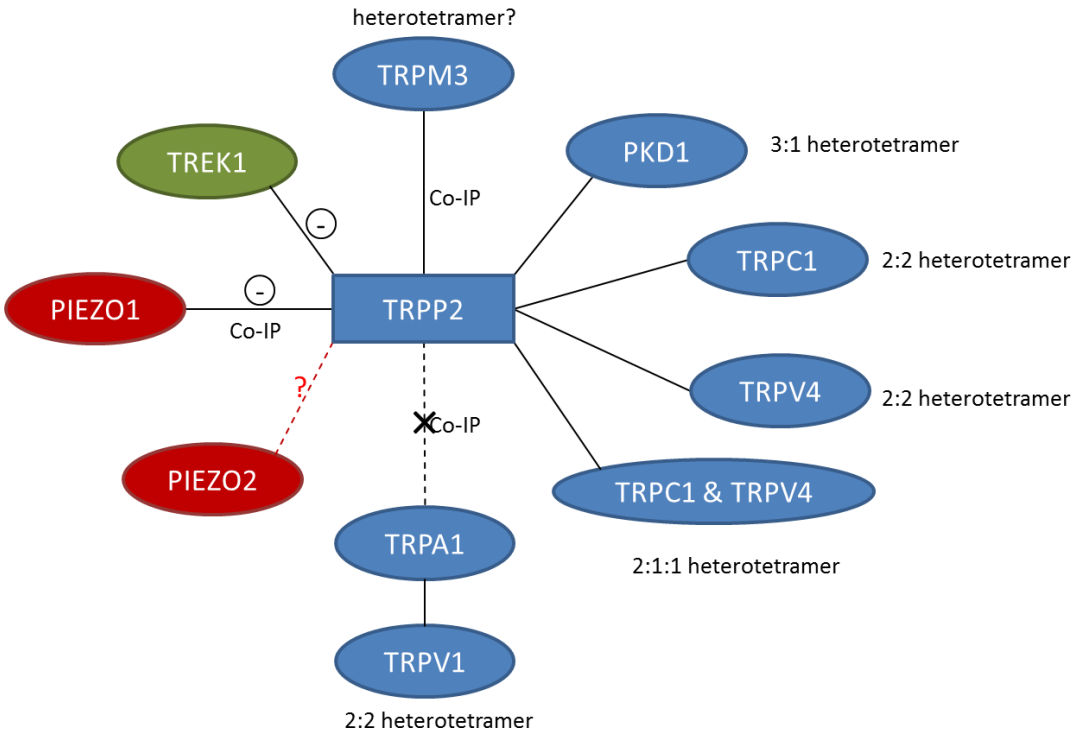

Figure 41. Schematic of interactions between TRPP2 and other MSCs.

In this study, after PIEZO2-siRNA cells with hydrostatic high pressure at 60 mmHg with a treatment for 24 hours, all the three isoforms of TRPP2 significantly decreased (Figure

40E). But in the same situation utilized on TRPP2-siRNA cells, there was no significant changes on PIEZO2 protein expression (Figure 37B). That shows that might be some connections within the two channels under high hydrostatic pressure.

Most interestingly, TRPP2 might have the function in regulating mechanosensitive processes through OCRL. The OCRL is a phosphoinositide 5-phosphatases, which can metabolize $PI(4,5)P_2$ into PI(4)P, while lack of / mutation of OCRL leads to accumulation of $PI(4,5)P_2$ and an inhibit of TRPP2 channel (Ma et al., 2005). Mutation of OCRL can cause Lowe syndrome, which includes congenital cataract and glaucoma (Luo et al., 2012), these data link TRPP2 to regulation of mechanosensitive processes. Our study revealed that TRPP2 was expressed in primary cilia of HNPCE cells, which may indicate that TRPP2 may play as a critical regulator to sense IOP of the eye, but needs further experimentation to be proven.

Since there is a lack of functional experiments, as to whether the IOP sensation of MSCs is more likely, less likely or has no function and which MSCs exactly are the mechanosensors would need to be investigated further.

5. Summary

In this study, the expression of seven MSCs (PIEZO1, PIEZO2, TRPA1, TRPM3, TRPV4, TRPP2 and TREK1) was shown in the CB by using immunofluorescence, WB and reverse transcription PCR (or qRT-PCR) analyses in the rat eye. MSCs were also present in the CB epithelium of human eyes as seen by using immunohistochemistry staining. In addition, the expression and localization of the selected MSCs were identified on HNPCE cells by western blotting, conventional PCR analysis and ICC. Highly expression of multiple MSCs on HNPCE cells may indicate a potential role in aqueous humor regulation.

The formation of primary cilia was confirmed in HNPCE cells after serum starvation by using ICC. Similar results were observed in human eye tissue paraffin sections when using electron microscopy observation and immunohistochemistry staining. The length of primary cilia is independent to the extension of the starvation time, because extension the starvation time from 24 hours to 48 hours or 72 hours did not affect the length of primary cilia. However, extending the serum starvation time from 24 hours to 48 or 72 hours caused increased frequency of HNPCE cells with primary cilia and almost all cells form primary cilia. Double immunofluorescence staining proved the co-localization of TRPP2 with primary cilia in HNPCE cells. As primary cilia have function in regulating mechanic sense, all these results may indicate that MSCs on HNPCE could be related to the mechanic sense.

By using a pressure elevation model, a change in the protein level of PIEZO2, TRPP2 and TREK1 was seen with increasing pressure. Similarly, the mRNA level of PIEZO1, PIEZO2, TRPA1, TRPM3 and TRPP2 clearly changed. Administration of PIEZO2-siRNA and hydrostatic high pressure at 60 mmHg for 24 hours caused significantly decreased protein levels of all the three isoforms of TRPP2 proteins in HNPCE cells. Within contrast, TRPP2-siRNA did not lead a change of PIEZO2 protein expression.

Characterizing the MSCs in ocular tissues may provide further insights into the potential function of mechanotransduction in IOP sensing and regulation, and finally could provide clues on suggesting new molecular targets for glaucoma treatment.

6. Zusammenfassung

In dieser Arbeit wurde die Expression sieben verschiedener mechano-sensitiver Kanäle (MSKs: PIEZO1, PIEZO2, TRPA1, TRPM3, TRPV4, TRPP2 und TREK1) im Bereich des Ziliarkörpers untersucht. Die Proteine wurden mittels Immunfluoreszenz, Western-Blot und Reverse-Transkriptions-PCR untersucht. MSCs waren sowohl im Ratten-Auge als auch humanen Ziliarkörper-Epithel vorhanden. Die Expression und Lokalisierung der ausgewählten MSKs wurden zudem in einer Zell-Linie des nicht-pigmentierten Ziliarkörperepithels (NPZE) untersucht. Die deutliche Expression mehrerer MSKs könnte auf eine mögliche Rolle bei der Regulierung des Kammerwassers hinweisen.

Die Bildung primärer Zilien nach Serumentzug konnte in der Zellkultur der NPZE-Zellen reproduziert und weiter analysiert werden. Entsprechende Befunde konnten in humanen Gewebsproben (Paraffinschnitten) mittels Elektronenmikroskopie und Immunhistologie bestätigt werden. Die Länge der primären Zilien war unabhängig von der Verlängerung des Serumentzugs von 24 auf 48 oder 72 Stunden, mit längerem Nährstoffentzug nahm die Häufigkeit von NPZE-Zellen mit primären Zilien jedoch deutlich zu. Eine doppelte Immunfluoreszenzfärbung zeigte eine Co-lokalisation von TRPP2 mit diesen primären Zilien.

In dem Modell der NPZE wurde die Expression der MSKs unter einem erhöhten hydrostatischen Druck untersucht: Es kam zu einer Zunahme der Proteinkonzentration von PIEZO2, TRPP2 und TREK1 mit steigendem Druck. Ebenso veränderte sich der mRNA-Spiegel von PIEZO1, PIEZO2, TRPA1, TRPM3 und TRPP2. Unter der Hemmung von PIEZO2 (siRNA) und hydrostatischem Druck von 60 mmHg für 24 Stunden wurde eine Abnahme aller drei Isoformen von TRPP2-Proteinen gesehen. Die Gabe von TRPP2-siRNA führte andererseits nicht zu einer Veränderung der PIEZO2-Proteinexpression.

Die weitere Charakterisierung der MSKs in Augengeweben könnte weitere Einblicke in die potenzielle Funktion okulärer Mechano-Sensoren für die Regulation des Augeninnendrucks liefern und somit Hinweise auf neue molekulare Ziele für die Behandlung des Glaukoms liefern.

7. Declaration of Contributions

The work was performed at the University Eye Hospital in Tübingen under the supervision of Prof. Dr. Focke Ziemssen.

The study was designed together with Prof. Dr. Focke Ziemssen, PD Dr. Bogomil Voykov and Dr. Sven Schnichels.

Prof. Dr. Ulrich Schraermeyer carried out the experiments of electron microscopy shown in Figure 32A. The experiments of immunohistochemistry were carried out with support of Claudia Riedinger and Monika Wild. Apl. Prof. Dr. Daniela Süsskind provided the histological sections of human eye. Dr. Fubo Cheng provided the rat eyes. Ms. Irena Stingl provided the picture for Figure 1, 2, 3, 5, 7.

All other experiments were carried out by independently after being trained by laboratory members and conducted with the support of Prof. Dr. Focke Ziemssen.

The statistical evaluation was carried out according to the instruction of Prof. Dr. Focke Ziemssen and Dr. Sven Schnichels.

I certify that I wrote the manuscript independently (following the guidance of Prof. Dr. Focke Ziemssen) and that I did not use any sources other than those I have indicated.

8. References

AbouAlaiwi, W.A., Takahashi, M., Mell, B.R., Jones, T.J., Ratnam, S., Kolb, R.J., Nauli, S.M., 2009. Ciliary polycystin-2 is a mechanosensitive calcium channel involved in nitric oxide signaling cascades. Circulation research 104, 860-869.

Adijanto, J., Castorino, J.J., Wang, Z.X., Maminishkis, A., Grunwald, G.B., Philp, N.J., 2012. Microphthalmia-associated transcription factor (MITF) promotes differentiation of human retinal pigment epithelium (RPE) by regulating microRNAs-204/211 expression. The Journal of biological chemistry 287, 20491-20503.

Alkozi, H.A., Perez de Lara, M.J., Sánchez-Naves, J., Pintor, J., 2017. TRPV4 Stimulation Induced Melatonin Secretion by Increasing Arylalkymine N-acetyltransferase (AANAT) Protein Level. International journal of molecular sciences 18.

Alkozi, H.A., Pintor, J., 2015. TRPV4 activation triggers the release of melatonin from human non-pigmented ciliary epithelial cells. Experimental eye research 136, 34-37.

Avci-Adali, M., Behring, A., Keller, T., Krajewski, S., Schlensak, C., Wendel, H.P., 2014. Optimized conditions for successful transfection of human endothelial cells with in vitro synthesized and modified mRNA for induction of protein expression. Journal of biological engineering 8, 8.

Baxter, S.L., Keenan, W.T., Athanas, A.J., Proudfoot, J.A., Zangwill, L.M., Ayyagari, R., Liebmann, J.M., Girkin, C.A., Patapoutian, A., Weinreb, R.N., 2020. Investigation of associations between Piezo1 mechanoreceptor gain-of-function variants and glaucoma-related phenotypes in humans and mice. Scientific reports 10, 19013.

Ben-Shahar, Y., 2011. Sensory functions for degenerin/epithelial sodium channels (DEG/ENaC). Advances in genetics 76, 1-26.

Bennett, T.M., Mackay, D.S., Siegfried, C.J., Shiels, A., 2014. Mutation of the melastatin-related cation channel, TRPM3, underlies inherited cataract and glaucoma. PloS one 9, e104000.

Berbari, N.F., O'Connor, A.K., Haycraft, C.J., Yoder, B.K., 2009. The primary cilium as a complex signaling center. Current biology : CB 19, R526-535.

Berkley, W.L., 1951. Glaucoma associated with polycystic kidney disease. American journal of ophthalmology 34, 1539-1542.

Bron, R., Wood, R.J., Brock, J.A., Ivanusic, J.J., 2014. Piezo2 expression in corneal afferent neurons. The Journal of comparative neurology 522, 2967-2979.

Brown, R.L., Xiong, W.H., Peters, J.H., Tekmen-Clark, M., Strycharska-Orczyk, I., Reed, B.T., Morgans, C.W., Duvoisin, R.M., 2015. TRPM3 expression in mouse retina. PloS one 10, e0117615.

Carreon, T.A., Castellanos, A., Gasull, X., Bhattacharya, S.K., 2017a. Interaction of cochlin and mechanosensitive channel TREK-1 in trabecular meshwork cells influences the regulation of intraocular pressure. Scientific reports 7, 452.

Carreon, T.A., Castellanos, A., Gasull, X., Bhattacharya, S.K., 2017b. Interaction of cochlin and mechanosensitive channel TREK-1 in trabecular meshwork cells influences the regulation of intraocular pressure. Scientific reports 7, 452.

Castellani, L., Root-Mccaig, J., Frendo-Cumbo, S., Beaudoin, M.S., Wright, D.C., 2014. Exercise training protects against an acute inflammatory insult in mouse epididymal adipose tissue. Journal of applied physiology (Bethesda, Md. : 1985) 116, 1272-1280.

Chemin, J., Patel, A.J., Duprat, F., Lauritzen, I., Lazdunski, M., Honore, E., 2005. A phospholipid sensor controls mechanogating of the K+ channel TREK-1. The EMBO journal 24, 44-53.

Cheng, Y.R., Jiang, B.Y., Chen, C.C., 2018. Acid-sensing ion channels: dual function proteins for chemo-sensing and mechano-sensing. Journal of biomedical science 25, 46.

Choi, H.J., Sun, D., Jakobs, T.C., 2015. Astrocytes in the optic nerve head express putative mechanosensitive channels. Molecular vision 21, 749-766.

Cinar, E., Zhou, S., DeCourcey, J., Wang, Y., Waugh, R.E., Wan, J., 2015. Piezo1 regulates mechanotransductive release of ATP from human RBCs. Proceedings of the National Academy of Sciences of the United States of America 112, 11783-11788.

Civan, M.M., Macknight, A.D., 2004. The ins and outs of aqueous humour secretion. Experimental eye research 78, 625-631.

Clark, A.F., Wordinger, R.J., 2009. The role of steroids in outflow resistance. Experimental eye research 88, 752-759.

Conte, I., Hadfield, K.D., Barbato, S., Carrella, S., Pizzo, M., Bhat, R.S., Carissimo, A., Karali, M., Porter, L.F., Urquhart, J., Hateley, S., O'Sullivan, J., Manson, F.D., Neuhauss, S.C., Banfi, S., Black, G.C., 2015. MiR-204 is responsible for inherited retinal dystrophy associated with ocular coloboma. Proceedings of the National Academy of Sciences of the United States of America 112, E3236-3245.

Cordeiro, S., Seyler, S., Stindl, J., Milenkovic, V.M., Strauss, O., 2010. Heat-Sensitive TRPV Channels in Retinal Pigment Epithelial Cells: Regulation of VEGF-A Secretion. Investigative ophthalmology & visual science 51, 6001-6008.

Corey, D.P., 2006. What is the hair cell transduction channel? The Journal of physiology 576, 23-28.

Corey, D.P., García-Añoveros, J., Holt, J.R., Kwan, K.Y., Lin, S.Y., Vollrath, M.A., Amalfitano, A., Cheung, E.L., Derfler, B.H., Duggan, A., Géléoc, G.S., Gray, P.A., Hoffman, M.P., Rehm, H.L., Tamasauskas, D., Zhang, D.S., 2004. TRPA1 is a candidate for the mechanosensitive transduction channel of vertebrate hair cells. Nature 432, 723-730.

Corey, D.P., Holt, J.R., 2016. Are TMCs the Mechanotransduction Channels of Vertebrate Hair Cells? The Journal of neuroscience : the official journal of the Society for Neuroscience 36, 10921-10926.

Coste, B., Mathur, J., Schmidt, M., Earley, T.J., Ranade, S., Petrus, M.J., Dubin, A.E., Patapoutian, A., 2010. Piezo1 and Piezo2 are essential components of distinct mechanically activated cation channels. Science (New York, N.Y.) 330, 55-60.

Cox, C.D., Bavi, N., Martinac, B., 2018. Bacterial Mechanosensors. Annual review of physiology 80, 71-93.

Delmas, P., Hao, J., Rodat-Despoix, L., 2011. Molecular mechanisms of mechanotransduction in mammalian sensory neurons. Nature reviews. Neuroscience 12, 139-153.

Denis, P., Nordmann, J.P., Elena, P.P., Saraux, H., Lapalus, P., 1994. Central nervous system control of intraocular pressure. Fundamental & clinical pharmacology 8, 230-237.

Du, J., Ma, X., Shen, B., Huang, Y., Birnbaumer, L., Yao, X., 2014. TRPV4, TRPC1, and TRPP2 assemble to form a flow-sensitive heteromeric channel. FASEB journal : official publication of the Federation of American Societies for Experimental Biology 28, 4677-4685.

Enyedi, P., Czirják, G., 2010. Molecular background of leak K+ currents: two-pore domain potassium channels. Physiological reviews 90, 559-605.

Faucherre, A., Kissa, K., Nargeot, J., Mangoni, M.E., Jopling, C., 2014. Piezo1 plays a role in erythrocyte volume homeostasis. Haematologica 99, 70-75.

Fernández-Trillo, J., Florez-Paz, D., Íñigo-Portugués, A., González-González, O., Del Campo, A.G., González, A., Viana, F., Belmonte, C., Gomis, A., 2020. Piezo2 Mediates Low-Threshold Mechanically Evoked Pain in the Cornea. The Journal of neuroscience : the official journal of the Society for Neuroscience 40, 8976-8993.

Fischer, M.J., Balasuriya, D., Jeggle, P., Goetze, T.A., McNaughton, P.A., Reeh, P.W., Edwardson, J.M., 2014. Direct evidence for functional TRPV1/TRPA1 heteromers. Pflugers Archiv : European journal of physiology 466, 2229-2241.

Fliegauf, M., Benzing, T., Omran, H., 2007. When cilia go bad: cilia defects and ciliopathies. Nature reviews. Molecular cell biology 8, 880-893.

Friedrich, E.E., Hong, Z., Xiong, S., Zhong, M., Di, A., Rehman, J., Komarova, Y.A., Malik, A.B., 2019. Endothelial cell Piezo1 mediates pressure-induced lung vascular hyperpermeability via disruption of adherens junctions. Proceedings of the National Academy of Sciences of the United States of America 116, 12980-12985.

Gallagher, A.R., Hoffmann, S., Brown, N., Cedzich, A., Meruvu, S., Podlich, D., Feng, Y., Könecke, V., de Vries, U., Hammes, H.P., Gretz, N., Witzgall, R., 2006. A truncated polycystin-2 protein causes polycystic kidney disease and retinal degeneration in transgenic rats. Journal of the American Society of Nephrology : JASN 17, 2719-2730.

Gao, F., Yang, Z., Jacoby, R.A., Wu, S.M., Pang, J.J., 2019. The expression and function of TRPV4 channels in primate retinal ganglion cells and bipolar cells. Cell death & disease 10, 364.

Gibbens, M.V., 1988. The consensual ophthalmotonic reaction. The British journal of ophthalmology 72, 746-749.

Gilliam, J.C., Wensel, T.G., 2011. TRP channel gene expression in the mouse retina. Vision research 51, 2440-2452.

Goel, M., Sienkiewicz, A.E., Picciani, R., Lee, R.K., Bhattacharya, S.K., 2011. Cochlin induced TREK-1 co-expression and annexin A2 secretion: role in trabecular meshwork cell elongation and motility. PloS one 6, e23070.

Goel, R., Murthy, K.R., Srikanth, S.M., Pinto, S.M., Bhattacharjee, M., Kelkar, D.S., Madugundu, A.K., Dey, G., Mohan, S.S., Krishna, V., Prasad Ts, K., Chakravarti, S., Harsha, H., Pandey, A., 2013. Characterizing the normal proteome of human ciliary body. Clinical proteomics 10, 9.

Gönczi, M., Szentandrássy, N., Johnson, I.T., Heagerty, A.M., Weston, A.H., 2006. Investigation of the role of TASK-2 channels in rat pulmonary arteries; pharmacological and functional studies following RNA interference procedures. British journal of pharmacology 147, 496-505.

Gradilone, S.A., Masyuk, A.I., Splinter, P.L., Banales, J.M., Huang, B.Q., Tietz, P.S., Masyuk, T.V., Larusso, N.F., 2007. Cholangiocyte cilia express TRPV4 and detect changes in luminal tonicity inducing bicarbonate secretion. Proceedings of the National Academy of Sciences of the United States of America 104, 19138-19143.

Greenbaum, D., Colangelo, C., Williams, K., Gerstein, M., 2003. Comparing protein abundance and mRNA expression levels on a genomic scale. Genome biology 4, 117.

Grimm, C., Kraft, R., Sauerbruch, S., Schultz, G., Harteneck, C., 2003. Molecular and functional characterization of the melastatin-related cation channel TRPM3. The Journal of biological chemistry 278, 21493-21501.

Guarino, B.D., Paruchuri, S., Thodeti, C.K., 2020. The role of TRPV4 channels in ocular function and pathologies. Experimental eye research 201, 108257.

Gudipaty, S.A., Lindblom, J., Loftus, P.D., Redd, M.J., Edes, K., Davey, C.F., Krishnegowda, V., Rosenblatt, J., 2017. Mechanical stretch triggers rapid epithelial cell division through Piezo1. Nature 543, 118-121.

Güler, A.D., Lee, H., Iida, T., Shimizu, I., Tominaga, M., Caterina, M., 2002. Heat-evoked activation of the ion channel, TRPV4. The Journal of neuroscience : the official journal of the Society for Neuroscience 22, 6408-6414.

Hackler, L., Jr., Wan, J., Swaroop, A., Qian, J., Zack, D.J., 2010. MicroRNA profile of the developing mouse retina. Investigative ophthalmology & visual science 51, 1823-1831.

Hirt, J., Liton, P.B., 2016. Autophagy and mechanotransduction in outflow pathway cells. Experimental eye research.

Honoré, E., 2007. The neuronal background K2P channels: focus on TREK1. Nature reviews. Neuroscience 8, 251-261.

Hu, R.G., Lim, J.C., Kalloniatis, M., Donaldson, P.J., 2011. Cellular localization of glutamate and glutamine metabolism and transport pathways in the rat ciliary epithelium. Investigative ophthalmology & visual science 52, 3345-3353.

Huang, M., Chalfie, M., 1994. Gene interactions affecting mechanosensory transduction in Caenorhabditis elegans. Nature 367, 467-470.

Hughes, S., Foster, R.G., Peirson, S.N., Hankins, M.W., 2017. Expression and localisation of two-pore domain (K2P) background leak potassium ion channels in the mouse retina. Scientific reports 7, 46085-46085.

Hughes, S., Pothecary, C.A., Jagannath, A., Foster, R.G., Hankins, M.W., Peirson, S.N., 2012. Profound defects in pupillary responses to light in TRPM-channel null mice: a role for TRPM channels in non-image-forming photoreception. The European journal of neuroscience 35, 34-43.

Iomini, C., Tejada, K., Mo, W., Vaananen, H., Piperno, G., 2004. Primary cilia of human endothelial cells disassemble under laminar shear stress. The Journal of cell biology 164, 811-817.

Iring, A., Jin, Y.J., Albarrán-Juárez, J., Siragusa, M., Wang, S., Dancs, P.T., Nakayama, A., Tonack, S., Chen, M., Künne, C., Sokol, A.M., Günther, S., Martínez, A., Fleming, I., Wettschureck, N., Graumann, J., Weinstein, L.S., Offermanns, S., 2019. Shear stress-induced endothelial adrenomedullin signaling regulates vascular tone and blood pressure. The Journal of clinical investigation 129, 2775-2791.

Ishikawa, H., Marshall, W.F., 2011. Ciliogenesis: building the cell's antenna. Nature reviews. Molecular cell biology 12, 222-234.

Ishikawa, M., Yoshitomi, T., Zorumski, C.F., Izumi, Y., 2014. Neurosteroids are endogenous neuroprotectants in an ex vivo glaucoma model. Investigative ophthalmology & visual science 55, 8531-8541.

Jaquemar, D., Schenker, T., Trueb, B., 1999. An ankyrin-like protein with transmembrane domains is specifically lost after oncogenic transformation of human fibroblasts. The Journal of biological chemistry 274, 7325-7333.

Jardín, I., López, J.J., Diez, R., Sánchez-Collado, J., Cantonero, C., Albarrán, L., Woodard, G.E., Redondo, P.C., Salido, G.M., Smani, T., Rosado, J.A., 2017. TRPs in Pain Sensation. Frontiers in physiology 8, 392.

Jin, P., Jan, L.Y., Jan, Y.N., 2020. Mechanosensitive Ion Channels: Structural Features Relevant to Mechanotransduction Mechanisms. Annual review of neuroscience 43, 207-229.

Jin, Y., Li, J., Wang, Y., Ye, R., Feng, X., Jing, Z., Zhao, Z., 2015. Functional role of mechanosensitive ion channel Piezo1 in human periodontal ligament cells. The Angle orthodontist 85, 87-94.

Jo, A.O., Lakk, M., Frye, A.M., Phuong, T.T.T., Redmon, S.N., Roberts, R., Berkowitz, B.A., Yarishkin, O., Križaj, D., 2016. Differential volume regulation and calcium signaling in two ciliary body cell types is subserved by TRPV4 channels. Proceedings of the National Academy of Sciences 113, 3885-3890.

Jo, A.O., Ryskamp, D.A., Phuong, T.T., Verkman, A.S., Yarishkin, O., MacAulay, N., Križaj, D., 2015. TRPV4 and AQP4 Channels Synergistically Regulate Cell Volume and Calcium Homeostasis in Retinal Müller Glia. The Journal of neuroscience : the official journal of the Society for Neuroscience 35, 13525-13537.

Kalapesi, F.B., Tan, J.C., Coroneo, M.T., 2005. Stretch-activated channels: a mini-review. Are stretch-activated channels an ocular barometer? Clinical & experimental ophthalmology 33, 210-217.

Karali, M., Peluso, I., Marigo, V., Banfi, S., 2007. Identification and characterization of microRNAs expressed in the mouse eye. Investigative ophthalmology & visual science 48, 509-515.

Katz, B., Payne, R., Minke, B., 2017. Frontiers in Neuroscience

TRP Channels in Vision, in: Emir, T.L.R. (Ed.), Neurobiology of TRP Channels. CRC Press/Taylor & Francis

© 2018 by Taylor & Francis Group, LLC., Boca Raton (FL), pp. 27-63.

Kerstein, P.C., del Camino, D., Moran, M.M., Stucky, C.L., 2009. Pharmacological blockade of TRPA1 inhibits mechanical firing in nociceptors. Molecular pain 5, 19.

Kim, S.E., Coste, B., Chadha, A., Cook, B., Patapoutian, A., 2012. The role of Drosophila Piezo in mechanical nociception. Nature 483, 209-212.

Kingman, S., 2004. Glaucoma is second leading cause of blindness globally. Bulletin of the World Health Organization 82, 887-888.

Kleene, S.J., Siroky, B.J., Landero-Figueroa, J.A., Dixon, B.P., Pachciarz, N.W., Lu, L., Kleene, N.K., 2019. The TRPP2-dependent channel of renal primary cilia also requires TRPM3. PloS one 14, e0214053.

Kobori, T., Smith, G.D., Sandford, R., Edwardson, J.M., 2009. The transient receptor potential channels TRPP2 and TRPC1 form a heterotetramer with a 2:2 stoichiometry and an alternating subunit arrangement. The Journal of biological chemistry 284, 35507-35513.

Köttgen, M., Buchholz, B., Garcia-Gonzalez, M.A., Kotsis, F., Fu, X., Doerken, M., Boehlke, C., Steffl, D., Tauber, R., Wegierski, T., Nitschke, R., Suzuki, M., Kramer-Zucker, A., Germino, G.G., Watnick, T., Prenen, J., Nilius, B., Kuehn, E.W., Walz, G., 2008. TRPP2 and TRPV4 form a polymodal sensory channel complex. The Journal of cell biology 182, 437-447.

Krol, J., Busskamp, V., Markiewicz, I., Stadler, M.B., Ribi, S., Richter, J., Duebel, J., Bicker, S., Fehling, H.J., Schübeler, D., Oertner, T.G., Schratt, G., Bibel, M., Roska, B., Filipowicz, W., 2010. Characterizing light-regulated retinal microRNAs reveals rapid turnover as a common property of neuronal microRNAs. Cell 141, 618-631.

Lakk, M., Young, D., Baumann, J.M., Jo, A.O., Hu, H., Križaj, D., 2018. Polymodal TRPV1 and TRPV4 Sensors Colocalize but Do Not Functionally Interact in a Subpopulation of Mouse Retinal Ganglion Cells. Frontiers in cellular neuroscience 12, 353.

Lee, N., Chen, J., Sun, L., Wu, S., Gray, K.R., Rich, A., Huang, M., Lin, J.H., Feder, J.N., Janovitz, E.B., Levesque, P.C., Blanar, M.A., 2003. Expression and characterization of human transient receptor potential melastatin 3 (hTRPM3). The Journal of biological chemistry 278, 20890-20897.

Li Fraine, S., Patel, A., Duprat, F., Sharif-Naeini, R., 2017. Dynamic regulation of TREK1 gating by Polycystin 2 via a Filamin A-mediated cytoskeletal Mechanism. Scientific reports 7, 17403.

Li, G., Liedtke, W., Challa, P., Luna, C., Epstein, D.L., Gonzalez, P., Liton, P., 2007. Expression of Transient Receptor Potential (TRP) Channels in the Outflow Pathway

and Ciliary Body of Porcine Eyes. Investigative ophthalmology & visual science 48, 2066-2066.

Li, J., Hou, B., Tumova, S., Muraki, K., Bruns, A., Ludlow, M.J., Sedo, A., Hyman, A.J., McKeown, L., Young, R.S., Yuldasheva, N.Y., Majeed, Y., Wilson, L.A., Rode, B., Bailey, M.A., Kim, H.R., Fu, Z., Carter, D.A., Bilton, J., Imrie, H., Ajuh, P., Dear, T.N., Cubbon, R.M., Kearney, M.T., Prasad, R.K., Evans, P.C., Ainscough, J.F., Beech, D.J., 2014. Piezo1 integration of vascular architecture with physiological force. Nature 515, 279-282.

Liedtke, W., Choe, Y., Martí-Renom, M.A., Bell, A.M., Denis, C.S., Sali, A., Hudspeth, A.J., Friedman, J.M., Heller, S., 2000. Vanilloid receptor-related osmotically activated channel (VR-OAC), a candidate vertebrate osmoreceptor. Cell 103, 525-535.

Lin, S.Y., Corey, D.P., 2005. TRP channels in mechanosensation. Current opinion in neurobiology 15, 350-357.

Liu, X., Vien, T., Duan, J., Sheu, S.H., DeCaen, P.G., Clapham, D.E., 2018. Polycystin-2 is an essential ion channel subunit in the primary cilium of the renal collecting duct epithelium. eLife 7.

Loi, M., 2006. Lowe syndrome. Orphanet journal of rare diseases 1, 16.

Lu, C.J., Du, H., Wu, J., Jansen, D.A., Jordan, K.L., Xu, N., Sieck, G.C., Qian, Q., 2008. Non-random distribution and sensory functions of primary cilia in vascular smooth muscle cells. Kidney & blood pressure research 31, 171-184.

Luo, N., Conwell, M.D., Chen, X., Kettenhofen, C.I., Westlake, C.J., Cantor, L.B., Wells, C.D., Weinreb, R.N., Corson, T.W., Spandau, D.F., Joos, K.M., Iomini, C., Obukhov, A.G., Sun, Y., 2014. Primary cilia signaling mediates intraocular pressure sensation. Proceedings of the National Academy of Sciences of the United States of America 111, 12871-12876.

Luo, N., West, C.C., Murga-Zamalloa, C.A., Sun, L., Anderson, R.M., Wells, C.D., Weinreb, R.N., Travers, J.B., Khanna, H., Sun, Y., 2012. OCRL localizes to the primary cilium: a new role for cilia in Lowe syndrome. Human molecular genetics 21, 3333-3344.

Ma, R., Li, W.P., Rundle, D., Kong, J., Akbarali, H.I., Tsiokas, L., 2005. PKD2 functions as an epidermal growth factor-activated plasma membrane channel. Molecular and cellular biology 25, 8285-8298.

Mandal, A., Shahidullah, M., Delamere, N.A., 2010. Hydrostatic pressure-induced release of stored calcium in cultured rat optic nerve head astrocytes. Investigative ophthalmology & visual science 51, 3129-3138.

Martínez-Rendón, J., Sánchez-Guzmán, E., Rueda, A., González, J., Gulias-Cañizo, R., Aquino-Jarquín, G., Castro-Muñozledo, F., García-Villegas, R., 2017. TRPV4 Regulates Tight Junctions and Affects Differentiation in a Cell Culture Model of the Corneal Epithelium. Journal of cellular physiology 232, 1794-1807.

Masyuk, A.I., Masyuk, T.V., Splinter, P.L., Huang, B.Q., Stroope, A.J., LaRusso, N.F., 2006. Cholangiocyte cilia detect changes in luminal fluid flow and transmit them into intracellular Ca^{2+} and cAMP signaling. Gastroenterology 131, 911-920.

Matsumoto, H., Sugio, S., Seghers, F., Krizaj, D., Akiyama, H., Ishizaki, Y., Gailly, P., Shibasaki, K., 2018. Retinal Detachment-Induced Müller Glial Cell Swelling Activates TRPV4 Ion Channels and Triggers Photoreceptor Death at Body Temperature. The Journal of Neuroscience 38, 8745-8758.

McHugh, B.J., Buttery, R., Lad, Y., Banks, S., Haslett, C., Sethi, T., 2010. Integrin activation by Fam38A uses a novel mechanism of R-Ras targeting to the endoplasmic reticulum. Journal of cell science 123, 51-61.

Meng, Q., Fang, P., Hu, Z., Ling, Y., Liu, H., 2015. Mechanotransduction of trigeminal ganglion neurons innervating inner walls of rat anterior eye chambers. American journal of physiology. Cell physiology 309, C1-10.

Mergler, S., Derckx, R., Reinach, P.S., Garreis, F., Böhm, A., Schmelzer, L., Skosyrski, S., Ramesh, N., Abdelmessih, S., Polat, O.K., Khajavi, N., Riechardt, A.I., 2014. Calcium regulation by temperature-sensitive transient receptor potential channels in human uveal melanoma cells. Cellular signalling 26, 56-69.

Mergler, S., Garreis, F., Sahlmüller, M., Lyras, E.M., Reinach, P.S., Dwarakanath, A., Paulsen, F., Pleyer, U., 2012. Calcium regulation by thermo- and osmosensing transient receptor potential vanilloid channels (TRPVs) in human conjunctival epithelial cells. Histochemistry and cell biology 137, 743-761.

Mergler, S., Garreis, F., Sahlmüller, M., Reinach, P.S., Paulsen, F., Pleyer, U., 2011a. Thermosensitive transient receptor potential channels in human corneal epithelial cells. Journal of cellular physiology 226, 1828-1842.

Mergler, S., Valtink, M., Taetz, K., Sahlmuller, M., Fels, G., Reinach, P.S., Engelmann, K., Pleyer, U., 2011b. Characterization of transient receptor potential vanilloid channel 4 (TRPV4) in human corneal endothelial cells. Experimental eye research 93, 710-719.

Miyamoto, T., Mochizuki, T., Nakagomi, H., Kira, S., Watanabe, M., Takayama, Y., Suzuki, Y., Koizumi, S., Takeda, M., Tominaga, M., 2014. Functional role for Piezo1 in stretch-evoked Ca(2)(+) influx and ATP release in urothelial cell cultures. The Journal of biological chemistry 289, 16565-16575.

Mochizuki, T., Wu, G., Hayashi, T., Xenophontos, S.L., Veldhuisen, B., Saris, J.J., Reynolds, D.M., Cai, Y., Gabow, P.A., Pierides, A., Kimberling, W.J., Breuning, M.H., Deltas, C.C., Peters, D.J., Somlo, S., 1996. PKD2, a gene for polycystic kidney disease that encodes an integral membrane protein. Science (New York, N.Y.) 272, 1339-1342.

Morozumi, W., Inagaki, S., Iwata, Y., Nakamura, S., Hara, H., Shimazawa, M., 2020. Piezo channel plays a part in retinal ganglion cell damage. Experimental eye research 191, 107900.

Nachury, M.V., Loktev, A.V., Zhang, Q., Westlake, C.J., Peränen, J., Merdes, A., Slusarski, D.C., Scheller, R.H., Bazan, J.F., Sheffield, V.C., Jackson, P.K., 2007. A core complex of BBS proteins cooperates with the GTPase Rab8 to promote ciliary membrane biogenesis. Cell 129, 1201-1213.

Nadal-Nicolas, F.M., Jimenez-Lopez, M., Sobrado-Calvo, P., Nieto-Lopez, L., Canovas-Martinez, I., Salinas-Navarro, M., Vidal-Sanz, M., Agudo, M., 2009. Brn3a as a

marker of retinal ganglion cells: qualitative and quantitative time course studies in naive and optic nerve-injured retinas. Investigative ophthalmology & visual science 50, 3860-3868.

Nakazawa, Y., Donaldson, P.J., Petrova, R.S., 2019. Verification and spatial mapping of TRPV1 and TRPV4 expression in the embryonic and adult mouse lens. Experimental eye research 186, 107707.

Nauli, S.M., Alenghat, F.J., Luo, Y., Williams, E., Vassilev, P., Li, X., Elia, A.E., Lu, W., Brown, E.M., Quinn, S.J., Ingber, D.E., Zhou, J., 2003. Polycystins 1 and 2 mediate mechanosensation in the primary cilium of kidney cells. Nature genetics 33, 129-137.

Nauli, S.M., Kawanabe, Y., Kaminski, J.J., Pearce, W.J., Ingber, D.E., Zhou, J., 2008. Endothelial cilia are fluid shear sensors that regulate calcium signaling and nitric oxide production through polycystin-1. Circulation 117, 1161-1171.

Nauta, J., Goedbloed, M.A., Herck, H.V., Hesselink, D.A., Visser, P., Willemsen, R., Dokkum, R.P., Wright, C.J., Guay-Woodford, L.M., 2000. New rat model that phenotypically resembles autosomal recessive polycystic kidney disease. Journal of the American Society of Nephrology : JASN 11, 2272-2284.

Nilius, B., Flockerzi, V., 2014. Mammalian transient receptor potential (TRP) cation channels. Preface. Handbook of experimental pharmacology 223, v - vi.

O'Neil, R.G., Heller, S., 2005. The mechanosensitive nature of TRPV channels. Pflugers Archiv : European journal of physiology 451, 193-203.

Obermüller, N., Gallagher, A.R., Cai, Y., Gassler, N., Gretz, N., Somlo, S., Witzgall, R., 1999. The rat pkd2 protein assumes distinct subcellular distributions in different organs. The American journal of physiology 277, F914-925.

Ohnishi, Y., Tanaka, M., 1980. Cilia in the ciliary epithelium. Albrecht von Graefes Archiv fur klinische und experimentelle Ophthalmologie. Albrecht von Graefe's archive for clinical and experimental ophthalmology 213, 161-167.

Okada, Y., Shirai, K., Miyajima, M., Reinach, P.S., Yamanaka, O., Sumioka, T., Kokado, M., Tomoyose, K., Saika, S., 2016. Loss of TRPV4 Function Suppresses Inflammatory Fibrosis Induced by Alkali-Burning Mouse Corneas. PloS one 11, e0167200.

Okada, Y., Shirai, K., Reinach, P.S., Kitano-Izutani, A., Miyajima, M., Flanders, K.C., Jester, J.V., Tominaga, M., Saika, S., 2014. TRPA1 is required for TGF-beta signaling and its loss blocks inflammatory fibrosis in mouse corneal stroma. Laboratory investigation; a journal of technical methods and pathology 94, 1030-1041.

Osbourne, N., 1994. Serotonin and melatonin in the iris/ciliary processes and their involvement in intraocular presence. Acta Neurobiol Exp 54, 57-64.

Pan, Z., Yang, H., Mergler, S., Liu, H., Tachado, S.D., Zhang, F., Kao, W.W., Koziel, H., Pleyer, U., Reinach, P.S., 2008. Dependence of regulatory volume decrease on transient receptor potential vanilloid 4 (TRPV4) expression in human corneal epithelial cells. Cell calcium 44, 374-385.

Papanikolaou, M., Lewis, A., Butt, A.M., 2017. Store-operated calcium entry is essential for glial calcium signalling in CNS white matter. Brain structure & function 222, 2993-3005.

Patel, A.J., Honoré, E., Maingret, F., Lesage, F., Fink, M., Duprat, F., Lazdunski, M., 1998. A mammalian two pore domain mechano-gated S-like K+ channel. The EMBO journal 17, 4283-4290.

Peyronnet, R., Martins, J.R., Duprat, F., Demolombe, S., Arhatte, M., Jodar, M., Tauc, M., Duranton, C., Paulais, M., Teulon, J., Honore, E., Patel, A., 2013. Piezo1-dependent stretch-activated channels are inhibited by Polycystin-2 in renal tubular epithelial cells. EMBO reports 14, 1143-1148.

Pintor, J., Peláez, T., Hoyle, C.H., Peral, A., 2003. Ocular hypotensive effects of melatonin receptor agonists in the rabbit: further evidence for an MT3 receptor. British journal of pharmacology 138, 831-836.

Polacheck, W.J., Li, R., Uzel, S.G., Kamm, R.D., 2013. Microfluidic platforms for mechanobiology. Lab on a chip 13, 2252-2267.

Ranade, S.S., Syeda, R., Patapoutian, A., 2015. Mechanically Activated Ion Channels. Neuron 87, 1162-1179.

Reinach, P.S., Mergler, S., Okada, Y., Saika, S., 2015. Ocular transient receptor potential channel function in health and disease. BMC ophthalmology 15 Suppl 1, 153.

Rhodes, J.D., Sanderson, J., 2009. The mechanisms of calcium homeostasis and signalling in the lens. Experimental eye research 88, 226-234.

Rode, B., Shi, J., Endesh, N., Drinkhill, M.J., Webster, P.J., Lotteau, S.J., Bailey, M.A., Yuldasheva, N.Y., Ludlow, M.J., Cubbon, R.M., Li, J., Futers, T.S., Morley, L., Gaunt, H.J., Marszalek, K., Viswambharan, H., Cuthbertson, K., Baxter, P.D., Foster, R., Sukumar, P., Weightman, A., Calaghan, S.C., Wheatcroft, S.B., Kearney, M.T., Beech, D.J., 2017. Piezo1 channels sense whole body physical activity to reset cardiovascular homeostasis and enhance performance. Nature communications 8, 350.

Roper, S.D., 2014. TRPs in taste and chemesthesis. Handbook of experimental pharmacology 223, 827-871.

Ryskamp, D.A., Frye, A.M., Phuong, T.T., Yarishkin, O., Jo, A.O., Xu, Y., Lakk, M., Iuso, A., Redmon, S.N., Ambati, B., Hageman, G., Prestwich, G.D., Torrejon, K.Y., Krizaj, D., 2016a. TRPV4 regulates calcium homeostasis, cytoskeletal remodeling, conventional outflow and intraocular pressure in the mammalian eye. Scientific reports 6, 30583.

Ryskamp, D.A., Frye, A.M., Phuong, T.T., Yarishkin, O., Jo, A.O., Xu, Y., Lakk, M., Iuso, A., Redmon, S.N., Ambati, B., Hageman, G., Prestwich, G.D., Torrejon, K.Y., Križaj, D., 2016b. TRPV4 regulates calcium homeostasis, cytoskeletal remodeling, conventional outflow and intraocular pressure in the mammalian eye. Scientific reports 6, 30583.

Ryskamp, D.A., Jo, A.O., Frye, A.M., Vazquez-Chona, F., MacAulay, N., Thoreson, W.B., Križaj, D., 2014. Swelling and eicosanoid metabolites differentially gate TRPV4 channels in retinal neurons and glia. The Journal of neuroscience : the official journal of the Society for Neuroscience 34, 15689-15700.

Ryskamp, D.A., Witkovsky, P., Barabas, P., Huang, W., Koehler, C., Akimov, N.P., Lee, S.H., Chauhan, S., Xing, W., Renteria, R.C., Liedtke, W., Krizaj, D., 2011a. The polymodal ion channel transient receptor potential vanilloid 4 modulates calcium flux, spiking rate, and apoptosis of mouse retinal ganglion cells. The Journal of neuroscience : the official journal of the Society for Neuroscience 31, 7089-7101.

Ryskamp, D.A., Witkovsky, P., Barabas, P., Huang, W., Koehler, C., Akimov, N.P., Lee, S.H., Chauhan, S., Xing, W., Rentería, R.C., Liedtke, W., Krizaj, D., 2011b. The polymodal ion channel transient receptor potential vanilloid 4 modulates calcium flux, spiking rate, and apoptosis of mouse retinal ganglion cells. The Journal of neuroscience : the official journal of the Society for Neuroscience 31, 7089-7101.

Sachs, F., 2010. Stretch-activated ion channels: what are they? Physiology (Bethesda, Md.) 25, 50-56.

Samanta, A., Hughes, T.E.T., Moiseenkova-Bell, V.Y., 2018. Transient Receptor Potential (TRP) Channels. Sub-cellular biochemistry 87, 141-165.

Samuel, W., Jaworski, C., Postnikova, O.A., Kutty, R.K., Duncan, T., Tan, L.X., Poliakov, E., Lakkaraju, A., Redmond, T.M., 2017. Appropriately differentiated ARPE-19 cells regain phenotype and gene expression profiles similar to those of native RPE cells. Molecular vision 23, 60-89.

Satir, P., 2005. Tour of organelles through the electron microscope: a reprinting of Keith R. Porter's classic Harvey Lecture with a new introduction. The anatomical record. Part A, Discoveries in molecular, cellular, and evolutionary biology 287, 1184-1185.

Satir, P., Christensen, S.T., 2007. Overview of structure and function of mammalian cilia. Annual review of physiology 69, 377-400.

Schulz, H.L., Rahman, F.A., Fadl El Moula, F.M., Stojic, J., Gehrig, A., Weber, B.H., 2004. Identifying differentially expressed genes in the mammalian retina and the retinal pigment epithelium by suppression subtractive hybridization. Cytogenetic and genome research 106, 74-81.

Shaham, O., Gueta, K., Mor, E., Oren-Giladi, P., Grinberg, D., Xie, Q., Cvekl, A., Shomron, N., Davis, N., Keydar-Prizant, M., Raviv, S., Pasmanik-Chor, M., Bell, R.E., Levy, C., Avellino, R., Banfi, S., Conte, I., Ashery-Padan, R., 2013. Pax6 regulates gene expression in the vertebrate lens through miR-204. PLoS genetics 9, e1003357.

Shahidullah, M., Mandal, A., Delamere, N.A., 2012. TRPV4 in porcine lens epithelium regulates hemichannel-mediated ATP release and Na-K-ATPase activity. American journal of physiology. Cell physiology 302, C1751-1761.

Sharif, N.A., Wang, Y., Katoli, P., Xu, S., Kelly, C.R., Li, L., 2014. Human Non-Pigmented Ciliary Epithelium Bradykinin B2-Receptors: Receptor Localization, Pharmacological Characterization of Intracellular Ca^{2+} Mobilization, and Prostaglandin Secretion. Current eye research 39, 378-389.

Shibukawa, Y., Sato, M., Kimura, M., Sobhan, U., Shimada, M., Nishiyama, A., Kawaguchi, A., Soya, M., Kuroda, H., Katakura, A., Ichinohe, T., Tazaki, M., 2015. Odontoblasts as sensory receptors: transient receptor potential channels, pannexin-1, and

ionotropic ATP receptors mediate intercellular odontoblast-neuron signal transduction. Pflugers Archiv : European journal of physiology 467, 843-863.

Shiels, A., 2020. TRPM3_miR-204: a complex locus for eye development and disease. Human genomics 14, 7.

Siroky, B.J., Kleene, N.K., Kleene, S.J., Varnell, C.D., Jr., Comer, R.G., Liu, J., Lu, L., Pachciarz, N.W., Bissler, J.J., Dixon, B.P., 2017. Primary cilia regulate the osmotic stress response of renal epithelial cells through TRPM3. American journal of physiology. Renal physiology 312, F791-f805.

Soattin, L., Fiore, M., Gavazzo, P., Viti, F., Facci, P., Raiteri, R., Difato, F., Pusch, M., Vassalli, M., 2016. The biophysics of piezo1 and piezo2 mechanosensitive channels. Biophysical chemistry 208, 26-33.

Soya, M., Sato, M., Sobhan, U., Tsumura, M., Ichinohe, T., Tazaki, M., Shibukawa, Y., 2014. Plasma membrane stretch activates transient receptor potential vanilloid and ankyrin channels in Merkel cells from hamster buccal mucosa. Cell calcium 55, 208-218.

Sruthi Sampathkumar and Carol B. Toris, Ciliary epithelium as a syncytium, digital image from 13 Structure and Mechanisms of Aqueous Production, EntoKey, accessed 2 June 2022, <https://entokey.com/structure-and-mechanisms-of-aqueous-production/>.

Startek, J.B., Boonen, B., Talavera, K., Meseguer, V., 2019. TRP Channels as Sensors of Chemically-Induced Changes in Cell Membrane Mechanical Properties. International journal of molecular sciences 20.

Stewart, A.P., Smith, G.D., Sandford, R.N., Edwardson, J.M., 2010. Atomic force microscopy reveals the alternating subunit arrangement of the TRPP2-TRPV4 heterotetramer. Biophysical journal 99, 790-797.

Suesskind, D., Schatz, A., Schnichels, S., Coupland, S.E., Lake, S.L., Wissinger, B., Bartz-Schmidt, K.U., Henke-Fahle, S., 2012. GDF-15: a novel serum marker for metastases in uveal melanoma patients. Graefe's archive for clinical and experimental ophthalmology = Albrecht von Graefes Archiv fur klinische und experimentelle Ophthalmologie 250, 887-895.

Talavera, K., Startek, J.B., Alvarez-Collazo, J., Boonen, B., Alpizar, Y.A., Sanchez, A., Naert, R., Nilius, B., 2020. Mammalian Transient Receptor Potential TRPA1 Channels: From Structure to Disease. Physiological reviews 100, 725-803.

Taylor, L., Arnér, K., Ghosh, F., 2017. Specific inhibition of TRPV4 enhances retinal ganglion cell survival in adult porcine retinal explants. Experimental eye research 154, 10-21.

Terrell, A.M., Anand, D., Smith, S.F., Dang, C.A., Waters, S.M., Pathania, M., Beebe, D.C., Lachke, S.A., 2015. Molecular characterization of mouse lens epithelial cell lines and their suitability to study RNA granules and cataract associated genes. Experimental eye research 131, 42-55.

Tham, Y.C., Li, X., Wong, T.Y., Quigley, H.A., Aung, T., Cheng, C.Y., 2014. Global prevalence of glaucoma and projections of glaucoma burden through 2040: a systematic review and meta-analysis. Ophthalmology 121, 2081-2090.

Thompson, C.L., Fu, S., Knight, M.M., Thorpe, S.D., 2020. Mechanical Stimulation: A Crucial Element of Organ-on-Chip Models. Frontiers in bioengineering and biotechnology 8, 602646.

Tran, V.T., Ho, P.T., Cabrera, L., Torres, J.E., Bhattacharya, S.K., 2014. Mechanotransduction channels of the trabecular meshwork. Current eye research 39, 291-303.

Tschulakow, A.V., Oltrup, T., Bende, T., Schmelzle, S., Schraermeyer, U., 2018. The anatomy of the foveola reinvestigated. PeerJ 6, e4482.

Tsutsumi, T., Kajiya, H., Fukawa, T., Sasaki, M., Nemoto, T., Tsuzuki, T., Takahashi, Y., Fujii, S., Maeda, H., Okabe, K., 2013. The potential role of transient receptor potential type A1 as a mechanoreceptor in human periodontal ligament cells. European journal of oral sciences 121, 538-544.

Voets, T., Prenen, J., Vriens, J., Watanabe, H., Janssens, A., Wissenbach, U., Bödding, M., Droogmans, G., Nilius, B., 2002. Molecular determinants of permeation through the cation channel TRPV4. The Journal of biological chemistry 277, 33704-33710.

Vranka, J.A., Kelley, M.J., Acott, T.S., Keller, K.E., 2015. Extracellular matrix in the trabecular meshwork: intraocular pressure regulation and dysregulation in glaucoma. Experimental eye research 133, 112-125.

Vriens, J., Owsianik, G., Hofmann, T., Philipp, S.E., Stab, J., Chen, X., Benoit, M., Xue, F., Janssens, A., Kerselaers, S., Oberwinkler, J., Vennekens, R., Gudermann, T., Nilius, B., Voets, T., 2011. TRPM3 is a nociceptor channel involved in the detection of noxious heat. Neuron 70, 482-494.

Wang, F.E., Zhang, C., Maminishkis, A., Dong, L., Zhi, C., Li, R., Zhao, J., Majerciak, V., Gaur, A.B., Chen, S., Miller, S.S., 2010. MicroRNA-204/211 alters epithelial physiology. FASEB journal : official publication of the Federation of American Societies for Experimental Biology 24, 1552-1571.

Wang, S., Chennupati, R., Kaur, H., Iring, A., Wettschureck, N., Offermanns, S., 2016. Endothelial cation channel PIEZO1 controls blood pressure by mediating flow-induced ATP release. The Journal of clinical investigation 126, 4527-4536.

Wann, A.K., Zuo, N., Haycraft, C.J., Jensen, C.G., Poole, C.A., McGlashan, S.R., Knight, M.M., 2012. Primary cilia mediate mechanotransduction through control of ATP-induced Ca^{2+} signaling in compressed chondrocytes. FASEB journal : official publication of the Federation of American Societies for Experimental Biology 26, 1663-1671.

Weinreb, R.N., Khaw, P.T., 2004. Primary open-angle glaucoma. Lancet (London, England) 363, 1711-1720.

Wheatley, D.N., 1995. Primary cilia in normal and pathological tissues. Pathobiology : journal of immunopathology, molecular and cellular biology 63, 222-238.

White, J.P., Cibelli, M., Urban, L., Nilius, B., McGeown, J.G., Nagy, I., 2016. TRPV4: Molecular Conductor of a Diverse Orchestra. Physiological reviews 96, 911-973.

Wimmers, S., Karl, M.O., Strauss, O., 2007. Ion channels in the RPE. Progress in retinal and eye research 26, 263-301.

Wistow, G., Bernstein, S.L., Ray, S., Wyatt, M.K., Behal, A., Touchman, J.W., Bouffard, G., Smith, D., Peterson, K., 2002. Expressed sequence tag analysis of adult human iris for the NEIBank Project: steroid-response factors and similarities with retinal pigment epithelium. Molecular vision 8, 185-195.

Wistow, G., Peterson, K., Gao, J., Buchoff, P., Jaworski, C., Bowes-Rickman, C., Ebright, J.N., Hauser, M.A., Hoover, D., 2008. NEIBank: genomics and bioinformatics resources for vision research. Molecular vision 14, 1327.

Woo, S.H., Ranade, S., Weyer, A.D., Dubin, A.E., Baba, Y., Qiu, Z., Petrus, M., Miyamoto, T., Reddy, K., Lumpkin, E.A., Stucky, C.L., Patapoutian, A., 2014. Piezo2 is required for Merkel-cell mechanotransduction. Nature 509, 622-626.

Wu, J., Du, H., Wang, X., Mei, C., Sieck, G.C., Qian, Q., 2009. Characterization of primary cilia in human airway smooth muscle cells. Chest 136, 561-570.

Wu, J., Lewis, A.H., Grandl, J., 2017. Touch, Tension, and Transduction - The Function and Regulation of Piezo Ion Channels. Trends in biochemical sciences 42, 57-71.

Xie, Q., Yang, Y., Huang, J., Ninkovic, J., Walcher, T., Wolf, L., Vitenzon, A., Zheng, D., Götz, M., Beebe, D.C., Zavadil, J., Cvekl, A., 2013. Pax6 interactions with chromatin and identification of its novel direct target genes in lens and forebrain. PloS one 8, e54507.

Yarishkin, O., Phuong, T.T.T., Baumann, J.M., De Ieso, M.L., Vazquez-Chona, F., Rudzitis, C.N., Sundberg, C., Lakk, M., Stamer, W.D., Križaj, D., 2021. Piezo1 channels mediate trabecular meshwork mechanotransduction and promote aqueous fluid outflow. The Journal of physiology 599, 571-592.

Yarishkin, O., Phuong, T.T.T., Bretz, C.A., Olsen, K.W., Baumann, J.M., Lakk, M., Crandall, A., Heurteaux, C., Hartnett, M.E., Križaj, D., 2018. TREK-1 channels regulate pressure sensitivity and calcium signaling in trabecular meshwork cells. The Journal of general physiology 150, 1660-1675.

Yarishkin, O., Phuong, T.T.T., Križaj, D., 2019. Trabecular Meshwork TREK-1 Channels Function as Polymodal Integrators of Pressure and pH. Investigative ophthalmology & visual science 60, 2294-2303.

Zanini, D., Göpfert, M.C., 2014. TRPs in hearing. Handbook of experimental pharmacology 223, 899-916.

Zanzouri, M., Lauritzen, I., Duprat, F., Mazzuca, M., Lesage, F., Lazdunski, M., Patel, A., 2006. Membrane potential-regulated transcription of the resting K+ conductance TASK-3 via the calcineurin pathway. The Journal of biological chemistry 281, 28910-28918.

Zeng, W.Z., Marshall, K.L., Min, S., Daou, I., Chapleau, M.W., Abboud, F.M., Liberles, S.D., Patapoutian, A., 2018. PIEZOs mediate neuronal sensing of blood pressure and the baroreceptor reflex. Science (New York, N.Y.) 362, 464-467.

Zhang, H., Shepherd, N., Creazzo, T.L., 2008. Temperature-sensitive TREK currents contribute to setting the resting membrane potential in embryonic atrial myocytes. The Journal of physiology 586, 3645-3656.

Zhang, X.-T., Xu, Z., Shi, K.-P., Guo, D.-L., Li, H., Wang, L., Zhu, X.-B., 2019. Elevated expression of TREK-TRAAK K(2P) channels in the retina of adult rd1 mice. Int J Ophthalmol 12, 924-929.

Zhao, P.Y., Gan, G., Peng, S., Wang, S.B., Chen, B., Adelman, R.A., Rizzolo, L.J., 2015. TRP Channels Localize to Subdomains of the Apical Plasma Membrane in Human Fetal Retinal Pigment Epithelium. Investigative ophthalmology & visual science 56, 1916-1923.

Zhou, Y., Suzuki, Y., Uchida, K., Tominaga, M., 2013. Identification of a splice variant of mouse TRPA1 that regulates TRPA1 activity. Nature communications 4, 2399.

Zhu, J., Yu, Y., Ulbrich, M.H., Li, M.H., Isacoff, E.Y., Honig, B., Yang, J., 2011. Structural model of the TRPP2/PKD1 C-terminal coiled-coil complex produced by a combined computational and experimental approach. Proceedings of the National Academy of Sciences of the United States of America 108, 10133-10138.

Zhu, W., Hou, F., Fang, J., Bahrani Fard, M.R., Liu, Y., Ren, S., Wu, S., Qi, Y., Sui, S., Read, A.T., Sherwood, J.M., Zou, W., Yu, H., Zhang, J., Overby, D.R., Wang, N., Ethier, C.R., Wang, K., 2021. The role of Piezo1 in conventional aqueous humor outflow dynamics. iScience 24, 102042.

Zufall, F., 2014. TRPs in olfaction. Handbook of experimental pharmacology 223, 917-933.

9. Acknowledgements

I would like to express my sincere appreciation and many thanks to my supervisor Prof. Dr. Focke Ziemssen for providing me the opportunity to do research in his lab and guiding me in my project, and for his encouragement and understanding. Thanks to your continuous support, I am able to complete my doctoral research, especially after my two children were born.

My appreciation also goes out to PD Dr. Bogomil Voykov for providing important ideas for this project and assisting me in initiating the study when arriving in Tübingen. I also would like to thank Dr. Sven Schnichels for his suggestions for my project and for his guidance in the lab. I also would like to thank Prof. Dr. Ulrich Schraermeyer for helping me do the electron microscopy observation. I also would like to thank Prof. Dr. Marlies Knipper for suggestions to siRNA technology. I also would like to thank Apl. Prof. Dr. Daniela Süsskind for providing me the histological sections of human eyes.

I want to thank Prof. Yajuan Zheng, my former supervisor in China, for encouraging me to study abroad, for her guidance in the clinical work which extended my knowledge of glaucoma and letting me focusing on this disease. I also would like to thank Prof. Wensong Zhang, for their guidance in clinical work and assistance whenever I have problems in life.

I am also very grateful to the people from neuroprotection and drug delivery research group at the Institute for Ophthalmic Research (University of Tübingen). Johanna Wude, thank you for your suggestions on my experiment and giving tips on my life in Germany. José Hurst, thank you for your assistance on working in the lab. Manuela Kübler and Henriette Rasp, thank you for your assistance in lab as well. I am also would like to thank people in the ophthalmic pathology laboratory at the Eye Hospital (University of Tübingen) who gave me assistance. Christiana Fischer-Lamprecht, Claudia Riedinger and Monika Wild, thank you for doing some immunohistochemistry experiments for me.

Thanks to Lena Riha for correcting my thesis and providing lots of useful comments. Also, thanks to the medical school, University of Tübingen, and especially to Dr. Inka

Montero and Dr. Tanja Mirjam Rieß, for their supervision and their kind help during my doctoral study.

A special thanks to my family, my husband, my daughter and my son, thank you for your love and support in my life, I love all of you. I would especially like to thank my parents for their constant support, understanding, and encouragement.